

Formation and Evolution of the Dust in Galaxies. II. The Solar Neighbourhood

L. Piovan^{1,2}, C. Chiosi¹, E. Merlin¹, T. Grassi¹, R. Tantalo¹, U. Buonomo¹ and L. P. Cassarà¹

¹ Department of Astronomy, Padova University, Vicolo dell'Osservatorio 3, I-35122, Padova, Italy

²Max-Planck-Institut für Astrophysik, Karl-Schwarzschild-Str. 1, Garching bei München, Germany
e-mail: lorenzo.piovan@unipd.it

Received: July 2011; Revised: *** ***; Accepted: *** ***

ABSTRACT

Context. Over the past decade a new generation of chemical models, in addition to the gas, have included the dust in the treatment of the interstellar medium (ISM). This major accomplishment has been spurred by the growing amounts of data on the highly obscured high- z Universe and the intriguing local properties of the Solar Neighbourhood (SoNe) of the Milky Way (MW) Disk.

Aims. We present here a new model able to simulate the formation and evolution of dust in the ISM of the MW. The model follows the evolution of 16 elemental species, with particular attention to those that are simultaneously present in form of gas and dust, e.g. C, N, O, Mg, Si, S, Ca and Fe. In this study we focus on the SoNe and the MW Disk as a whole which are considered as laboratories to test the physical ingredients governing the dust evolution.

Methods. The MW is described as a set of concentric rings of which we follow the time evolution of gas and dust. Infall of primordial gas, birth and death of stars, radial flows of matter between contiguous shells, presence of a central bar, star-dust emission by SN α and AGB stars, dust destruction and accretion are taken into account. The model reproduces the local depletion of the elements in the gas, and simultaneously satisfies other constraints obtained from the observations.

Results. The evolution of the element abundances in the gas and dust has been well reproduced for plausible choices of the parameters. The Mg/Si ratio, in particular, drives the formation of silicates. We show that for most of the evolution of the MW, the main process for dust enrichment is the accretion in the cold regions of the ISM. SN α dominate in the early phases of the evolution. We have also examined the main factors controlling the temporal window in which SN α govern the dust budget both in low and high star forming environments. The role played by AGB stars is also discussed. We find that IMFs with regular slope in the range of massive stars better reproduce the observed depletions.

Conclusions. The classical chemical models nicely reproduce the abundances, depletion factors and dust properties of the SoNe and the main ingredients of the models are tested against observational data. The results obtained for the SoNe lead us to safely extend the model to the whole Galactic Disk or galaxies of different morphological types.

Key words. Galaxies - Dust; Galaxies – Spirals; Galaxies – Milky Way

1. Introduction

In the fascinating subject of the origin and evolution of galaxies, the interstellar dust is acquiring a primary role because of its growing importance in the observations of the high- z Universe (Omout et al. 2001; Shapley et al. 2001; Bertoldi et al. 2003; Robson et al. 2004; Wang et al. 2008a,b; Gallerani et al. 2010; Michałowski et al. 2010b,a) and the theoretical spectro-photometric, dynamical, and chemical modeling of galaxies (Schurer et al. 2009; Narayanan et al. 2010; Jonsson et al. 2010; Grassi et al. 2010; Pipino et al. 2011; Popescu et al. 2011).

Indeed, the evidence of highly obscured QSOs and galaxies already in place at high- z leads necessarily to a new generation of theoretical models where dust is a key ingredient that cannot be neglected, if we want to obtain precious clues on the fundamental question about when and how galaxies formed and evolved. First of all, dust absorbs the stellar radiation and re-emits it in the infrared deeply changing the shape of the observed spectral energy distributions (SEDs) of obscured galaxies (Silva et al. 1998; Piovan et al. 2006; Popescu et al. 2011); second, it

strongly affects the production of molecular hydrogen and the local amount of UV radiation in galaxies thus playing a strong role in the star formation process via the cooling mechanisms (Yamasawa et al. 2011). The inclusion of dust in the models leads to a growing complexity and typically to a much larger set of parameters influencing the results of the simulations to be then compared with the observations. Indeed several questions must be addressed, each one easily expanding the model: who are the main stardust injectors in the interstellar medium (ISM) (Gail et al. 2009; Valiante et al. 2009; Gall et al. 2011a; Piovan et al. 2011a)? How much dust do they produce and on which timescales (Draine 2009; Dwek et al. 2009)? What is the contribution and the role played by the molecular clouds (MCs)-grown dust that form in the cold dense regions of the ISM (Zhukovska et al. 2008; Pipino et al. 2011)? How much dust is destroyed by SN α shocks (Nozawa et al. 2006, 2007; Bianchi & Schneider 2007; Jones & Nuth 2011)? What is the typical minimal set of dust grains whose evolution should be followed and what could be a minimal set of dust grains to be used for a satisfactory description

of the chemical or spectrophotometric properties of the galaxy?

To answer all these questions the theoretical models must include (i) a set of grains with suitable composition and properties and/or an ISM made of gas and dust in which the abundances of the elements are followed, (ii) a recipe for their formation/accretion and destruction in the ISM and (iii) a prescription for the yields of dust by the stellar sources. The duty cycle of the dust can be schematically summarized as follows (Jones 2004). Stars, mainly AGBs and SN α , inject material in the ISM, mainly in form of gas, but with a variable amount that condenses into the so-called star-dust. Once injected into the ISM, star-dust grains are subjected to destruction processes that reconstitute the material to the gaseous phase. However in cold and dense regions dust can accrete on the so-called seeds: the competition between the accretion and destruction processes, mainly via shocks, determines the total budget of dust in the ISM and the observed depletion of the elements that are involved in the formation of dust grains (Dwek 1998). Dust accretion mainly occurs in the very cold molecular clouds (MCs), where it induces strong cooling thus leading to the formation of new stars. The stellar winds from AGB stars and SN α explosions more and more enrich the ISM with new metals and star-dust grains that are able to survive to the local shocks caused by SN α explosions.

The Milky Way (MW) is the ideal laboratory to our disposal to study the dust cycle (Zhukovska et al. 2008) and its impact on the wider subject of galaxy formation. For obvious reasons, the MW provides plenty of observational data to which we can compare theoretical predictions, thus setting useful constraints on theoretical simulations and highlighting the role of the most important physical quantities leading the whole problem. Once this important step is accomplished, our modelling of the role played by dust can be extended to other galaxies such as local disk and spheroidal galaxies, high- z galaxies and QSOs.

Starting from these considerations, in this paper we simulate the formation, evolution and composition of dust in the MW, both locally in the Solar Neighbourhood (SoNe) and radially along the Galactic Disk. We build up a detailed chemical model (the theoretical simulation is still the main tool to investigate the formation and evolution of dust in galaxies) starting from the pioneering study by Dwek (1998) and taking into account the more recent ones by Zhukovska et al. (2008), Calura et al. (2008), Valiante et al. (2009), Gall et al. (2011a), Gall et al. (2011b), Mattsson (2011), Valiante et al. (2011), Kemper et al. (2011) and Dwek & Cherchneff (2011). The theoretical model we are building up stems from the basic one with infall by Chiosi (1980), however updated to the more recent version with radial flows of matter and presence of a central bar developed by Portinari & Chiosi (2000). The stellar yields of chemical elements in form of gas are those calculated by Portinari et al. (1998). The model follows the evolution of the abundances of a number of elements composing the ISM gas, includes the formation/destruction and evolution of dust and, finally, follows in detail also the abundances of those elements that are embedded in the dust grains. To this aim, the model makes use of the best prescriptions available in literature concerning dust accretion, destruction and condensation in the AGB winds and SN α explosions. These prescriptions

have been already presented by Piován et al. (2011a) to whom the reader should refer and will also be discussed in some detail here.

The main test for any model of dust formation is given by the data on element depletion provided by SoNe of the MW to which we will compare our results. In a forthcoming paper (Piován et al. 2011c) we will investigate the radial dependence of chemical abundances and dust depletion across the Disk of the MW.

The plan of the paper is as follows. In Sect. 2 we introduce the formalism and basic equations governing the temporal evolution of the gas, stars, and dust in an open model with radial flows of gas and dust for the galactic Disk of the MW. In Sect. 3 we summarize the current prescriptions for the star formation rate and initial mass function. In Sect. 4 we introduce and describe in some detail the various processes responsible for the formation and growth of dust grains in the ISM, whereas in Sect. 5 we present the accretion rates into dust grains for a number of important elements we have considered. The yields of dust from AGB stars and SN α explosions are adopted according to Piován et al. (2011a) to whom the reader should refer for all the details. In Sect. 6 the problem of dust destruction by SN α shocks is faced. Then, in Sect. 7 we present the observational data for the elemental abundances in the Solar Neighborhood and define the reference set of abundances we have adopted. In Sect. 8 after summarizing the main ones between the many available parameters, we discuss and compare the effect of them on the formation and evolution of dust, at varying them between the many possible choices. In particular we examine the influence on dust of a different CO fraction in the ISM (Sect. 8.1), the effect of the IMF (Sect. 8.2) and of the SF law (Sect. 8.3), the choice between different models for the accretion of dust in cold regions (Sect. 8.4) and, finally we discuss some interesting parameters however not discussed in our model. In Sect. 9 we present the results for our models of the Solar Vicinity in presence of dust and as a function of three important ingredients, namely, the initial mass function, the efficiency of star formation, the accretion time scale of primordial gas onto the system mimicking the evolution of the MW Disk. The effect of radial flows and central bar are always included according to the prescription developed in previous studies (Portinari & Chiosi 2000) and also adopted in Piován et al. (2011c). The simulations are compared with the depletion of the elements in the SoNe under the constraints that we want that the local chemical properties are satisfied, such as the time evolution of the elemental abundances, the metallicity and iron enrichment. In Sect. 10 we discuss the results we have obtained and draw some general conclusions.

2. Chemical Evolution Model

In classical models of chemical evolution, the Disk of the MW is subdivided in N concentric circular rings of a certain thickness Δr , where r is the galacto-centric distance, in the case of plane geometry or N concentric cylindrical shells if the third dimension is considered. Each ring or shell is identified by the mid radius r_k with $k = 1, \dots, N$. In most cases, radial flows of interstellar gas and dust are neglected, so that each ring / shell evolves independently from the others. The physical quantity used to describe the Disk is the surface mass density as a function of the radial

coordinate r and time t : $\sigma(r_k, t)$ is the mass surface density at radius r_k and time t . Depending on the model, σ can refer to the ISM ($\sigma^{\mathcal{M}}$), in turn split into dust or gas (σ^D or σ^G respectively), to the stars (σ^*) or to the total mass (simply σ). At every radius r_k , the surface mass density is supposed to slowly grow by infall of either primordial or already enriched gas and to fetch at the present age t_G the mass density profile across the Galactic Disk for which an exponential profile is best suited to represent the surface mass density distribution: $\sigma(r_k, t_G) \propto \exp(-r_k/r_d)$, where r_d is the scale radius of the Galactic Disk, that is typically estimated of the order of 4 – 5 kpc. Since the final density profile is *a priori* known, one may normalize to it the current total surface mass density of the ISM " \mathcal{M} " (sum of gas and dust),

$$\mathcal{M}(r_k, t) = \frac{\sigma^{\mathcal{M}}(r_k, t)}{\sigma(r_k, t_G)}. \quad (1)$$

Introducing the fractionary mass of the generic i -th element we have:

$$\mathcal{M}_i(r_k, t) = \frac{\sigma_i^{\mathcal{M}}(r_k, t)}{\sigma(r_k, t_G)} = \chi_i(r_k, t) \mathcal{M}(r_k, t) \quad (2)$$

and therefore the fractional mass abundance $\chi_i(r_k, t) = \mathcal{M}_i(r_k, t)/\mathcal{M}(r_k, t)$, with $\sum_i \chi_i(r_k, t) = 1$.

Similar expressions can be derived for the dust (indicated by " D ") and the gas (indicated by " G ")

$$D(r_k, t) = \frac{\sigma^D(r_k, t)}{\sigma(r_k, t_G)} \quad (3)$$

$$G(r_k, t) = \frac{\sigma^G(r_k, t)}{\sigma(r_k, t_G)} \quad (4)$$

with $\sigma^{\mathcal{M}}(r_k, t) = \sigma^G(r_k, t) + \sigma^D(r_k, t)$ and $\sigma(r_k, t) = \sigma^{\mathcal{M}}(r_k, t) + \sigma^*(r_k, t)$, where $\sigma^*(r_k, t)$ is the surface mass density of stars. For single chemical elements we may write:

$$D_i(r_k, t) = \frac{\chi_i^D(r_k, t) \sigma^D(r_k, t)}{\sigma(r_k, t_G)} = \chi_i^D(r_k, t) D(r_k, t) \quad (5)$$

$$G_i(r_k, t) = \frac{\chi_i^G(r_k, t) \sigma^G(r_k, t)}{\sigma(r_k, t_G)} = \chi_i^G(r_k, t) G(r_k, t) \quad (6)$$

with $\sum_i [\chi_i^D(r_k, t) + \chi_i^G(r_k, t)] = 1$, from which it follows that $\sum_i \chi_i^D(r_k, t) \neq 1$ and $\sum_i \chi_i^G(r_k, t) \neq 1$.

The fundamental equation describing the evolution of the ISM in absence of radial flows of matter between contiguous shells (Portinari & Chiosi 2000) and processes of dust accretion/destruction (Dwek 1998) is:

$$\begin{aligned} \frac{d}{dt} \mathcal{M}_i(r_k, t) &= -\chi_i(r_k, t) \psi(r_k, t) \\ &+ \int_{M_l}^{M_u} \psi(r_k, t - \tau_M) R_i(M) \phi(M) dM \\ &+ \left[\frac{d}{dt} \mathcal{M}_i(r_k, t) \right]_{inf} \end{aligned} \quad (7)$$

where $\phi(M)$ is the IMF and M_l and M_u are the lower and upper limits for the stellar masses, $\psi(r_k, t - \tau_M)$ is the star formation rate (SFR) at the radius r_k and at the time $t' = t - \tau_M$, $R_i(M) = E_{iM}/M$ (Portinari et al. 1998) is the fraction of a star of initial mass M ejected back in form of the chemical species i -th. The three terms at the r.h.s.

represent the depletion of the ISM due to star formation, its increase by stellar ejecta, and the increase by infall of external gas (either primordial or already enriched).

Adding supernovae and radial flows. Type Ia supernovae originate in binary systems and have a fundamental role, in particular concerning the iron enrichment. The supernovae rate and the adopted formalism are the ones of Greggio & Renzini (1983) and the formulation of equation describing chemical evolution of the ISM is modified following Matteucci & Greggio (1986). The contribution of single stars, corresponding to a fraction $(1 - A)$ of the total, is separated from the contribution of binary system, a fraction A of the total. Inserting the contribution of type Ia supernovae and integrating in time, instead that in mass, the equation for the evolution of the i -th component of the ISM is,

$$\begin{aligned} \frac{d}{dt} \mathcal{M}_i(r_k, t) &= -\chi_i \psi + \\ &+ \int_0^{t-\tau_{MB,l}} \psi \left[\phi(M) R_i \cdot \left(-\frac{dM}{d\tau_M} \right) \right]_{M(\tau)} dt' + \\ &+ (1 - A) \int_{t-\tau_{MB,l}}^{t-\tau_{MB,u}} \psi \left[\phi R_i \cdot \left(-\frac{dM}{d\tau_M} \right) \right]_{M(\tau)} dt' + \\ &+ \int_{t-\tau_{MB,u}}^{t-\tau_{Mu}} \psi \left[\phi R_i \cdot \left(-\frac{dM}{d\tau_M} \right) \right]_{M(\tau)} dt' + \\ &+ A \int_{t-\tau_{M_1,min}}^{t-\tau_{M_1,max}} \psi \left[f(M_1) R_{i,1} \cdot \left(-\frac{dM_1}{d\tau_{M_1}} \right) \right]_{M_1(\tau)} dt' + \\ &+ R_{SNI} \cdot E_{SNI,i} + \\ &+ \left[\frac{d}{dt} \mathcal{M}_i(r_k, t) \right]_{inf} - \left[\frac{d}{dt} \mathcal{M}_i(r_k, t) \right]_{out} \\ &+ \left[\frac{d}{dt} \mathcal{M}_i(r_k, t) \right]_{rf} \end{aligned} \quad (8)$$

where $\psi = \psi(r_k, t')$, $\phi = \phi(M)$, $\chi = \chi_i(r_k, t)$, $R_i = R_i(M)$, $R_{i,1} = R_i(M_1)$ and $M(t - t') = M(\tau)$. The first term at the r.h.s. is as usual the one describing the depletion of interstellar material because of the process of star formation and it depends from the star formation rate and from the abundance of the i -th element considered. The next three terms represent the contribution of single stars to the enrichment of the i -th element. The fifth term is the contribution of the primary star in a binary system (assumed to be independent from the secondary star as far as it concerns the chemical yields). The sixth term is the contribution of type Ia supernovae. Finally, the last three terms are the infall rate of external gas, the outflow rate of matter due for example to the onset of galactic winds powered by supernovae explosions, and the radial flows of gas that determine the ISM exchange between contiguous shells (Portinari & Chiosi 2000), respectively. Furthermore, $f(M_1)$ is the distribution function of the mass of the primary star M_1 in a binary system, between $M_{1,min} = M_{B,l}/2$ and $M_{1,max} = M_{B,u}$, where $M_{B,l}$ and $M_{B,u}$ are the lower and upper limit of the binary systems assumed respectively $3M_\odot$ and $12M_\odot$. R_{SNI} is the rate of type Ia SNæ and $E_{SNI,i}$ their ejecta of the i -th chemical species. $M(\tau) = M(t - t')$ is the mass of a star of lifetime τ , born at t' . It is worth noticing that various quantities depend on the metallicity $Z(t)$ as well as on M : $M(\tau) = M(t - t') = M(t - t', Z(t - t'))$ and $R_i(M) = R_i(M, Z(t - t'))$ as stellar lifetimes and ejecta

depend on metallicity. $R_i(M)$ are calculated on the base of the detailed stellar yields from Portinari et al. (1998) and keep track of finite stellar lifetimes (no instantaneous recycling approximation). Eqns. (8) govern the evolution of the ISM.

Separating gas from dust. For our purposes we need to formulate the equations governing the evolution of the dust in the ISM. Separating the ISM in gas and dust, the equations governing the evolution of the generic elemental species i -th in the dust are

$$\begin{aligned}
 \frac{d}{dt}D_i(r_k, t) = & -\chi_i^D \psi + \\
 & + \int_0^{t-\tau_{MB,l}} \psi \left[\phi \delta_{c,i}^w R_i \cdot \left(-\frac{dM}{d\tau_M} \right) \right]_{M(\tau)} dt' + \\
 & + (1-A) \int_{t-\tau_{MSN\ae}}^{t-\tau_{MB,l}} \psi \left[\phi \delta_{c,i}^w R_i \cdot \left(-\frac{dM}{d\tau_M} \right) \right]_{M(\tau)} dt' + \\
 & + (1-A) \int_{t-\tau_{MSN\ae}}^{t-\tau_{MB,u}} \psi \left[\phi \delta_{c,i}^{II} R_i \cdot \left(-\frac{dM}{d\tau_M} \right) \right]_{M(\tau)} dt' + \\
 & + \int_{t-\tau_{MB,u}}^{t-\tau_{Mu}} \psi \left[\phi \delta_{c,i}^{II} R_i \cdot \left(-\frac{dM}{d\tau_M} \right) \right]_{M(\tau)} dt' + \\
 & + A \int_{t-\tau_{MSN\ae}}^{t-\tau_{M_1, max}} \psi \left[f(M_1) \delta_{c,i}^{II} R_{i,1} \cdot \left(-\frac{dM_1}{d\tau_{M_1}} \right) \right]_{M(\tau)} dt' + \\
 & + A \int_{t-\tau_{M_1, min}}^{t-\tau_{MSN\ae}} \psi \left[f(M_1) \delta_{c,i}^w R_{i,1} \cdot \left(-\frac{dM_1}{d\tau_{M_1}} \right) \right]_{M(\tau)} dt' + \\
 & + R_{SNI} E_{SNI,i} \delta_{c,i}^I + \\
 & - \left[\frac{d}{dt} D_i(r_k, t) \right]_{out} + \left[\frac{d}{dt} D_i(r_k, t) \right]_{rf} + \\
 & + \left[\frac{d}{dt} D_i(r_k, t) \right]_{accr} - \left[\frac{d}{dt} D_i(r_k, t) \right]_{SN} \quad (9)
 \end{aligned}$$

where $\chi_i^D = \chi_i^D(r_k, t)$. The first term at the r.h.s. of Eqn. (9) is the depletion of dust because of star formation that consumes both gas and dust (uniformly mixed in the ISM). The second term is the contribution by stellar winds from low mass stars to the enrichment of the i -th component of the dust. Following Dwek (1998), we introduce the so-called condensation coefficients $\delta_{c,i}^w$ that determines the fraction of material in stellar winds that goes into dust with respect to that in gas (local condensation). The third term is the contribution by stars not belonging to binary systems and not going into type II SN \ae (the same coefficients $\delta_{c,i}^w$ are used). The fourth term is the contribution by stars not belonging to binary systems, but going into type II SN \ae . For the condensation efficiency in the ejecta of type II SN \ae we introduce the coefficients $\delta_{c,i}^{II}$, the analog of $\delta_{c,i}^w$. The possible choices for these coefficients are discussed in detail in Pivon et al. (2011a). The fifth term is the contribution of massive stars going into type II SN \ae . The sixth and seventh term represent the contribution by the primary star of a binary system, distinguishing between those becoming type II SN \ae from those failing this stage and using in each situation the correct coefficients. The eighth term is the contribution of type Ia SN \ae , where again we introduced the condensation coefficients $\delta_{c,i}^I$ to describe the mass fraction of the ejecta going into dust. The last four terms describe: (1) the outflow of dust due to galactic winds (in the case of disk galaxies this term can be set to zero); (2) the radial flows of matter between contiguous shells; (3) the accretion

term describing the accretion of grain onto bigger particles in cold clouds; (4) the destruction term taking into account the effect of the shocks of SN \ae on grains, obviously giving a negative contribution. The infall term in the case of dust can be neglected because we can safely assume that the material entering the galaxy is made by gas only without a solid dust component mixed to it.

Finally, from the equation for $D_i(r_k, t)$ we can get the equation describing the evolution of the gaseous component $G_i(r_k, t)$, where $G_i(r_k, t) = \mathcal{M}_i(r_k, t) - D_i(r_k, t)$:

$$\begin{aligned}
 \frac{d}{dt}G_i(r_k, t) = & -\chi_{G,i} \psi + \\
 & + (1-A) \int_{t-\tau_{MB,l}}^{t-\tau_{MSN\ae}} \psi \left[\phi (1 - \delta_{c,i}^w) R_i \cdot \left(-\frac{dM}{d\tau_M} \right) \right]_{M(\tau)} dt' + \\
 & + (1-A) \int_{t-\tau_{MSN\ae}}^{t-\tau_{MB,u}} \psi \left[\phi (1 - \delta_{c,i}^{II}) R_i \cdot \left(-\frac{dM}{d\tau_M} \right) \right]_{M(\tau)} dt' + \\
 & + \int_0^{t-\tau_{MB,l}} \psi \left[\phi (1 - \delta_{c,i}^w) R_i \cdot \left(-\frac{dM}{d\tau_M} \right) \right]_{M(\tau)} dt' + \\
 & + \int_{t-\tau_{MB,u}}^{t-\tau_{Mu}} \psi \left[\phi (M) (1 - \delta_{c,i}^{II}) R_i \cdot \left(-\frac{dM}{d\tau_M} \right) \right]_{M(\tau)} dt' + \\
 & + A \int_{t-\tau_{MSN\ae}}^{t-\tau_{M_1, max}} \psi \left[f(M_1) (1 - \delta_{c,i}^{II}) R_{i,1} \cdot \left(-\frac{dM_1}{d\tau_{M_1}} \right) \right]_{M(\tau)} dt' + \\
 & + A \int_{t-\tau_{M_1, min}}^{t-\tau_{MSN\ae}} \psi \left[f(M_1) (1 - \delta_{c,i}^w) R_{i,1} \cdot \left(-\frac{dM_1}{d\tau_{M_1}} \right) \right]_{M(\tau)} dt' + \\
 & + R_{SNI} E_{SNI,i} (1 - \delta_{c,i}^I) + \left[\frac{d}{dt} G_i(r_k, t) \right]_{inf} + \\
 & - \left[\frac{d}{dt} G_i(r_k, t) \right]_{out} + \left[\frac{d}{dt} G_i(r_k, t) \right]_{rf} + \\
 & - \left[\frac{d}{dt} D_i(r_k, t) \right]_{accr} + \left[\frac{d}{dt} D_i(r_k, t) \right]_{SN} \quad (10)
 \end{aligned}$$

where again the outflow term $-\left[\frac{d}{dt} G_i(r_k, t) \right]_{out}$ will be fixed to zero because we do not have galactic wind for spirals with continuous star formation. Since the primordial material is likely dust-free we have $\left[\frac{d}{dt} \mathcal{M}_i(r, t) \right]_{in} = \left[\frac{d}{dt} G_i(r, t) \right]_{in}$.

It is worth noticing the following point: the stellar models, upon which are based our yields, predict that stars with mass higher than $6M_\odot$ go into SN \ae , whereas those with mass lower than $6M_\odot$ first become AGB stars and later White Dwarfs. We must therefore split the third and the fifth member of Eqn. (8) in two parts, both in Eqns. (10) and (9), because the minimum mass dividing the intervals of AGB and/or SN \ae belongs to the mass interval ($3 - 12M_\odot$) describing binary systems going into type Ia SN \ae ¹.

¹ For example in Eqn. (9), using $\delta_{c,i}$ to indicate the generic condensation coefficient we have the following split:

$$(1-A) \int_{t-\tau_{MB,l}}^{t-\tau_{MB,u}} \psi \left[\phi \delta_{c,i} R_i(M) \left(-\frac{dM}{d\tau_M} \right) \right]_{M(\tau)} dt'$$

is divided into:

$$\begin{aligned}
 & (1-A) \int_{t-\tau_{MB,l}}^{t-\tau_{MSN\ae}} \psi \left[\phi \delta_{c,i}^w R_i \left(-\frac{dM}{d\tau_M} \right) \right]_{M(\tau)} dt' \\
 & + (1-A) \int_{t-\tau_{MSN\ae}}^{t-\tau_{MB,u}} \psi \left[\phi \delta_{c,i}^{II} R_i \left(-\frac{dM}{d\tau_M} \right) \right]_{M(\tau)} dt'
 \end{aligned}$$

To summarize. Indicating the contribution to the yields by stellar winds and type Ia and II SNæ with the symbols $W_{i,D}(r_k, t)$, $W_{i,G}(r_k, t)$ and $W_{i,\mathcal{M}}(r_k, t)$ (they can easily be reconstructed by comparison) and neglecting the outflow term, Eqns. (8), (9) and (10) become:

$$\begin{aligned} \frac{d}{dt} \mathcal{M}_i(r_k, t) &= -\chi_i^{\mathcal{M}}(r_k, t) \psi(r_k, t) + W_{i,\mathcal{M}}(r_k, t) \\ &+ \left[\frac{d}{dt} \mathcal{M}_i(r_k, t) \right]_{rf} \end{aligned} \quad (11)$$

$$\begin{aligned} \frac{d}{dt} D_i(r_k, t) &= -\chi_i^D(r_k, t) \psi(r_k, t) + W_{i,G}(r_k, t) \\ &+ \left[\frac{d}{dt} D_i(r_k, t) \right]_{accr} - \left[\frac{d}{dt} D_i(r_k, t) \right]_{SN} \\ &+ \left[\frac{d}{dt} D_i(r_k, t) \right]_{rf} \end{aligned} \quad (12)$$

$$\begin{aligned} \frac{d}{dt} G_i(r_k, t) &= -\chi_{G,i}(r_k, t) \psi(r_k, t) + W_{i,G}(r_k, t) \\ &- \left[\frac{d}{dt} D_i(r_k, t) \right]_{accr} + \left[\frac{d}{dt} D_i(r_k, t) \right]_{SN} \\ &+ \left[\frac{d}{dt} G_i(r_k, t) \right]_{inff} + \left[\frac{d}{dt} G_i(r_k, t) \right]_{rf}. \end{aligned} \quad (13)$$

It is soon evident that the dust creation/destruction and the radial flows make the system of differential equations more complicated than the original one by Talbot & Arnett (1975) for a one-zone closed-box model. As the ISM is given by the sum of gas and dust, only two of these equations are required, furthermore Eqn. (11) can be used only if gas and dust flow with the same velocity. To proceed further we must now specify the law of star formation, the IMF, the stellar ejecta and the various rates describing gas infall, dust accretion/destruction, and radial flows/bar effect. No details will be given about these ones. They are included into the model and they are mainly useful in order to reproduce the radial gradients of abundance in the MW. The reader should refer to Portinari & Chiosi (2000) and Piovan et al. (2011c).

where $M_{SNæ}$ is the separation mass that tell us if we must use the condensation coefficients of stellar winds (condensation of dust in the envelopes of AGB stars) in the mass interval between $M_{B,l}$ and $M_{SNæ}$ or the condensation coefficients of supernovæ between $M_{SNæ}$ e $M_{B,u}$. In the same way:

$$A \int_{t-\tau_{M_1, min}}^{t-\tau_{M_1, max}} \psi \left[f(M_1) \delta_{c,i} R_{i,1} \left(-\frac{dM_1}{d\tau_{M_1}} \right) \right]_{M_1(\tau)} dt'$$

splits itself into:

$$\begin{aligned} &A \int_{t-\tau_{M_{SNæ}}}^{t-\tau_{M_1, max}} \psi \left[f(M_1) \delta_{c,i}^I R_{i,1} \left(-\frac{dM_1}{d\tau_{M_1}} \right) \right]_{M(\tau)} dt' \\ &+ A \int_{t-\tau_{M_1, min}}^{t-\tau_{M_{SNæ}}} \psi \left[f(M_1) \delta_{c,i}^w R_{i,1} \left(-\frac{dM_1}{d\tau_{M_1}} \right) \right]_{M(\tau)} dt'. \end{aligned}$$

3. The Star Formation Laws and Initial Mass Functions

Star Formation. The law of Star Formation (SF) is a key ingredient of any model of galaxy formation and evolution. Unfortunately it is poorly known, so that many prescriptions for the SF rate can be found in literature. In this study we have considered several well known SF laws adopted for the MW (see Portinari & Chiosi 1999, for details).

A very popular prescription is the Schmidt (1959) law. In our formalism it becomes:

$$\Psi(r_k, t) = - \left[\frac{dG(r_k, t)}{dt} \right]_* = \nu \left[\frac{\sigma(r_k, t_G)}{\sigma(r_\odot, t_G)} \right]^{\kappa-1} G^\kappa(r_k, t) \quad (14)$$

where the normalization factor is $\sigma(r_\odot, t_G)^{-(\kappa-1)}$ and ν is in $[t^{-1}]$. Following Portinari & Chiosi (1999) we adopt $\kappa = 1.5$.

This simple dependence of the SFR can be complicated by including other physical effects. For instance, the SF suited to spiral galaxies such as the MW, may include the effect of gas compression by density waves (Roberts 1969; Shu et al. 1972; Wyse & Silk 1989; Prantzos & Silk 1998) or gravitational instabilities (Wang & Silk 1994). We have:

$$\Psi(r_k, t) = \nu \left[\frac{r}{r_\odot} \right]^{-1} \left[\frac{\sigma(r_k, t_G)}{\sigma(r_\odot, t_G)} \right]^{\kappa-1} G^\kappa(r_k, t) \quad (15)$$

where ν is always in $[t^{-1}]$ and $k = 1$ (Kennicutt 1998; Portinari & Chiosi 1999).

Another possibility is to describe the SF as a balance between cooling and heating processes, that is the gravitational settling of the gas onto the Disk and the energy injection from massive stars (Talbot & Arnett 1975; Dopita 1985; Dopita & Ryder 1994). In our formalism, we have

$$\Psi(r_k, t) = \nu \left[\frac{\sigma^n(r_k, t) \sigma^{m-1}(r_k, t_G)}{\sigma(r_\odot, t_G)^{n+m-1}} \right] G^m(r_k, t) \quad (16)$$

where $n = 1/3$, $m = 5/3$ (Portinari & Chiosi 1999) and ν in $[t^{-1}]$. This formulation is similar to the original one by Talbot & Arnett (1975) thus leading to similar results (Portinari et al. 1998).

Initial Mass Function. The initial mass function (IMF) is perhaps the most important ingredient of chemical models of any kind (see Kroupa 2002b, for a recent review of the subject). Brown dwarfs and very low mass stars whose lifetimes are longer than the age of the Universe, in practice lock up forever the chemical elements present in the ISM at the age of their birth, whereas intermediate and high mass stars of short life continuously enrich the environment with the products of thermonuclear reactions, thus driving the chemical evolution of the host system. They are also the factories of star-dust to be injected into the ISM by SNæ explosions and strong stellar winds. The adoption of an IMF has two effects worth being mentioned here. First of all, a different slope of the IMF in the intermediate-high mass range would imply a different relative population of the stars contributing to the dust yields. Second, the net yield of metals and dust per stellar generation varies. According to its definition (see for instance Tinsley 1980; Pagel 1997; Portinari et al. 2004a) the net yield is the the amount of metals globally produced by a stellar generation over the

the fraction of mass locked up in living stars and remnants. Therefore, efficiency of metal and dust enrichment depends not just on the amount of metals produced per unit mass involved in star formation but on the ratio between this and the mass that remains locked in remnants or ever-lived low mass stars. The locked-up fraction, is therefore as crucial to the metal and dust enrichment as is the absolute number of the high-mass stars directly responsible for the production of dust itself. In a given model of fixed total mass, it is clear that an IMF bending down steeply at low masses will lead to a different locked up fraction with respect to a power-law, low-mass oriented IMF. The metal and dust production is accordingly affected.

In this section we shortly present the IMFs we have included in our model of the Galactic Disk and SoNe. For the purposes of our study the IMF is assumed to be constant in time and space. All the IMFs are normalized assuming that the total mass encompassed by the IMF from the lower, M_L , to the upper, M_U , mass limit of stars is equal to $1 M_\odot$. To this aim, following Talbot & Arnett (1975) and Bressan et al. (1994), we define the parameter ζ , which describes the fraction of total mass in form of stars stored in the IMF above a given mass M_\star . In other words, M_\star is the minimum mass contributing to the nucleo-synthetic enrichment of the ISM over a timescale of the order of the galaxy life

$$\zeta = \frac{\int_{M_\star}^{M_U} \phi(M) dM}{\int_{M_L}^{M_U} \phi(M) dM}. \quad (17)$$

This equation, at varying ζ and for fixed M_U and M_\star , can be reversed numerically to determine the lower limit of the distribution M_L . The IMFs included in our model are:

- **The Salpeter IMF.** Salpeter-like IMFs are very popular. These are an extension over the desired mass range of the original Salpeter IMF (Salpeter 1955). This IMF is $\phi(M) = C_S M^{-1.35}$ with C_S depending on the value of ζ . For a mass range $[0.1 - 100] M_\odot$ (Portinari et al. 2004a) we have $C_S = 0.1716$ and a $\zeta = 0.3925$.

- **The Kroupa IMF.** In a series of papers Kroupa revised and updated the power-law IMF with a set of continuous multi-slope power-laws (Kroupa et al. 1993; Kroupa 2001, 2002b,a, 2007, e.g.). In the following we consider two cases. First, the IMF derived by Kroupa (1998) for field stars in the SoNe and used by Portinari et al. (2004b). This IMF is typical of models of chemical evolution of disk galaxies (Boissier & Prantzos 1999, 2000; Prantzos & Boissier 2000; Hou et al. 2008)². For $M_L = 0.1 M_\odot$ and $M_U = 100 M_\odot$, we obtain $\zeta = 0.405$. Second, the Kroupa (2007) IMF, where taking $M_L = 0.01 M_\odot$ and $M_U = 100 M_\odot$ we get $\zeta = 0.38$, slightly lower than in the above Kroupa (1998) because of the lower limit extended to brown dwarf regime.

- **The Larson IMF.** Larson (1998) proposed an IMF in which the relative percentage of very low mass stars and sub-stellar objects is decreased due to the presence of an exponential cut-off. As a consequence of this there is a negligible contribution to the locked-up mass, and in contrast

a very high net yield per stellar generation, and a high production of metals and dust. The Larson (1986) IMF is

$$\phi(M) = C_L M^{-1.35} \exp\left(-\frac{M_L}{M}\right). \quad (18)$$

In practice this IMF recovers the Salpeter IMF at high masses, whereas at low masses the exponential cut-off determines the steep downfall after the peak mass $M_P = M_L/1.35 = 0.25 M_\odot$. For a typical mass range $[0.01 - 100] M_\odot$ we have $\zeta = 0.653$ thus allowing for a high number of intermediate-high mass stars. For the present aims, we will simply keep M_L constant with time or metallicity. We also consider the possibility for a modified Larson IMF adapted to the SoNe, in which the slope in the power-law factor for the high mass range has the value $M^{-1.7}$, according to Scalo (1986) and in agreement with recent IMFs proposed by Kroupa (see above). In this last case with the same mass range $[0.01 - 100]$, we have $\zeta = 0.5$, lower than the other case.

- **The Chabrier IMF.** Along the line of thought of Larson (1998), Chabrier (2001) proposes:

$$\phi(M) = C_C M^{-2.3} \exp\left[\left(-\frac{M_C}{M}\right)^{1/4}\right]. \quad (19)$$

The two parameters in equation (19) are tuned on local field low mass stars and the functional form is proved to be valid down to the brown dwarfs regime (Chabrier 2002). With a mass range $[0.01 - 100] M_\odot$ and $M_C = 716.4$ we get $C_C = 40.33$ and $\zeta = 0.545$, not as high as in the Larson IMF, but still leading to high net yield and low locked up mass fraction.

- **The Kennicutt IMF.** The Kennicutt (1983) IMF is used in literature to describe the global properties of spiral galaxies and it is inspired by the observations of $H\alpha$ luminosities and equivalent width in external galaxies (Kennicutt et al. 1994; Portinari et al. 2004b; Sommer-Larsen 1996). With a mass range $[0.1 - 100] M_\odot$, we get $\zeta = 0.59$.

- **The Arimoto IMF.** This top-heavy IMF has been suggested by Arimoto & Yoshii (1987) to simulate elliptical galaxies and is introduced just for the sake of comparison as an extreme case: $\phi(M) = C_{Ari} M^{-1.0}$. With a mass range $[0.1 - 100] M_\odot$, we get $\zeta = 0.5$.

4. Growth dust grains in the ISM

Dust grains form by a number of physical processes (see below) and once in the ISM they may grow in mass by accreting a number of atoms or molecules. In the following we examine in some detail the accretion mechanisms for which two different models are proposed.

4.1. The Dwek (1998) model or case A

Dwek (1998) view of grain growth can be summarized as follows. Let us consider an ISM whose dust component is formed by grains made of a single element i -th with mass $m_{gr,i}$. Let m_i be the mass of an atom (or molecule) of the element i -th in the gaseous phase. N_i is the number of atoms (molecules) of the element i -th locked up into the mono-composition grains that we are considering and $n_{gr,i}$ the density of grains of i -th type in the ISM, considered in this

² Along this line it worth recalling that IMF with slope $(1.6 \sim 1.7)$ in the high mass range, i.e. steeper than the Salpeter value, is from Scalo (1986) and it is widely used in literature in chemical models of the MW even with dust (Matteucci & François 1989; Chiappini et al. 1997; Dwek 1998; Romano et al. 2000; François et al. 2004; Calura et al. 2008)

model as a *single phase*, without distinction between diffuse ISM and cold molecular clouds. Let now α_i be the sticking coefficient, telling us the probability that an atom (molecule) of the element i in the gaseous phase binds to the grains increasing the number of atoms/molecules on it. Finally $n_{gas,i}$ is the number density the gas made of atoms

(molecules) of type i -th and $\bar{v} = \left(\frac{8K_B T}{\pi m_i}\right)^{\frac{1}{2}}$ is the mean thermal velocity of the particles of the element i in the gaseous phase with respect to the dust grains. We get:

$$\frac{dN_i}{dt} = \alpha_i \pi a^2 n_{gr,i} n_{gas,i} \bar{v}. \quad (20)$$

Multiplying both members of the equation by the constant mass m_i , multiplying and dividing the second member by the mass of one grain $m_{gr,i}$, introducing the mean thermal velocity \bar{v} and using the following relation³ (Dwek 1998):

$$m_i n_{gas,i} = 2m_H n_{H_2} \left(1 - \frac{\sigma_i^D}{\sigma_i^M}\right) \quad (21)$$

where $\sigma_i^D(r, t)$ and $\sigma_i^M(r, t)$ are functions of position and time, we obtain:

$$\frac{d\sigma_i^D}{dt} = \frac{\sigma_i^D}{\tau_{i,0}} \left(1 - \frac{\sigma_i^D}{\sigma_i^M}\right). \quad (22)$$

For the dimensional consistency of the equation, the multiplying quantity has the dimension of the inverse of a time indicated by $\tau_{i,0}$

$$\frac{1}{\tau_{i,0}} = 2n_{H_2} \alpha_i \frac{\pi a^2}{A_i} \left(\frac{8K_B T}{\pi m_i}\right)^{\frac{1}{2}}. \quad (23)$$

It may be worth of interest to give an estimate of the involved timescale: by means of typical values of the involved quantities, Dwek (1998) obtains $\sim 3 \times 10^4$ yrs. It is possible now to define the accretion time scale of our i -th element onto the grains as:

$$\frac{1}{\tau_{i,accr}} = \frac{1}{\tau_{0,i}} \cdot \left(1 - \frac{\sigma_i^D}{\sigma_i^M}\right) \quad (24)$$

that is the inverse of $\tau_{0,i}$ multiplied by the fraction of the i -th element in the gaseous phase. Again, we drop the dependence from r and t . Dwek (1998) adopting the ratio $\sigma_i^D/\sigma_i^M \approx 0.7$ gets $\tau_{i,accr} \approx 10^5$ yrs which turns out to be significantly shorter than the lifetime of molecular clouds where accretion takes place. This lifetime is estimated to be of the order of $t_{MC} \sim 2 - 3 \times 10^6 - 10^7$ yrs. The lifetime of a molecular cloud is comparable to the lifetime of the most massive stars born in it. These stars indeed injecting great amounts of energy by stellar winds and SNæ explosions eventually disrupt the cloud. Similar estimates have been made in studies on the temporal evolution of dust in the ISM by Calura et al. (2008), $\sim 5 \cdot 10^7$ yrs, and Zhukovska et al. (2008), $\sim 10^7$ yrs, and are consistent with observational and theoretical estimates of the lifetimes of molecular clouds (Matzner 2002; Krumholz et al. 2006; Blitz et al. 2007, see e.g.). One may argue that we are comparing two different timescales, i.e. with $t_{i,accr} \ll t_{MC}$.

³ The above relation says that the mass of the element i -th in the gaseous phase can be expressed by means of the density of the molecular clouds, i.e. the site in which the grains grow. $2m_H n_{H_2}$ is the mass of the molecular cloud, $\left(1 - \sigma_i^D/\sigma_i^M\right)$ is the fraction of the element i -th in the gaseous phase as a function of the abundance of the same element in the dust and ISM.

However, inside molecular clouds there are many physical processes continuously stripping atoms and molecules from the grains, like UV radiation and cosmic rays. The net effect of it could be that $\tau_{i,accr}$ is considerably lengthened (Dwek 1998), likely up to $6 \cdot 10^7$ yrs, so that $t_{i,accr} \simeq t_{MC}$. Furthermore, all the dust grains are in cold molecular clouds where the growing occurs. The simplest way to take this into account is to divide the above estimate for $t_{i,accr}$ by the fraction of dust in molecular clouds. The resulting accretion timescale would be $t_{i,accr} \sim 1 - 2 \times 10^8$ yrs.

There is another important point to consider on which indeed several studies of the ISM evolution are based: both the destruction timescale (driven by SNæ explosions) and the accretion timescale $t_{i,accr}$ have the same dependence on the star formation rate ψ and surface mass density σ_i . SNæ rate can be expressed as $\tau_{i,snr} \propto \sigma/\psi$. The lower the star formation rate, the lower is the number of supernovae explosions and finally the longer the destruction time of grains due to shocks. We clearly expect $\tau_{i,accr}$ to vary over the evolutionary history of the Galaxy: Dwek (1998) divides the accretion timescale by σ^{MC}/σ and reasonably assumes that $\psi \propto \sigma^{MC}$. In this way, $\tau_{i,accr} \propto \sigma\psi$. Since both $\tau_{i,accr}$ and $\tau_{i,snr}$ have the same dependence from σ^{ISM}/ψ Dwek (1998) suggests that the ratio between the two timescales is constant: $\tau_{i,accr}/\tau_{i,snr} = 1/2$. If now we consider the accretion/destruction terms in eqn. (12) we have:

$$\begin{aligned} \left(\frac{d\sigma_i^D}{dt}\right)_{accr} + \left(\frac{d\sigma_i^D}{dt}\right)_{snr} &= \frac{\sigma_i^D}{\tau_{i,accr}} - \frac{\sigma_i^D}{\tau_{i,snr}} = \\ &= 2 \cdot \frac{\sigma_i^D}{\tau_{i,snr}} - \frac{\sigma_i^D}{\tau_{i,snr}} = \frac{\sigma_i^D}{\tau_{i,snr}}. \end{aligned} \quad (25)$$

The contribution of the creation/destruction terms is greatly simplified and the numerical solution of the differential equations describing the dust evolution becomes very simple. More refined is the solution adopted by Calura et al. (2008). In brief, (i) only $\tau_{0,i}$ is fixed and $\tau_{i,accr}$ remains an explicit function of the ratio σ_i^D/σ_i^M ; (ii) no *a priori* correlation between $\tau_{i,accr}$ and $\tau_{i,snr}$ is supposed to exist, the two timescales are defined independently, and both plays a role in the σ_i^D evolution. In our model we adopt the same strategy.

4.2. The Zhukovska et al. (2008) model or case B

A step forward in modelling grain accretion has been made by Zhukovska et al. (2008). In brief, Zhukovska et al. (2008)'s picture can be summarized as follows: (i) grain accretion is tightly related to molecular clouds and a multi-phase description of the ISM would be required; (ii) the evolution of chemical elements is calculated in presence of some typical dust compounds that are representative of the grain families growing inside the cold regions of the ISM or ejected by the stars, namely silicates, carbonaceous grains, iron grains, and silicon carbide. This model has two important advantages. First, it allows for different physical situations each of which implying different timescales for each elements and different relationships between $\tau_{i,accr}$ and $\tau_{i,snr}$ which are independent; second, accretion in cold regions is described in a realistic way; third, the model can be easily incorporated in a multi-phase description of the ISM to estimate the amounts of gas in the warm and cold phases.

Let us now examine some of the key points and basic equations of the model and how they are adapted to our description, where contrary to what made in Zhukovska et al. (2008) we track the evolution *abundances of single elements in dust* instead of *ad-hoc* families of dust grains.

The growth of the generic type of grains j -th is driven by the least abundant element indicated as element i -th (otherwise called the *key element*) among those forming the grain. All the other elements concurring to form the j -th compound adapt their abundances to that of the *key element*. For a mixture of accreting grains made of silicates (pyroxenes and olivines, i.e. magnesium-iron sulfates), carbonaceous and iron grains, the key elements are Mg, Si or Fe for silicates, depending on which has the lowest abundance, C for carbon grains, and Fe for iron grains. Most of these elements accrete some specific atomic or molecular species called *growth species*. The growth in mass of a single j -th type grain is:

$$\frac{dm_j}{dt} = S_j \alpha_j v_j^{gw} A_j^D m_H \frac{\nu_{i,j}^{gw}}{\nu_{i,j}^D} n_j^{gw} \quad (26)$$

where m_j is the mass of one grain of the j -th type, S_j is the surface area, α_j is the sticking coefficient, v_j^{gw} is the relative velocity of the accreting species with respect to the grain, $A_j^D m_H$ is the mass of one atom (or molecule) that is accreting on the grain of type of type j -th, n_j^{gw} is the number density of the growth species j , and finally $\nu_{i,j}^{gw}/\nu_{i,j}^D$ is the ratio between the number of atoms of the key element i -th in the growth species for the dust grain of type j -th and the number of atoms of i -th element we need to build one grain of the j -th type.

After some substitutions and simplifications for which all the details can be found in Zhukovska et al. (2008), it comes out:

$$\frac{df_{i,j}}{dt} = \frac{1}{\tau_j^{gr}} f_{i,j} (1 - f_{i,j}) \quad (27)$$

where $f_{i,j} \propto \rho_j^D$ is the fraction of the key element i -th that is already condensed onto the dust type j -th, called degree of condensation. $1 - f_{i,j}$ is therefore the fraction of the key element i -th still in the gaseous phase and available to form growth species for the j -th dust component. An explicit formula for τ_j^{gr} as a function of all the relevant quantities (Zhukovska et al. 2008, see Eqn. 31) is:

$$\tau_j^{gr} = 46 \frac{(A_j^{gw})^{1/2} \nu_{i,j}^D}{A_j^D} \left(\frac{\rho_j^C}{3} \right) \left(\frac{10^3}{n_H} \right) \left(\frac{3.5 \cdot 10^{-5}}{\epsilon_{i,j}} \right) \text{Myr}. \quad (28)$$

Integrating eqn. (27) with the initial conditions $f_{i,j} = f_{0,i,j}$ for $t = 0$ we get the final equation describing the evolution of the condensed fraction:

$$f_{i,j}(t) = \frac{f_{0,i,j} e^{t/\tau_j^{gr}}}{1 - f_{0,i,j} + f_{0,i,j} e^{t/\tau_j^{gr}}}. \quad (29)$$

As in real conditions the grain accretion takes place in cold MCs with a finite lifetime τ_{MC} , the above accretion time scale must be compared with τ_{MC} . As already discussed for model A of accretion, the molecular lifetime constrains the real time interval during which the exchange of matter between cold clouds and surrounding medium can happen. It is the interplay between the accretion/disruption timescales to determine if and how much material can be condensed inside the cloud before it dissolves into the surrounding

ISM. If $f_{0,i,j}$ is the initial degree of condensation of the key element i -th of the grains j -th and the molecular cloud will be destroyed after a lifetime t we have that the effective amount of material that is given back to the ISM after the cloud dissolution is:

$$M_j^{MC}(t) = (f_{i,j}(t) - f_{0,i,j}) \chi_{j,max}^D M_{MC} \quad (30)$$

where $f_{i,j}(t) - f_{0,i,j}$ is the fraction of key element condensed with respect to the initial condensation fraction, $\chi_{j,max}^D$ is the maximum possible fraction of dust of the kind j -th that can be formed in the molecular cloud and that would exist if all the material is condensed in dust of type j -th. Multiplying by the mass of the cloud we get the mass of newly formed material M_j^{MC} returned to the ISM. The fraction $\chi_{j,max}^D$ is given by

$$\chi_{j,max}^D = \frac{A_j^D \epsilon_{i,j}}{(1 + 4\epsilon_{He}) \nu_{i,j}^D} \quad (31)$$

as shown in the footnote below ⁴.

Not all the MCs have the same lifetime: therefore there is a certain probability $P(t)$ that a molecular cloud is destroyed in the time interval $t - t + dt$. According to Zhukovska et al. (2008) the probability is well represented by an exponential law with time scale τ_{MC} . The instantaneous condensation fraction at the time t of the key element i -th relative to the dust compound j -th is derived from integrating over time and considering for each cloud of lifetime x , born at $t - x$ the condensation fraction holding at the time of birth $f_{0,i,j}(t - x)$. Since the lifetime distribution function quickly decays over time, only the MCs born some τ_{MC} before t will contribute in practice. The instantaneous condensation fraction is

$$f_{i,j}(t) = \frac{1}{\tau_{MC}} \int_0^t \frac{f_{0,i,j}(t-x) e^{x/\tau_j^{gr}} e^{-x/\tau_{MC}}}{1 - f_{0,i,j}(t-x)(1 - e^{x/\tau_j^{gr}})} dx. \quad (32)$$

This procedure is however time consuming when applied in practice. A much simpler approach is provided by using the average restitution mass \bar{R}_j^{MC} and the average condensation fraction $\bar{f}_{i,j}$ assuming $f_{0,i,j}$ as a constant. Using Eqn. (30) and integrating between 0 and $t = \infty$ we obtain the mean value of $f_{i,j}$:

$$\bar{f}_{i,j} = \frac{1}{\tau_{MC}} \int_0^\infty \frac{f_{0,i,j} e^{t/\tau_j^{gr}}}{1 - f_{0,i,j} + f_{0,i,j} e^{t/\tau_j^{gr}}} e^{-t/\tau_{MC}} dt. \quad (33)$$

⁴ The number density n_H of hydrogen atoms is given by $n_H = \rho_{MC} / [(1 + 4\epsilon_{He}) m_H]$ which in turn follows from the series of equalities: $\rho_{MC} = m_H n_H + 4m_H n_{He} = m_H n_H + 4m_H n_H \epsilon_{He} = m_H n_H (1 + 4\epsilon_{He})$, where $\epsilon_{He} = n_{He}/n_H$. The fraction $\chi_{j,d,max}$ is given by $\chi_{j,max}^D = \frac{\rho_{j,max}^D}{\rho_{MC}} = \frac{A_j^D m_H (\epsilon_{i,j} n_H)}{\nu_{i,j}^D \cdot m_H n_H (1 + 4\epsilon_{He})} = \frac{A_j^D \epsilon_{i,j}}{(1 + 4\epsilon_{He}) \nu_{i,j}^D}$. The explanation is quite simple: dividing the number of atoms $\epsilon_{i,j} n_H$ of the key element available in the molecular cloud by the number of atoms $\nu_{i,j}^D$ of the same key element that are tied up when we form one dust grain, we get the maximum number of dust grains that we can form per unit volume. Knowing the mass of a single dust grain, $A_j^D m_H$, the mass density $\rho_{j,max}^D$ immediately follows.

Inserting Eqn. (33) into Eqn. (30) we get $\overline{M}_{j,MC}$, that is the time averaged mass of dust of type j -th returned to the ISM. However, this is only part of the story, because the molecular clouds have also different mass, so we need to evaluate their mean mass \overline{M}_{MC} and use this instead of M_{MC} .

Fractionary mass of dust grains of j -type. With aid of Eqn. (33) we can derive the fractionary mass of dust of type j -th produced by the accretion of grains in cold clouds per unit area and unit time:

$$\left(\frac{d\sigma_i^D}{dt}\right)_{accr} = \frac{1}{\tau_{MC}} (\overline{f}_{i,j} - f_{0,i,j}) \cdot \chi_{j,max}^D \sigma_{MC}. \quad (34)$$

Looking at Eqn. (34), it requires to know the amount of molecular gas of the galaxy we are going to model. To do this, a multi-phase description of the ISM taking into account the exchange of matter between cold and warm phases would be required. This is not possible with the present model because Eqns. (8), (9), and (10) have been formulated for the single phase description and without a description of the gas exchange between cold and warm phases. To overcome this limitation some adjustment of the model are needed. Introducing $\chi_{MC} = \sigma^{MC}/\sigma^M$ as the fraction of molecular gas and with some passages (Zhukovska et al. 2008) the final equation for grain growth in MCs in the frame of a single-phase ISM.

$$\left(\frac{d\sigma_i^D}{dt}\right)_{accr} = \frac{\chi_{MC}}{(1 - \chi_{MC})\tau_{MC}} (\overline{f}_{i,j}\sigma_{j,max}^D - \sigma_j^D). \quad (35)$$

We need however to fix χ_{MC} : in Zhukovska et al. (2008) is fixed to 0.2 in agreement to the observations for the SoNe at the current time. However this approximation could not probably hold for other phases of the evolution of the SoNe or other regions of the MW. In Piovan et al. (2011c), by means of the data available for the MW disk about molecular hydrogen, neutral hydrogen, total amount of gas and star formation we suitably extended χ_{MC} by means of Artificial Neural Networks (ANNs) in such a way to have the amount of MCs as a function of the current local variables describing the system. This recipe will be adopted in this work. For more details see Piovan et al. (2011c).

Degree of condensation. Another critical parameter to be examined with accuracy is the condensation degree $\overline{f}_{i,j}$. It depends on the comparison between τ_{MC} , the average lifetime of the MC, and the typical accretion time of grains τ_j^{gr} of Eqn. (28). If $\tau_j^{gr} \gg \tau_{MC}$ then we expect that only small amounts of dust are produced because the cold clouds will be destroyed before that dust has enough time to grow. On the contrary, if $\tau_j^{gr} \ll \tau_{MC}$, we expect the condensation of dust grains to occur almost completely and consequently dust to increase. Zhukovska et al. (2008) propose an analytical expression for the condensation degree as a function of the ratio τ_j^{gr}/τ_{MC} (assuming a constant $f_{0,i,j}$):

$$\overline{f}_{i,j} = \left[\frac{1}{f_{0,i,j}^2 \left(1 + \frac{\tau_{MC}}{\tau_j^{gr}}\right)^2} + 1 \right]^{-\frac{1}{2}}. \quad (36)$$

According to Zhukovska et al. (2008), this expression is no longer valid only for very small values of $f_{0,i,j}$. The situation for our models is more complicated because we are dealing

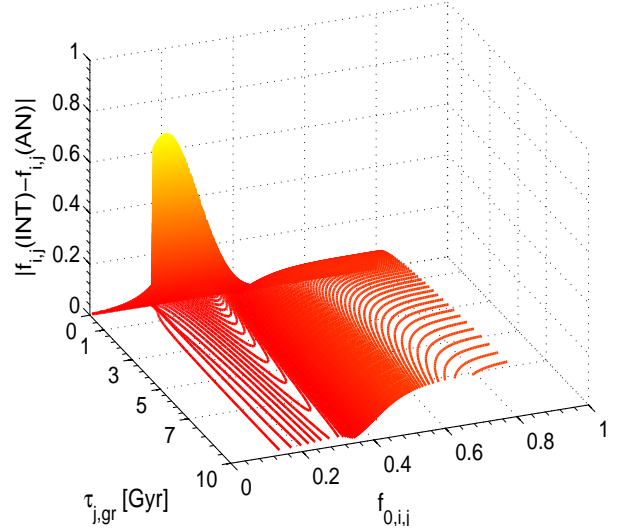


Fig. 1. Absolute value of the differences between the $\overline{f}_{i,j}$ calculated integrating and averaging on the MCs lifetimes as in Eqn. (33) and the same quantity derived from the analytical formula of Eqn. (36) suggested by Zhukovska et al. (2008). A grid of 200×200 suitably discrete values of $f_{0,i,j}$ and τ_j^{gr} has been considered.

with large variations of $f_{0,i,j}$ and τ_j^{gr} . To clarify the issue, we checked in advance whether or not the above relation can be still used. To this aim we have calculated the differences between $\overline{f}_{i,j}$ from Eqn. (36) and the relation of Eqn. (33). This comparison is made for $\tau_j^{gr} < 1000\tau_{MC}$ and $\tau_j^{gr} > \tau_{MC}/50$. If $\tau_j^{gr} > 1000\tau_{MC}$ or $\tau_j^{gr} < \tau_{MC}/50$ we use the Taylor expansion suggested by Zhukovska et al. (2008) deal with the extreme cases of very slow or very fast accretion time.

The results are presented in Fig. 4.2 for a 200×200 grid of models with uniform spacing of $f_{0,i,j}$ and τ_j^{gr} growing linearly from low to high values. The error can be significant, in particular for very low $f_{0,i,j}$ and very short τ_j^{gr} or high τ_j^{gr} and average $f_{0,i,j}$. As we discussed in Sect. 4.1, the same accretion term in Dwek (1998) and Calura et al. (2008) is

$$\left(\frac{d\sigma_i^D}{dt}\right)_{accr} = \frac{\sigma_i^D}{\tau_{i,accr}} = \frac{\sigma_i^D}{\tau_{0,i}} \cdot \left(1 - \frac{\sigma_i^D}{\sigma_i^M}\right). \quad (37)$$

The basic difference between the two approaches is that while Dwek (1998) and Calura et al. (2008) with describes the evolution of the abundance of the element i -th in the dust, Zhukovska et al. (2008) follow the evolution of the abundance of the j -th type dust in a given sample molecules considered to represent the situation of the ISM. To adapt the equations to our formulation for single elements (see Sect. 2), we start from:

$$\sigma_i^G = \sigma_i^M - \sigma_i^D \quad (38)$$

which summing up all the types of dust j -th in which a given element is locked up the element i -th is locked (independently on whether or not it is a key element for that kind of molecule) becomes:

$$\sigma_i^G = \sigma_i^M - \sum_j \nu_{i,j}^D \frac{A_{i,j}}{A_j^D} \sigma_j^D \quad (39)$$

$$\text{with} \quad \sigma_i^D = \sum_j \nu_{i,j}^D \frac{A_{i,j}}{A_j^D} \sigma_j^D \quad (40)$$

where as usual σ_i^D is the surface mass density of the i -th element in dust, while σ_j^D is the surface mass density of the j -th type dust. The above relations says that the amount of element i -th contained in the dust is given by the sum of the contributions by all the j -th kinds of dust in which i is involved. For each one of the j -th types, we divide σ_j^D by the unit mass $A_j^D m_H$ of one species j -th and find the number density of dust of type j -th. Then, for each one of these molecules j -th we have $\nu_{i,j}^D$ atoms of the element i -th. Finally, we multiply by the atomic mass $A_{i,j} m_H$ of the element i -th to get the mass of the i -th element coming from the j -th type dust. If we derive respect to time we obtain

$$\left(\frac{d\sigma_i^D}{dt} \right)_{TOT} = \sum_j \nu_{i,j}^D \frac{A_{i,j}}{A_j^D} \left(\frac{d\sigma_j^D}{dt} \right)_{TOT} \quad (41)$$

where the total evolution of dust is given by the sum of the variations due to the star formation, the stardust injected in the ISM, the destruction of the grains by SNa shocks, and the accretion process in the cold regions. Taking into account only this last one:

$$\left(\frac{d\sigma_i^D}{dt} \right)_{accr} = \sum_j \nu_{i,j}^D \frac{A_{i,j}}{A_j^D} \left(\frac{d\sigma_j^D}{dt} \right)_{accr} \quad (42)$$

The amount of element i -th contained in dust is given by the sum of the contributions by all the j th kinds of dust in which i is involved. For each j -th type, we divide σ_j^D by the unit mass $A_j^D m_H$ of one species j -th of dust and find the number density of the j -th type dust. For each j -th dust we have $\nu_{i,j}^D$ atoms of the element i -th. Finally, we multiply by the atomic mass $A_{i,j} m_H$ of the element i -th to get the mass of this coming from the j -th type dust. Inserting the expression for $(d\sigma_j^D/dt)_{accr}$ we have:

$$\begin{aligned} \left(\frac{d\sigma_i^D}{dt} \right)_{accr} &= \sum_j \nu_{i,j}^D \frac{A_{i,j}}{A_j^D} \left(\frac{d\sigma_j^D}{dt} \right)_{gg} = \\ &= \sum_j \frac{\nu_{i,j}^D A_{i,j}}{A_j^D} \frac{\chi_{MC}}{(1 - \chi_{MC}) \tau_{MC}} (\bar{f}_{k,j} \sigma_{j,max}^D - \sigma_j^D). \end{aligned} \quad (43)$$

Let's now introduce $\sigma_{j,max}^D$, which is related to the amount of key-element k -th in the dust of type j -th present in the ISM, i.e. σ_k^M . We can express σ_j^D by means of the key-element k -th of the j -th dust that is locked up into the j -th component itself. This quantity is not known and not tracked by our model. All we know is how much of a given element is locked up into dust, but *we do not know how much of that element is locked in every kind of dust*. For example we are able to follow how much silicon is locked up into dust, but not how much silicon is stored in pyroxene, olivine and quartz. Doing the substitution we have:

$$\begin{aligned} \left(\frac{d\sigma_i^D}{dt} \right)_{accr} &= \sum_j \frac{\nu_{i,j}^D A_{i,j}}{A_j^D \tau_{MC}} \frac{\chi_{MC}}{(1 - \chi_{MC})} \\ &\cdot \left[\bar{f}_{k,j} \frac{A_j^D}{A_{k,j} \nu_{k,j}^D} \sigma_{k,j}^M - \frac{A_j^D}{A_{k,j} \nu_{k,j}^D} \sigma_{k,j}^D \right] \end{aligned} \quad (44)$$

$$\begin{aligned} \left(\frac{d\sigma_i^D}{dt} \right)_{accr} &= \frac{\chi_{MC}}{(1 - \chi_{MC}) \tau_{MC}} \sum_j \frac{A_{i,j} \nu_{i,j}^D}{A_{k,j} \nu_{k,j}^D} \\ &\cdot [\bar{f}_{k,j} \sigma_{k,j}^M - \sigma_{k,j}^D] \end{aligned} \quad (45)$$

Posing $K = \chi_{MC} / (\tau_{MC} (1 - \chi_{MC}))$, we have:

$$\begin{aligned} \left(\frac{d\sigma_i^D}{dt} \right)_{accr} &= K \left[\sum_{j,i=k} (\bar{f}_{i,j} \sigma_{i,j}^M - \sigma_{i,j}^D) + \right. \\ &\left. + \sum_{j,i \neq k} \frac{A_{i,j} \nu_{i,j}^D}{A_{k,j} \nu_{k,j}^D} (\bar{f}_{k,j} \sigma_{k,j}^M - \sigma_{k,j}^D) \right] \end{aligned} \quad (46)$$

where k indicates the key element of the dust of type j -th, because it may occur that a dust molecule contains the element i -th of which we tracking the evolution, but *not* the key element that could be of another type. For example, we could be following the evolution of carbon and considering the silicon carbide that contains carbon, but not as key-element. As a consequence of this, the above has been split in two parts: in the first one we include the part of the j -th type dust grain in which the element i -th is locked *as key-element*; in the second part we have the dust molecules containing the i -th element but *not as key element*, which instead corresponds to the element k -th. Therefore the summation goes for all the $k \neq i$. The notation $\sigma_{k,j}^D$ is meant to indicate the surface mass density of the k -th element locked up into the dust compounds of type j -th.

5. Dust accretion rates for a few important elements

At this stage we need to specify the dust accretion rate given by Eqn. (46) for some specific elements whose evolution we intend to study. The model follows 16 elements (Portinari et al. 1998): H, ^4He , ^{12}C , ^{13}C , ^{14}N , ^{15}N , ^{16}O , ^{17}O , ^{18}O , ^{22}Ne , ^{20}Ne , ^{24}Mg , ^{28}Si , ^{32}S , ^{40}Ca , ^{56}Fe .

Four families of dust can be identified and tracked by the model: they are the silicates, carbonaceous and iron grains, and silicon carbide (it is worth clarifying that SiC does not form by accretion in MCs). We must distribute the 16 elements followed by the model in the four families of dust. First of all, H, ^4He , ^{20}Ne , ^{22}Ne are noble gases not involved into the dust formation process by accretion. Second, since the hydrogen is by far the most abundant element in the Universe, even if it may be contained in many dust molecules (such as for instance the PAHs), its abundance in the ISM gas will not be significantly affected by dust. For what concern ^{16}O , ^{17}O , ^{18}O , ^{24}Mg , ^{28}Si , ^{56}Fe , according to the simplified Zhukovska et al. (2008) scheme, they are involved in silicates (all of them) and iron grains (just some of them). For ^{14}N , ^{15}N , ^{32}S and ^{40}Ca there is no specific dust family to associate them. However, the observations tell us that they are or could be depleted –see for instance the case of Calcium (Whittet 2003; Tielens 2005)–, so we must set a plausible yet simple scheme to describe them. Finally, ^{12}C and ^{13}C are both involved into the formation of carbonaceous grains and silicon carbide. In the following we will examine the case of ^{12}C , ^{13}C , ^{16}O , ^{17}O , ^{18}O , ^{24}Mg , ^{28}Si and ^{56}Fe in some detail.

5.1. Carbon

Carbon is present in dust as key constituent of many molecules containing carbon (C-molecules), otherwise named carbonaceous grains. It is also part of important dust molecules like silicon carbide (SiC) where, however, the key element ruling the process is silicon. SiC grains are mainly related to AGB carbon stars and for them there is no process of accretion in cold clouds of the ISM. Finally, the problem of the formation of SiC in the ejecta of supernovæ is still debated.

Nozawa et al. (2003), studying dust formation in population III supernovæ argues that they cannot form SiC grains with radii comparable to the pre-solar SiC grains identified as supernova condensates, because silicon and carbon are firstly locked into other carbonaceous grains or silicates before the formation of SiC grains can take place. However, we observe a small but significant percentage of X-type SiC grains (one of the minor types A, B, X, Y and Z, that is believed to be formed in the ejecta of type II SNæ because of the isotopic signature) with respect to the mainstream SiC (about 90% of the total and whose origin is attributed to AGB C-stars, because of their similar $^{12}\text{C}/^{13}\text{C}$ ratio, signatures of s-processes and the 11.3 SiC μm feature in C-stars). The ratio between X-type and mainstream type can be quantified in about 0.01 (Hoppe et al. 2000). Therefore, as proposed by Deneault et al. (2003), special conditions and/or chemical pathways might have to be considered in order to realize the formation in type II SNæ of SiC grains. To reproduce the observed X-type over mainstream ratio, Zhukovska et al. (2008) considers a small formation of SiC in Type II SNæ, however this is just an *ad-hoc* recipe based on meteorites and does not throw light over the uncertain amount of dust, and X-type SiC, produced by SNæ.

The equation describing the accretion of carbonaceous grains of the ISM is:

$$\left(\frac{d\sigma_C^D}{dt}\right)_{\text{accr}} = K \{ \bar{f}_{C,C} (1 - \xi_{CO}) \sigma_{C,C}^M - \sigma_{C,C}^D \} \quad (47)$$

where $\sigma_{C,C}^M$ is the amount of the available carbon, ξ_{CO} a factor accounting for the carbon embedded in molecules like CO that do not take part to the accretion process, $\sigma_{C,C}^D$ is the carbon already condensed into dust, and $\bar{f}_{C,C}$ is the average condensation factor (see Sect. 4 model B). The accretion of C-molecules in molecular clouds happens according to a time scale defined by Eqn. 28 which for the specific case of carbon is:

$$\tau_C^{gr} = 46 \frac{(A_C^{gw})^{\frac{1}{2}} \nu_{C,C}^D}{A_C^D} \left(\frac{\rho_C^D}{3}\right) \left(\frac{10^3}{n_H}\right) \left(\frac{3.5 \cdot 10^{-5}}{\epsilon_{C,C}}\right) \text{Myr}. \quad (48)$$

This relation deserves some comments. First of all $\nu_{C,C}^D = 1$ because carbon is present in the cold regions of molecular clouds as single atoms or molecules with typically one atom of carbon. Second, $\rho_C^D = 2.26 \text{ g cm}^{-3}$ (Li & Draine 2001). To determine A_C^D we should average the masses of the various type of molecules present in the molecular clouds. Carbon is embedded in CO (with a percentage easily up to 20 or 40%). There are also lots of C-molecules like: CO_2 , H_2CO , HCN , CS , CH_4 , C_2H_2 , C_2H_6 , HCOOH , OCS , We consider $A_C^D = 28$ corresponding to CO as a sort of mean value fairly representing the above group. $A_C^{gw} = 12$

assuming single atoms as the typical accreting species. Finally, we need to specify $\epsilon_{C,C}$ the abundance by number with respect to H of the key-species C driving the process of accretion of dusty C-molecules. We have:

$$\epsilon_{C,C} = (1 - \xi_{CO}) \frac{\sigma_C^M - \sigma_C^D}{12\sigma_H^M}. \quad (49)$$

In this relation, the factor $(1 - \xi_{CO})$ takes into account that fact that the carbon already in CO is not available to the accretion process. This correction is not negligible. Second, we subtract from the carbon atoms available for accretion, those ones already embedded in dust or belonging to unreactive species like SiC. Finally, we obtain for the typical accretion time:

$$\tau_C^{gr} = \frac{1.80}{(1 - \xi_{CO}) n_H} \left(\frac{\sigma_H^M}{\sigma_C^M - \sigma_C^D}\right) \text{Myr}. \quad (50)$$

A similar relation is assumed for ^{13}C , in which the only difference is the 2.03 instead of 1.80. This assumption stands on the notion that ^{13}C , much less abundant than ^{12}C , undergoes the same kind of accretion processes and forms similar C-molecules. Clearly this is a simplified view of the subject, however sustained by the fact that, on average, the mean $N(^{12}\text{CO})/N(^{13}\text{CO})$ ratio in diffuse clouds is close or compatible with the local interstellar isotope ratio $^{12}\text{C}/^{13}\text{C}$, even if the $N(^{12}\text{CO})/N(^{13}\text{CO})$ can be easily enhanced or reduced by a factor of two with a large spread (Liszt 2007; Visser et al. 2009). This allows to think that the relative percentage of carbon isotopes in molecules and dust should not be on average too different.

To practically use Eqn. (47), we need $f_{0,C,C}$ to get the average condensation factor $\bar{f}_{C,C}$: $f_{0,C,C}$ is the initial condensation of the key-element C of the carbonaceous dust compound. If $\tilde{\chi}_j^D$ is the mass fraction of dust j-th contained in the part of the ISM that is not stored in cold clouds, we have:

$$f_{0,C,C} \approx \frac{\tilde{\chi}_C^D}{\chi_{C,max}^D} \approx \frac{\chi_C^D}{\chi_{C,max}^D} \approx \frac{\sigma_{C,C}^D}{\sigma_{C,C}^M} \quad (51)$$

where to derive it, we simply replaced the mass fraction of dust in the ISM not belonging to cold regions with the mass fraction embedded in the cold ones: $\tilde{\chi}_C^D \approx \chi_C^D$. This simply means that after every cycle of MCs there is complete restitution and mixing with the ISM, so that on the average the ISM dust content always mirrors the initial mass-fraction already condensed at the formation of the MC.

5.2. Silicon

Silicon is present in many types of grains generically referred to as silicates, one of the most complicated families of minerals. We consider only some kinds of silicates, commonly used in models of dust formation. First of all, we list the pyroxenes that are inosilicates (i.e. a family containing single chain and double chain silicates) in general indicated by $\text{XY}(\text{Si}, \text{Al})_2\text{O}_6$, where X represents ions such as calcium, sodium, iron $^{2+}$ and magnesium, whereas Y represents ions of smaller size such as chromium, aluminum, iron $^{+3}$, magnesium. Aluminum, while commonly replacing in other silicates, does not often do it in pyroxenes. Typical pyroxenes used in dust models are the end members of the enstatite-hypersthene-ferrosilite series described by $\text{Mg}_x\text{Fe}_{1-x}\text{SiO}_3$ with $0 < x < 1$ determining the partition between the two possibilities. Enstatite is the

magnesium end-member MgSiO_3 of the series, while ferrosilite is the iron end-member FeSiO_3 : both are found in iron and stony meteorites. Second, we have the olivines. They are a series of minerals falling in between two end-members, fayalite and forsterite. They can be described by $[\text{Mg}_x\text{Fe}_{1-x}]_2\text{SiO}_4$ with $0 < x < 1$ determining the partition. Fayalite is the iron-rich member with Fe_2SiO_4 . Forsterite is the magnesium-rich member with Mg_2SiO_4 . The two minerals form a series where the iron and magnesium can be interchanged without much effect, also difficult to detect, on the crystal structure. Olivine can be found for example in many meteorites like the iron-nickel ones, in the tails of comets, and in the disks of dust around young stars. Both pyroxenes and olivines are expected to exist in the interstellar dust because they form from magnesium and iron that are abundant. In addition to this and limited to the calculation of stellar dust yields, we included quartz, the most common mineral on the surface of the Earth, composed by SiO_2 and silicon carbide, SiC . Silicon carbide is expected to form in the ejecta of carbon-rich stars and type II SN α , but not by accretion in cold clouds.

Two parameters control the pyroxene-olivine mixture: the Mg fraction x , assumed to be the same for pyroxenes and olivines, and the abundance ratio between the amount of magnesium and silicon bound in dust A_{Mg}^D/A_{Si}^D . This latter determines the fraction of silicates with olivine stoichiometry $F_{Ol} = A_{Mg}^D/(A_{Si}^D \cdot x) - 1$, while for pyroxenes we can define $F_{Pyr} = 1 - F_{Ol}$. The two parameters are fixed and chosen according to present day observations of IR emission and abundances in the diffuse ISM (Dwek et al. 1997; Whittet 2003; Dwek 2005; Zhukovska et al. 2008), i.e. $x = 0.8$ and $A_{Mg}^D/A_{Si}^D = 1.06 - 1.07$. Varying these parameters does not significantly affect the total efficiency of dust production by the MCs (Zhukovska et al. 2008). For the purposes of this study, they can be kept fixed. The equation describing the evolution of silicon is nearly the same no matter whether or not silicon is the key-element for pyroxenes and olivines.

The Mg/Fe case. Let us first suppose that the key-element is magnesium/iron and not silicon. Using Eqn. (46) we get:

$$\begin{aligned} \left(\frac{d\sigma_{Si}^D}{dt}\right)_{accr} &= K \frac{A_{Si,Pyr} \nu_{Si,Pyr}^D}{A_{i,Pyr} \nu_{i,Pyr}^D} \cdot \{\bar{f}_{i,Pyr} \sigma_{i,Pyr}^M - \\ &- \sigma_{i,Pyr}^D\} + K \frac{A_{Si,Ol} \nu_{Si,Ol}^D}{A_{i,Ol} \nu_{i,Ol}^D} \{\bar{f}_{i,Ol} \cdot \\ &\cdot \sigma_{i,Ol}^M - \sigma_{i,Ol}^D\} \end{aligned} \quad (52)$$

where $\bar{f}_{i,Pyr}$ and $\bar{f}_{i,Ol}$ are the average condensation fractions of pyroxenes and olivines, obtained according to the procedure described in Sect. 4. Furthermore, $\nu_{Si,Pyr}^D$ is the number of silicon atoms needed for one molecule of pyroxene, i.e. $\nu_{Si,Pyr}^D = 1$. Since for each molecule we have just one Si atom, $\nu_{Si,Pyr}^D \cdot A_{Si,Pyr} = 28$. The quantity $A_{i,Pyr} = 24$ or 56 (magnesium or iron). We must also define $\nu_{i,Pyr}^D$ (a number between 0 and 1). Assuming a fixed partition x : $\nu_{Mg,Pyr}^D = 0.8$ and $\nu_{Fe,Pyr}^D = 0.2$. Finally, we have the physical constants for olivines: $\nu_{Si,Ol}^D = 1$, $A_{Si,Ol} = 28$, $A_{Mg,Ol} = 24$, $A_{Fe,Ol} = 56$, $\nu_{Mg,Ol}^D = 1.6$, finally $\nu_{Fe,Ol}^D = 0.4$. Since F_{Pyr} and F_{Ol} are the fractions of

pyroxenes and olivines in which silicates are subdivided, we have the following partition of magnesium in dust $\sigma_{Mg}^D = \sigma_{Mg,Ol}^D + \sigma_{Mg,Pyr}^D = (x \cdot F_{Pyr})/(x \cdot F_{Pyr} + 2x \cdot F_{Ol}) \sigma_{Mg}^D + (2x \cdot F_{Ol})/(x \cdot F_{Pyr} + 2x \cdot F_{Ol}) \sigma_{Mg}^D = Mg_{Pyr} \sigma_{Mg}^D + Mg_{Ol} \sigma_{Mg}^D$ and of iron in silicates (once subtracted the iron embedded in iron grains) $\sigma_{Fe,Sil}^D = \sigma_{Fe}^D - \sigma_{Fe,Fe}^D = \sigma_{Fe,Ol}^D + \sigma_{Fe,Pyr}^D = (1-x) \cdot F_{Pyr}/((1-x) \cdot F_{Pyr} + 2(1-x) \cdot F_{Ol}) \sigma_{Fe,Sil}^D + 2(1-x) \cdot F_{Ol}/((1-x) \cdot F_{Pyr} + 2(1-x) \cdot F_{Ol}) \sigma_{Fe,Sil}^D = Fe_{Pyr} \sigma_{Fe,Sil}^D + Fe_{Ol} \sigma_{Fe,Sil}^D$.

It is worth also noting that the dust compounds of which we follow the accretion, i.e. pyroxenes/olivines for silicates, carbonaceous grains and iron grains (the same considered by Zhukovska et al. (2008)), are fewer in number than the dust molecules considered by the stellar yields of dust in the most detailed models calculated by CNT theory (see Piovan et al. 2011a, for more details). The number and variety of the dust molecules injected into the ISM are wider than the number of accreting species. For this reason, before splitting σ_{Mg}^D , $\sigma_{Fe,Sil}^D$ and σ_{Si}^D (see below) between pyroxenes/olivines, we need to keep memory of the evolution of the other dust species injected by AGB/SN α (also eventually swept up and destroyed by shocks in the ISM), which are not included in the accretion scheme.

The Si case. In alternative, silicon can be the key-element for olivines and pyroxenes:

$$\begin{aligned} \left(\frac{d\sigma_{Si}^D}{dt}\right)_{accr} &= K \{\bar{f}_{Si,Pyr} \sigma_{Si,Pyr}^M - \sigma_{Si,Pyr}^D\} \\ &+ K \{\bar{f}_{Si,Ol} \sigma_{Si,Ol}^M - \sigma_{Si,Ol}^D\} \end{aligned} \quad (53)$$

where again $\bar{f}_{Si,Pyr}$ and $\bar{f}_{Si,Ol}$ are the average condensation fractions of silicon in pyroxenes and olivines. The corresponding partition of silicon in dust is $\sigma_{Si}^D = \sigma_{Si,Pyr}^D + \sigma_{Si,Ol}^D = F_{Pyr} \sigma_{Si}^D + F_{Ol} \sigma_{Si}^D$. We need to calculate the accretion time scales of pyroxenes and olivines, to be compared with the lifetime of molecular clouds and included into the integrations for $\bar{f}_{Mg,Pyr}$, $\bar{f}_{Mg,Ol}$, $\bar{f}_{Si,Pyr}$ and $\bar{f}_{Si,Ol}$. Applying Eqn. (28) we get:

$$\begin{aligned} \tau_{Pyr}^{gr} &= 46 \frac{(A_{Pyr}^{gw})^{1/2} \nu_{i,Pyr}^D}{A_{Pyr}^D} \left(\frac{\rho_{Pyr}^D}{3}\right) \left(\frac{10^3}{n_H}\right) \left(\frac{3.5 \cdot 10^{-5}}{\epsilon_{i,Pyr}}\right) = \\ &= \frac{\tau_{0,Pyr,i}^{gr} \sigma_H^M}{\sigma_i^M n_H} \end{aligned} \quad (54)$$

$$\begin{aligned} \tau_{Ol}^{gr} &= 46 \frac{(A_{Ol}^{gw})^{1/2} \nu_{i,Ol}^D}{A_{Ol}^D} \left(\frac{\rho_{Ol}^D}{3}\right) \left(\frac{10^3}{n_H}\right) \left(\frac{3.5 \cdot 10^{-5}}{\epsilon_{i,Ol}}\right) = \\ &= \frac{\tau_{0,Ol,i}^{gr} \sigma_H^M}{\sigma_i^M n_H} \end{aligned} \quad (55)$$

where $\tau_{0,Pyr,i}^{gr}$ and $\tau_{0,Ol,i}^{gr}$ are two constants that depend on the key-element. $\tau_{0,Pyr,i}^{gr}$ is equal to 2.05, 1.30 and 1.16 for the key-elements Si, Mg and Fe respectively, while $\tau_{0,Ol,i}^{gr}$ is equal to 2.05, 2.60 and 2.32 again for Si, Mg and Fe. A_{Ol}^{gw} and A_{Pyr}^{gw} are the atomic weight of the growing species. Finally, $A_{d,Ol} = A_{d,Pyr} = 121.41$. It is important to note that in the calculation of the abundances of species available for dust accretion, we do not subtract the amount of dust already formed σ_i^D from the total ISM abundance σ_i^M ; this is equivalent to assume that the grains of silicates already formed act as reactive species in the accretion process. Dropping this assumption (and simplification), the

accretion process would be too slow. There is one exception though in the case of iron as the key-element for the mixture of silicates mixture. In such a case we subtract from σ_i^M the amount of iron already embedded in the iron dust grains (that do not react with silicates), thus obtaining $\sigma_i^M = \sigma_{Fe}^M - \sigma_{Fe,Fe}^D$.

The initial condensation fractions $f_{0,i,Pyrr}$, $f_{0,i,Ol}$ needed to derive $\bar{f}_{i,Pyrr}$, $\bar{f}_{i,Ol}$ can be obtained as in Eqn. (51).

5.3. Oxygen

Oxygen is much more abundant than the refractory elements Si, Fe, Mg, Ca and S. Therefore, oxygen (at least the most abundant isotope ^{16}O) will never become a key-element determining the growth of the typical dust grains in the ISM. The equation describing the evolution of the mass abundance of the ^{16}O is obtained from Eqn. (46), dropping the terms giving the contribution of the O as key-element. Therefore, considering the accretion of pyroxenes and olivines, the temporal evolution of the ^{16}O abundance (we drop the mass number of the isotope) is:

$$\begin{aligned} \left(\frac{d\sigma_O^D}{dt}\right)_{accr} &= K \frac{A_{O,Pyrr}\nu_{O,Pyrr}^D}{A_{i,Pyrr}\nu_{i,Pyrr}^D} \{\bar{f}_{i,Pyrr}\sigma_{i,Pyrr}^M - \\ &\quad - \sigma_{i,Pyrr}^D\} + K \frac{A_{O,Ol}\nu_{O,Ol}^D}{A_{i,Ol}\nu_{i,Ol}^D} \{\bar{f}_{i,Ol}\sigma_{i,Ol}^M - \\ &\quad - \sigma_{i,Ol}^D\} \end{aligned} \quad (56)$$

where once again the key-element could be Mg, Si or Fe, depending on which has the lowest abundance. The subscript i indicates a generic key-element. As usual, $\bar{f}_{i,Pyrr}$ and $\bar{f}_{i,Ol}$ are the average condensation fractions when the MC is dispersed, and $\sigma_{i,Pyrr}^D$ and $\sigma_{i,Ol}^D$ are defined as in Sect. 5.2. Introducing the Dirac delta function notation we have: $A_{i,Pyrr} = 28\delta(A_i - 28) + 24\delta(A_i - 24) + 56\delta(A_i - 56)$ where A_i is the mass number of the key-element i . Furthermore, $A_{O,Pyrr} = 16$ and, since in pyroxenes we have sulfite SiO_3 with 3 oxygen atoms, $\nu_{O,Pyrr}^D = 3$, $\nu_{i,Pyrr}^D = 1\delta(A_i - 28) + 0.8\delta(A_i - 24) + 0.2\delta(A_i - 56)$, and $A_{O,Ol} = 16$. Similarly, $\nu_{O,Ol}^D = 4$ because in the olivines we have sulfate SiO_4 , $A_{i,Ol} = 28\delta(A_i - 28) + 24\delta(A_i - 24) + 56\delta(A_i - 56)$, and $\nu_{i,Ol}^D = 1\delta(A_i - 28) + 1.6\delta(A_i - 24) + 0.4\delta(A_i - 56)$. The accretion time scales τ_{Pyrr}^{gr} and τ_{Ol}^{gr} that we need for $\bar{f}_{i,Pyrr}$ and $\bar{f}_{i,Ol}$, the elemental abundances of the key-elements and the initial condensation fractions are the same as in Sect. 5.2.

In this context, we need also a simple description for ^{17}O and ^{18}O . First of all let us examine how they behave in the inert CO molecule. The way in which the isotopes of O and C combine to form many isotopologues other than $^{12}\text{C}^{16}\text{O}$ is very complicated and thoroughly studied, because of the importance of CO molecule, its easy detection and chemical stability (van Dishoeck & Black 1988; Liszt 2007; Visser et al. 2009). The photo-dissociation of CO is a line process and consequently subject to self-shielding that in turn depends on the column density. Therefore, isotopologues other than C^{16}O are not self-shielded unless located very deeply into the molecular clouds due to the much lower abundance of ^{17}O and ^{18}O (Clayton 2003; Lee et al. 2008; Visser et al. 2009). Looking at the case of

the Sun, where the isotopic ratios are about $^{16}\text{O}/^{18}\text{O} \approx 500$ and $^{16}\text{O}/^{17}\text{O} \approx 2600$ (Lodders et al. 2009; Asplund et al. 2009), the regions with abundances of the isotopologues different than C^{16}O significantly reduced with respect to other isotopologues are located very deeply in the atmosphere. Basing on these considerations, we set the reduction factor of ^{17}O and ^{18}O , ξ'_{CO} , equal to 1/3 of the reduction factor assumed for CO in Eqn. (49). All this agrees with the observational ratios $\text{C}^{16}\text{O}/\text{C}^{17}\text{O}$ and $\text{C}^{16}\text{O}/\text{C}^{18}\text{O}$ in ζ Oph, > 5900 and ≈ 1550 respectively (Savage & Sembach 1996)).

Another point to note is that the ratios ^{16}O to ^{17}O and ^{18}O in the interstellar dust could be different from the same ratios in the ISM (Clayton 1988; Leshin et al. 1997). The subject is a matter of debate, because the above ratios strongly depend on the site where those isotopes condense into dust (Meyer 2009). Consequently, we should not simply scale to ^{17}O and ^{18}O the results obtained for ^{16}O . However, a detailed analysis of this issue is far beyond the purposes of this paper and we leave it to future improvements of our model. For the time being, basing on the following considerations we adopt a simple recipe. As in the dust grains, ^{17}O and ^{18}O are much less abundant than other elements, consider them as the key element of the dust accretion process. Therefore, Eqn. (46) applied to ^{17}O and ^{18}O (briefly indicated as ^{n}O) becomes:

$$\begin{aligned} \left(\frac{d\sigma_{(n)O}^D}{dt}\right)_{accr} &= K \left\{ \bar{f}_{(n)O,Pyrr} (1 - \xi'_{CO}) \sigma_{(n)O,Pyrr}^M - \right. \\ &\quad \left. \sigma_{(n)O,Pyrr}^D \right\} + K \left\{ \bar{f}_{(n)O,Ol} (1 - \xi'_{CO}) \sigma_{(n)O,Ol}^M - \right. \\ &\quad \left. - \sigma_{(n)O,Ol}^D \right\} \end{aligned} \quad (57)$$

where ξ'_{CO} takes into account that not all ^{17}O and ^{18}O in the ISM can be used to form new grains because part of them are locked in the CO.

The relative amounts of ^{17}O and ^{18}O available to form silicates are $\epsilon_{(n)O,Sil} = (1 - \xi'_{CO}) \left(\frac{\sigma_{(n)O}^M}{\sigma_{H}^M} \right) / (A_{(n)O} \sigma_{H}^M)$ and the accretion timescales for ^{17}O and ^{18}O are:

$$\tau_{^{17}\text{O}}^{gr} = \frac{0.97}{(1 - \xi'_{CO}) n_H} \left(\frac{\sigma_{H}^M}{\sigma_{^{17}\text{O}}^M} \right) Myr \quad (58)$$

$$\tau_{^{18}\text{O}}^{gr} = \frac{1.00}{(1 - \xi'_{CO}) n_H} \left(\frac{\sigma_{H}^M}{\sigma_{^{18}\text{O}}^M} \right) Myr \quad (59)$$

where we have considered a typical silicate in which just one atom of ^{17}O and/or ^{18}O is involved in the accretion process.

5.4. Magnesium

In our simple picture of the the grain accretion process, magnesium intervenes in pyroxenes and olivines, often as the key-element. Furthermore, magnesium is present also in other dust compounds such as MgO contained in the SNæ yields of dust. In analogy to the case of Si, the set of equations governing the temporal evolution of the Mg abundance is different depending on whether or not Mg is the key, similarly to silicon. If Mg is a key element:

$$\left(\frac{d\sigma_{Mg}^D}{dt}\right)_{accr} = K \cdot \left\{ \bar{f}_{Mg,Pyrr} \sigma_{Mg,Pyrr}^M - \sigma_{Mg,Pyrr}^D \right\} + K \cdot \left\{ \bar{f}_{Mg,Ol} \sigma_{Mg,Ol}^M - \sigma_{Mg,Ol}^D \right\} \quad (60)$$

with the usual meaning of the symbols. The accretion time scales and the initial condensation fractions of Mg can be obtained in the same way as in Sect. 5.2, following Eqns. (54), (55) and (51). If Mg is not the key-element, but Si or Fe are playing the role, we have the following equation for the Mg accretion:

$$\left(\frac{d\sigma_{Mg}^D}{dt}\right)_{accr} = K \cdot \frac{A_{Mg,Pyrr} \nu_{Mg,Pyrr}^D}{A_{i,Pyrr} \nu_{i,Pyrr}^D} \left\{ \bar{f}_{i,Pyrr} \sigma_{i,Pyrr}^M - \sigma_{i,Pyrr}^D \right\} + K \cdot \frac{A_{Mg,Ol} \nu_{Mg,Ol}^D}{A_{i,Ol} \nu_{i,Ol}^D} \cdot \left\{ \bar{f}_{i,Ol} \sigma_{i,Ol}^M - \sigma_{i,Ol}^D \right\} \quad (61)$$

in which $A_{Mg,Pyrr} = 24$, $\nu_{Mg,Pyrr}^D = 0.8$, $A_{i,Pyrr} = 28$ or 56 (silicon/iron), $\nu_{Si,Pyrr}^D = 1$, $\nu_{Fe,Pyrr}^D = 0.2$, $A_{Mg,Ol} = 48$, $\nu_{Mg,Ol}^D = 1.6$, $A_{Si,Ol} = 28$, $\nu_{Si,Ol}^D = 1$ and $\nu_{Fe,Ol}^D = 0.4$. The time scales for accretion of pyroxenes/olivines and the initial condensation fractions are again from Eqns. (54), (55) and (51). For $\sigma_{i,Pyrr}^D$ and $\sigma_{i,Ol}^D$ see Sect. 5.2.

5.5. Iron

Even considering the small number of accreting compounds included in our model, iron can be locked up in grains of various type thanks to accretion processes in cold regions of the ISM. First of all, iron is locked up in iron grains that act as the key element. Second, iron is also present in pyroxene and olivine grains. In such a case, iron may or may not be the key element. In any case it is removed from the gaseous phase and stored in grains. The existence of two channels for locking up iron into grains leads to a rather complicated equation for the evolution of the iron. There are the main terms to consider: in the first and second, iron participates to the formation of silicates (pyroxenes and olivines) *as or not a key-element*, and in the third one iron plays the role of a *key-element* for the formation of iron grains. Furthermore, the equation will be slightly different depending on whether magnesium, silicon or iron is the key-element for the formation of pyroxenes/olivines. The final equation is

$$\left(\frac{d\sigma_{Fe}^D}{dt}\right)_{accr} = K \frac{A_{Fe,Pyrr} \nu_{Fe,Pyrr}^D}{A_{i,Pyrr} \nu_{i,Pyrr}^D} \left\{ \bar{f}_{i,Pyrr} \sigma_{i,Pyrr}^M - \sigma_{i,Pyrr}^D \right\} + K \frac{A_{Fe,Ol} \nu_{Fe,Ol}^D}{A_{i,Ol} \nu_{i,Ol}^D} \left\{ \bar{f}_{i,Ol} \sigma_{i,Ol}^M - \sigma_{i,Ol}^D \right\} + K \left\{ \bar{f}_{Fe,Fe} (\sigma_{Fe}^M - \sigma_{Fe,Sil}^D) - (\sigma_{Fe}^D - \sigma_{Fe,Sil}^D) \right\} \quad (62)$$

where the subscript i stands for Si , Mg or Fe itself. Using the Dirac delta function notation, we have $A_{i,Pyrr} = 28 \cdot \delta(A_i - 28) + 24 \cdot \delta(A_i - 24) + 56 \cdot \delta(A_i - 56)$. The same

expression holds good for $A_{i,Ol}$. We have also: $A_{Fe,Pyrr} = A_{Fe,Ol} = 56$, $\nu_{Fe,Pyrr}^D = 0.2$ (according to $Mg_x Fe_{1-x} SiO_3$ with $x = 0.8$), $\nu_{i,Pyrr}^D = 1 \cdot \delta(A_i - 28) + 0.8 \cdot \delta(A_i - 24) + 0.2 \cdot \delta(A_i - 56)$, $\nu_{Fe,Ol}^D = 0.4$ (according to $[Mg_x Fe_{1-x}]_2 SiO_4$ with $x = 0.8$) and finally $\nu_{i,Ol}^D = 1 \cdot \delta(A_{i,Ol} - 28) + 1.6 \cdot \delta(A_{i,Ol} - 24) + 0.4 \cdot \delta(A_{i,Ol} - 56)$. Also, with the usual meaning, $\bar{f}_{i,Pyrr}$, $\bar{f}_{i,Ol}$ and $\bar{f}_{Fe,Fe}$ are the average condensations before cloud dispersion.

For internal consistency, the system of equations must take into account that the iron abundance used to describe the evolution of the iron grains should be corrected for the iron already condensed into pyroxenes and olivines, subtracting it from σ_{Fe}^M and σ_{Fe}^D . If the key-element is magnesium, the amount of iron $\sigma_{Fe,Sil}^D$ embedded into pyroxenes and olivines is given by:

$$\sigma_{Fe,Sil}^D = \frac{\sigma_{Mg}^D A_{Fe}}{24} \left(\frac{\nu_{Fe,Ol}^D}{\nu_{Mg,Ol}^D} Mg_{Ol} + \frac{\nu_{Fe,Pyrr}^D}{\nu_{Mg,Pyrr}^D} Mg_{Pyrr} \right) \quad (63)$$

where A_{Fe} is the atomic weight of the iron and Mg_{Ol} and Mg_{Pyrr} are defined in Sect. 5.2. Doing the correct substitution we get

$$\sigma_{Fe,Sil}^D = \sigma_{Mg}^D (0.583 \cdot Mg_{Ol} + 0.583 \cdot Mg_{Pyrr}) \quad (64)$$

In a similar way, if the role of key element is played by silicon we have:

$$\sigma_{Fe,Sil}^D = \sigma_{Si}^D (0.8 \cdot F_{Ol} + 0.4 \cdot F_{Pyrr}) \quad (65)$$

where F_{Ol} and F_{Pyrr} have been defined in Sect. 5.2. If iron is the key element for silicates, we simply have:

$$\sigma_{Fe,Sil}^D = \sigma_{Fe}^D - \sigma_{Fe,Fe}^D \quad (66)$$

This clearly requires to keep track of the accretion/destruction and injection of the iron grains by SN α and AGB stars. The accretion time scales for pyroxenes/olivines are the same as in Eqns. (54) and (55), whereas for iron grains:

$$\tau_{Fe}^{gr} = 46 \frac{(A_{Fe}^{gw})^{1/2} \nu_{Fe,Fe}^D}{A_{Fe}^D} \left(\frac{\rho_{Fe}^{Fe}}{3} \right) \left(\frac{10^3}{n_H} \right) \cdot \left(\frac{3.5 \cdot 10^{-5}}{\epsilon_{Fe,Fe}} \right) = \frac{31.56}{n_H} \frac{\sigma_H}{(\sigma_{Fe}^M - \sigma_{Fe,Sil}^D)} Myr. \quad (67)$$

where $\nu_{Fe,Fe}^D = 1$ and $\rho_{Fe}^D = 7.86 \text{ g cm}^{-3}$. Concerning the accreting elements we consider the simplest case in which they are in form of atoms. The initial condensation fractions for magnesium/silicon as key-elements in pyroxenes/olivines follow Eqns. (??) and (??), while for iron we have:

$$f_{0,Fe,Fe} = \frac{\chi_{Fe}^D}{\chi_{Fe,max}^D} = \frac{\sigma_{Fe}^D - \sigma_{Fe,Sil}^D}{\sigma_{Fe}^M - \sigma_{Fe,Sil}^D}. \quad (68)$$

where we subtract the amount of iron already locked up in silicates and therefore not available to for iron grains.

5.6. Calcium

This element has a complicate behaviour difficult to follow. First of all it is usually heavily depleted in the ISM (Whittet 2003; Tielens 2005), and its abundance in the solar system is quite low. The difficult arises from the total condensation efficiency and the big fluctuations generated by the low abundance, compared to other refractory elements. Second there is not an average molecule that could be used to represent typical calcium grains in a simple theoretical description. Furthermore, the measurements of depletion cannot be easily derived from observational data: in principle the ionization equilibrium equation should be solved to derive the Ca abundance from the observations of Ca II. Possible estimates of Ca abundances by electron densities and strengths of the ionizing radiation fields are not easy and relying on ratios of ionization and recombination rates between different elements (like CaII to those of NaI or KI for instance) is a cumbersome affair (Weingartner & Draine 2001). For all these reasons, Jenkins (2009, and 2011, private communication) leaved Ca (and also Na and K) aside. Trying to overcome this difficulty, we simplify the problem as follows. Thanks to its low abundance, we consider Ca as the key-element of the associated grains of dust; the equation for the evolution of Ca is:

$$\left(\frac{d\sigma_{Ca}^D}{dt}\right)_{accr} = K \{ \bar{f}_{Ca,Ca} \sigma_{Ca}^M(Ca) - \sigma_{Ca}^D(Ca) \} \quad (69)$$

where all the symbols have their usual meaning. To derive the accretion time scale τ_{Ca}^{gr} we do not refer to a typical Ca dust grain but simply take *the shortest* timescale among those of refractory elements that are most depleted, i.e. Mg, Si and Fe ($\tau_{Si}^{gr}, \tau_{Mg}^{gr}, \tau_{Fe}^{gr}$), and a timescale $\tau_{Ca,Ca}^{gr}$ for the formation of dust silicates-like molecules with one calcium atom as key atom. This last-named timescale is multiplied for a correction factor Ca_X , eventually allowing for a fast accretion. Therefore $\tau_{Ca}^{gr} = \min\{\tau_{Si}^{gr}, \tau_{Mg}^{gr}, \tau_{Fe}^{gr}, Ca_X \cdot \tau_{Ca,Ca}^{gr}\}$. The initial condensation fraction at the MC formation is as usual $f_{Ca,Ca} = \sigma_{Ca}^D / \sigma_{Ca}^M$.

5.7. Sulfur

Sulfur is a very important element: it is often used as a reference case of nearly zero depletion in studies of local and distant objects (Jenkins 2009). However the real depletion efficiency of this element is a matter of debate and the assumption of nearly zero depletion cannot be safe. Calura et al. (2009) reviews data and theoretical interpretations gathered over the past years to convincingly show that S can be depleted in considerable amounts. Jenkins (2009) points out the depletion of sulfur can be significant along some lines of sight. We take Jenkins (2009) results into account to set upper and lower limits to the sulfur depletion. Considering sulfur as a refractory element, its evolution in dust is given by

$$\left(\frac{d\sigma_S^D}{dt}\right)_{accr} = K \{ \bar{f}_{S,S} \sigma_S^M(S) - \sigma_S^D(S) \} \quad (70)$$

where all the symbols have their usual meaning. Current observations do allow us to choose a grain as representative of the accretion process. In analogy to what made for calcium, the accretion time $\tau_{S,gr}$ is supposed to be *the longest* between the timescales of the refractory elements, i.e. Mg,

Si and Fe, and a timescale $\tau_{S,S}^{gr}$ for the formation of dust silicates-like molecules with one sulfur atom as key atom, allowing therefore for a slow accretion. We also introduce a multiplying scaling factor S_X to eventually correct this timescale. Therefore $\tau_S^{gr} = S_X \cdot \max\{\tau_{Si}^{gr}, \tau_{Mg}^{gr}, \tau_{Fe}^{gr}, \tau_{S,S}^{gr}\}$. The initial condensation fraction for $\bar{f}_{S,S}$ is $f_{S,S} = \sigma_S^D / \sigma_S^M$.

5.8. Nitrogen

Nitrogen is known to be poorly depleted and if not depleted at all (Whittet 2003; Tielens 2005). Jenkins (2009) suggests that depletion is independent from the line of sight depletion strength factor and that in any case depletion is very low, thus confirming the poor ability of nitrogen to condense into dust grains. As nitrogen is included in our list of elements (both ^{14}N and ^{15}N), the evolution of both isotopes in dust is governed by:

$$\left(\frac{d\sigma_N^D}{dt}\right)_{accr} = K \{ \bar{f}_{N,N} \sigma_N^M(N) - \sigma_N^D(N) \} \quad (71)$$

where for the accretion time we simply take the *longest* between C and O and the accretion timescale with one nitrogen atom as growing species for a nitrogen molecule. Carbon and oxygen are the nearest elements, both do not show a strong depletion and, finally, similarly to nitrogen both indicate (at least along some lines of sight) low values of depletion. Taking the longest timescale, we implicitly assume that nitrogen very slowly accretes onto dust. As usual $f_{N,N} = \sigma_N^D / \sigma_N^M$.

6. Supernovae: destruction time scales

Dust grains in the ISM can be destroyed by other physical process such as the passage of shock waves by supernovæ explosions. The destruction time scale of the element i -h in dust grains in the ISM because of the shocks by local SNæ is defined as the ratio between the available amount of that element locked up into dust (the surface mass density of the element i -th $\sigma_i^D(r, t)$, at a given radius and evolutionary time) and the rate at which grains containing that element are destroyed refueling the gaseous phase :

$$\tau_{SNR,i} = \sigma_i^D / \left(\frac{d\sigma_i^D}{dt}\right)_{SNR} \quad (72)$$

as usual, we drop the dependence from r and t . The destruction time scale can be expressed as follows:

$$\left(\frac{d\sigma_i^D}{dt}\right)_{SNR} = M_i^{destr} \cdot R_{SN} \quad (73)$$

where $M_i^{destr} = M_i^{destr}(r, t)$ is the amount of mass destroyed by a single SNa event, while $R_{SN} = R_{SN}(r, t)$ is the global rate of SNæ, obtained by adding together the rate of Type I and II SNæ. Multiplying numerator and denominator by σ_i^D and combining together Eqns. (72) and (73) it follows:

$$\tau_{SNR,i} = \sigma_i^D / \left(\frac{d\sigma_i^D}{dt}\right)_{SNR} = \frac{1}{R_{SN}} \frac{\sigma_i^D}{M_i^{destr}} \quad (74)$$

The amount of mass destroyed by the interstellar shocks can be defined as the amount of mass swept by the SNa shock, multiplied by the fraction of dust mixed with the ISM (in this way we get the total swept up mass of dust)

and finally by a factor of dust destruction ϵ_i that depends on the element we are taking into account:

$$M_i^{destr} = \frac{\sigma_i^D}{\sigma_i^M} \cdot M_{swept} \cdot \epsilon_i. \quad (75)$$

Inserting this expression into Eqn. (74) we have:

$$\tau_{SNR,i} = \frac{1}{R_{SN}} \frac{\sigma_i^D}{M_i^{destr}} = \frac{1}{M_{swept}\epsilon_i} \left(\frac{\sigma_i^M}{R_{SN}} \right). \quad (76)$$

We need now to get an estimate of the mass swept up by a SNa shock propagating through the ISM. To describe the evolution of the SNa remnant we follow Cioffi et al. (1988) and Gibson (1994). In brief, the evolution of the remnant after the SNa explosion is subdivided into three main phases: (i) free expansion that lasts until the mass of the swept up material is comparable to the mass of the expelled material; (ii) adiabatic expansion, or so-called Sedov-Taylor phase, lasting until when the radiative cooling time of the shocked gas is about equal to the expansion time of the remnant; (iii) radiative expansion, with the formation of a cold and dense shell behind the shock front, starting when at least some sections of the shocked gas have radiated most of their thermal energy (Ostriker & McKee 1988). Phase (i) has a simple solution that can be obtained using the obvious relation $(4/3)\pi R^3 \rho_0 = M_{SN}$ where M_{SN} is the mass of the expelled material. The duration of the phase is $\tau = R/v \approx 200$ years (very short indeed). For the phase (ii) we have the classical auto-similar adiabatic solution of Sedov-Taylor (Ostriker & McKee 1988);

$$R_S(t) = 1.15 \left(\frac{E_0}{\rho_g(t)} \right)^{1/5} t^{2/5} \quad (77)$$

where E_0 is the energy of the blast wave in units of 10^{50} erg and $\rho_g(t)$ is the density of the environment. The radiative cooling leads to the formation of a thin and dense shell at t_{sf} :

$$t_{sf} = 3.61 \cdot 10^4 \cdot \varepsilon_0^{3/14} n_H^{-4/7} \left(\frac{Z}{Z_\odot} \right)^{-5/14} \quad (78)$$

n_H is the number density of hydrogen atoms, Z the metallicity of the ISM and Z_\odot the solar value. ε_0 is the energy in units of 10^{51} erg. The blast wave decelerates until when the radiative losses start dominating. At about $t_{PDS} \approx 0.37t_{sf}$, the remnant enters the so-called Pressure Driven Snowplow phase (PDS) lasting or Phase (iii). In the early stages of the PDS phase, the radius of the remnant changes according to the following equation (where $t_{SN} = t - t'$):

$$R_S(t_{SN}) = R_{PDS} \left(\frac{4}{3} \frac{t_{SN}}{t_{PDS}} - \frac{1}{3} \right)^{3/10} \quad (79)$$

where the radii are in parsec. R_{PDS} is the radius at the start of the PDS phase:

$$R_{PDS} = 14 \cdot \varepsilon_0^{2/7} n_0^{3/7} \left(\frac{Z}{Z_\odot} \right). \quad (80)$$

The inner side of the shock continuously loses energy because of the radiative cooling and it pushes forward the shell in the ISM. At the time t_{merge} , given by:

$$t_{merge} = 21.1 \cdot t_{sf} \varepsilon_0^{5/49} n_0^{10/49} \left(\frac{Z}{Z_\odot} \right)^{15/49}. \quad (81)$$

The remnant and the ISM lose their identity as single entities and merge together. Subsequently, in the time interval for $t_{merge} \leq t_{SN} \leq t_{cool}$ the radius of the shell is given by:

$$R_{merge} = 3.7 R_{PDS} \varepsilon_0^{3/98} n_0^{3/49} \left(\frac{Z}{Z_\odot} \right)^{9/98} \quad (82)$$

in parsec, where the time scale t_{cool} is:

$$t_{cool} = 203 t_{sf} \left(\frac{Z}{Z_\odot} \right)^{-9/14} \quad (83)$$

in years. There are four time intervals, with the corresponding radii, to consider:

$$\begin{aligned} R_S(t_{SN}) &= 1.15 \left(\frac{E_0}{\rho_g(t)} \right)^{1/5} t_{SN}^{2/5} & 0 \leq t_{SN} < t_{PDS}; \\ R_S(t_{SN}) &= R_{PDS} \left(\frac{4}{3} \frac{t_{SN}}{t_{PDS}} - \frac{1}{3} \right)^{3/10} & t_{PDS} \leq t_{SN} < 1.17 t_{sf}; \\ R_S(t_{SN}) &= R_{PDS} \left(\frac{4}{3} \frac{t_{SN}}{t_{PDS}} - \frac{1}{3} \right)^{3/10} & 1.17 t_{sf} \leq t_{SN} < t_{merge}; \\ R_S &= 3.7 R_{PDS} \varepsilon_0^{3/98} n_0^{3/49} \left(\frac{Z}{Z_\odot} \right)^{9/98} & t_{merge} \leq t_{SN} < t_{cool}. \end{aligned} \quad (84)$$

To obtain the shock velocity in the various time intervals, we need the R_S as functions of time. Approximating $\rho_g(t) \approx \bar{\rho}_g$, we get:

$$\begin{aligned} v_S(t_{SN}) &= \frac{2}{5} \frac{R_S(t)}{t} & 0 \leq t_{SN} < t_{PDS}; \\ v_S(t_{SN}) &= \frac{2}{5} \frac{R_{PDS}}{t_{PDS}} \left(\frac{4}{3} \frac{t}{t_{PDS}} - \frac{1}{3} \right)^{-7/10} & t_{PDS} \leq t_{SN} < 1.17 t_{sf}; \\ v_S(t_{SN}) &= \frac{2}{5} \frac{R_{PDS}}{t_{PDS}} \left(\frac{4}{3} \frac{t}{t_{PDS}} - \frac{1}{3} \right)^{-7/10} & 1.17 t_{sf} \leq t_{SN} < t_{merge}; \\ v_S(t_{SN}) &= 0 & t_{merge} \leq t_{SN} < t_{cool}. \end{aligned} \quad (85)$$

After t_{merge} there is no longer expansion and we simply have $v_S(t_{SN}) = 0$. How do we proceed in the chemical simulation? First of all we need n_H , the number density of hydrogen atoms. This is a spatial density, in atoms per cubic centimeter; we must derive it from the surface mass density of hydrogen in our flat geometry. This is done assuming as parameters the scale height and thickness of the disk suggested by the observational data. Once n_H is known, we derive the time scales t_{sf} , t_{PDS} and t_{merge} , and finally the radii of the remnant and velocity of the shock at the beginning and end of the three evolutionary phases we have described. At this point we must fix the velocity v_{low} setting the limit at which the shock stops disrupting the dust grains. A typical value is about 50 km/s (see Nozawa et al. 2006, 2007, for a thorough discussion of this point). Knowing the limit velocity, we can soon determine the time in which the remnant expanding at the limit velocity covers a distance equal to its own radius. The swept up mass is:

$$M_{swept} = \frac{4}{3} \pi R (v_{low})^3 n_H. \quad (86)$$

The other factors of Eqn. (76) are the ratio σ_i^M/R_{SN} and the coefficients ϵ_i that describe the fraction of the element i -th condensed into dust that is destroyed by the shock. While the ratio σ_i^M/R_{SN} is simply provided by the chemical model in use, to calculate ϵ_i we refer to the studies by Nozawa et al. (2006, 2007). In brief, the Nozawa et al. (2006) data are used in the first evolutionary phases of the galaxies to derive the destruction coefficients for the ISM dust. From Table (6) of Nozawa et al. (2006) we take the a_i and b_i to be used in:

$$\epsilon_j = a_j E_{51}^{b_j} \quad (87)$$

where E_{51} is the energy of the supernova in units of 10^{51} erg. For simplicity we assume $E_{51} = 1$, typical energy of the explosion of SN α of mass not too high, that according to the IMF are also the most numerous. In this way we get the coefficients to be used for destruction by forward shocks in the ISM. Furthermore, the results by Nozawa et al. (2007) are used to constrain the yields by the SN α progenitors, before dust is injected into the ISM where it will interact with the shocks generated by the surrounding SN α . Therefore we take into account the amount of material injected into the ISM (Nozawa et al. 2003) corrected for the effect of the internal reverse shock.

7. Solar System Abundances

To validate the results of our model we need a reference set of chemical abundances to compare. They are also known as the *cosmic reference abundances*. Usually, the Solar System abundances provide the comparison set of values, but other choices are possible (Savage & Sembach 1996; Asplund et al. 2009; Whittet 2010). Since the solar system abundances can not be determined directly from measurements of the ISM, because of the depletion of the elements accreted into dust, two main sources of information are usually adopted: spectroscopic data inferred from the Sun and Meteoritic Abundances.

Photospheric abundances of the Sun can not be determined directly, but only by means of a model atmosphere of the solar spectrum. The model must be able to calculate lines formation (classical 1D or hydrodynamical 3D), and takes into account radiative transfer and non-LTE processes (see Basu & Antia 2008, for a review about solar abundances obtained from spectroscopy). However, since there are no lines of noble gases in the solar photosphere, coronal lines, energetic particles or solar wind are also studied, in particular to determine the crucial abundances of He and Ne.

Between the tens of thousands meteorites fell on the earth, only five are C1 carbonaceous chondrites (Lodders et al. 2009). They form the only group of meteorites allowing us to determine the abundances in the proto-solar environment that match the solar ones, and keep some memory of the original proto-environment. However, volatile elements and noble gases like H, He, C, N, O, and Ne, therefore including the most abundant elements, are heavily depleted in these meteorites. We can not rely on mass spectrometry to safely determine their abundances, but an additional source of information must be adopted.

It is common practice to combine photospheric and meteoritic measurements to get the compilations of abundances commonly used in literature and continuously updated year after year (Anders & Grevesse 1989; Grevesse & Noels 1993; Grevesse & Sauval 1998; Lodders 2003; Asplund et al. 2005a; Grevesse et al. 2007; Lodders et al. 2009; Asplund et al. 2009).

Two points are worth of mention. (i) According to the most recent models, the present photospheric abundances of the Sun are lower than the bulk abundances of the proto-Sun formed about 4.6 Gyr ago because of the physical processes taking place in the deep convective region under the solar surface. The effects of thermal diffusion, gravitational settling due to differential gravity and radiative acceleration (Turcotte & Wimmer-Schweingruber 2002) allow helium and heavy elements to deposit in the interiors

Table 1. Chemical abundances for the Sun at the present age according to the classical compilation by Grevesse & Sauval (1998) (GS98 - photospheric solar abundances) and the more recent ones by Asplund et al. (2009) (AGSS09 - photospheric solar abundances) and Lodders et al. (2009) (LPG09 - photospheric and meteoritic abundances compilation). Finally, in the last column we present the abundances we have adopted in this study. The Abundance A(X) of the element X is in units of $\log_{10}(N(X)/N(H))+12$. Only the elements included in our chemical model are reported and discussed

Element	GS98	AGSS09	LPG09	This work
H	12.00	12.00	12.00	12.00
He	10.93±0.004	10.93±0.01	10.93±0.02	10.93±0.02
C	8.52±0.06	8.43±0.05	8.39±0.04 ¹	8.50±0.06 ⁷
N	7.92±0.06	7.83±0.05	7.86±0.12 ²	7.83±0.05
O	8.83±0.06	8.69±0.05	8.73±0.07 ³	8.73±0.06
Ne	8.08±0.06	7.93±0.10	8.05±0.10 ⁴	7.99±0.10
Mg	7.58±0.05	7.60±0.04	7.54±0.06 ⁵	7.57±0.05
Si	7.55±0.05	7.51±0.03	7.53±0.01 ⁶	7.53±0.01
S	7.33±0.11	7.12±0.03	7.16±0.02 ⁵	7.14±0.03
Ca	6.36±0.02	6.34±0.04	6.31±0.02 ⁶	6.34±0.04
Fe	7.50±0.05	7.50±0.04	7.46±0.08 ⁵	7.50±0.04
z/X	0.0231±0.018	-	-	-

¹This is the same low photosphere value as in Lodders (2003), selected from Allende Prieto et al. (2002), and confirmed in Asplund et al. (2005b) and Scott et al. (2006). ²N is taken from Caffau et al. (2009), from solar photospheric models. ³The O abundance is an average from solar photospheric models by Caffau et al. (2008); Ludwig & Steffen (2008); Meléndez & Asplund (2008). ⁴Ne abundance is an average from Morel & Butler (2008); Landi et al. (2007). ⁵Average between solar and meteoritic values. ⁶Meteoritic value. ⁷Caffau et al. (2010).

of the Sun. The decay of radioactive elements affects the isotopic compositions (Piersanti et al. 2007; Lodders et al. 2009). The correction needed to obtain the unfractionated abundances of the proto-Sun is of about 0.05 dex for He and 0.04 dex for heavier elements (Asplund et al. 2009) or slightly higher of 0.01 dex for both corrections (Lodders et al. 2009). With these corrections there is agreement with the abundances observed in nearby B stars by Przybilla et al. (2008). (ii) The He and Ne abundances determined with coronal lines or solar wind suffer from the FIP effect. Therefore the most precise method to determine the He abundance is helioseismology and the adiabatic index Γ_1 , whereas for Ne abundance are the photospheric ratios Ne/O and Ne/Mg together with their systematic errors (Basu & Antia 2008).

Starting from Allende Prieto et al. (2001, 2002), the widely used compilation of abundances by Grevesse & Sauval (1998) has been the subject of a continuous revision of the photospheric C, N, O abundances toward a significantly lower value, i.e. about 0.2 dex lower than before (Asplund et al. 2004, 2005a,b). These new values, derived from 3D hydrodynamical models with updated input physics and no macro- and micro-turbulence, bring the Sun to better agree with the metal content of the Galactic neighbourhood (Turck-Chièze et al. 2004). They are also in good agreement with recent determinations of B-star abundances (Nieva & Przybilla 2008b,a) and car-

bonaceous C1 chondrites for many elements (Asplund et al. 2005b; Lodders et al. 2009; Asplund et al. 2009). There is also a better agreement between different diagnostics (OI, [OI] and OH vibrational and roto-vibrational bands for Oxygen, CI, [CI], CH, C₂ and CO for Carbon), but a strong disagreement with the helioseismological models (Antia & Basu 2005; Bahcall et al. 2005a,b; Antia & Basu 2006; Basu & Antia 2008). In brief, the position of the base of the convective zone, the helium abundance, sound speed and density profiles are all affected by the revised abundances (Basu & Antia 2008). Many suggestions have been advanced to solve this discrepancy, e.g. increased input opacities, increased abundances of neon or other elements, fine tuning of the diffusion process, inclusion of other additional physical processes etc. All this, however, without removing the discrepancy. The recent revision of the abundance compilation by Asplund et al. (2009), reversed the trend toward higher abundances, thus in closer agreement with helioseismology, even if the differences are still significant. Also, a series of models calculated over the past few years (all based on the so-called CO⁵BOLD 3D hydrodynamical code) go toward a reconciliation with helioseismology (Caffau et al. 2008; Caffau & Ludwig 2008; Caffau et al. 2009; Ludwig et al. 2009; Maiorca et al. 2009; Caffau et al. 2010). Anyway, as pointed out in Caffau et al. (2010), results from different 3D hydrodynamical simulations may still mutually differ by as much as 0.1 dex, suggesting that better validation of the hydrodynamical models and more and more updated solar models are needed (Turck-Chièze et al. 2008).

In Table 1 we show the classical set of abundances by Grevesse & Sauval (1998) (GS98), the two most recent compilations available in literature by Asplund et al. (2009) (AGSS09) and Lodders et al. (2009) (LPG09) and, finally, in the last column, our adopted reference set for the present-day solar abundances. The abundances by number of the various elements are indicated by $A(X)$ which stands for $\log_{10} (N(X)/N(H)) + 12$.

Let us now examine in some detail the choice we made for the abundances of the various elements included in our model:

Carbon: the carbon abundance is $A(C)=8.50\pm 0.06$ according to Caffau et al. (2010). It corresponds to a weak efficiency of the collisions with neutral hydrogen atoms ($S_H = 1/3$). The uncertainty is the sum of statistical (0.02) and systematic (0.04) errors. This value is similar to the old GS98 determination and very close to the average estimate of the carbon abundance during the past thirty years (see Table 4 in Caffau et al. 2010).

Nitrogen: the abundance of Nitrogen determined by AGSS09 does not much differ from that by LPG09, but it is significantly lower than GS98. We adopt the value by AGSS09 $A(N)=7.83\pm 0.05$. As this is derived from both atomic and molecular lines, the error is minimized.

Oxygen: Oxygen, together with Neon, are the most debated and uncertain elements (Asplund et al. 2009). LPG09 adopted the average value between the estimate from CO⁵BOLD atmosphere models by Caffau et al. (2008) (8.76 ± 0.07), that by Ludwig & Steffen (2008) (8.72 ± 0.06), and the one by Meléndez & Asplund (2008) (8.71 ± 0.02). AGSS09 recommends 8.69 ± 0.05 obtained from atmosphere models with updated physics and taking the mean value of estimates based on [OI], OI, OH vibration-rotation and OH pure rotation. Whittet (2010) adopts 8.76 ± 0.03 based

upon observations of nearby B-stars (Przybilla et al. 2008). Averaging all these values, we adopt 8.73 ± 0.06 .

Neon: the abundance of Neon proposed by AGSS09 (7.93 ± 0.10) is determined from their O abundance and the Ne/O ratio. LPG09 (8.05 ± 0.10) takes the mean value between measurements in B-type stars and UV-flares. The proposed values are very different. We adopt the average value of 7.99 ± 0.10 . The corresponding Ne/O ratio is 0.182 in very good agreement with Young (2005) and Schmelz et al. (2005).

Magnesium: magnesium *gf*-values for the two ionization stages MgI and MgII suffer of well know uncertainties, as underlined in AGSS09. For this reason we adopt the weighed average between the LPG09 meteoritic abundance 7.55 ± 0.01 and the AGSS09 value, obtaining 7.55 ± 0.05 .

Silicon: silicon is the element linking meteoritic and photospheric measurements. Since H is very depleted in C1 chondrites, meteoritic abundances are usually expressed in the cosmochemical scale as number of atoms per 10^6 Si atoms. If the abundance by number of Si is known, we may easily obtain the abundance by number of any element in the usual scale $A(X) = \log_{10} (N(X)/N(H)) + 12$. The various estimates of the Si abundance listed in Table 1 agree quite well each other. Therefore we can adopt the estimate by LPG09 that is the average between the solar photospheric and meteoritic values.

Sulfur: the sulfur abundance has been revised by AGSS09, including additional lines and NLTE corrections. We take the mean between this value and the meteoritic abundance by LPG09 (see their Table 4).

Calcium: for the abundance of Calcium we choose the value proposed by AGSS09, which is in good agreement with LPG09 and GS98 and is based upon recent NLTE abundance corrections by Mashonkina et al. (2007).

Iron: we adopt the value given by AGSS09, in excellent agreement with the meteoritic measurement by LPG09 and GS98.

Once the reference abundances are assigned, we can tackle the element depletion in the ISM, that is the underabundance of some elements compared to the corresponding reference value, because a fraction of the element under consideration is locked up in the interstellar dust. The depletion of the element X in the ISM is measured in the following way. Following Jenkins (2009) and Whittet (2010) we define

$$[X_{gas}/H] = \log [N(X)/N(H)] - \log (X/H)_{ISM} \quad (88)$$

where $N(X)$ is the column density of the element X and $N(H) = N(HI) + N(H_2)$ the same for hydrogen and, finally, and $(X/H)_{ISM}$ the assumed reference abundance. If part of the element X is locked up into dust grains ($[X_{gas}/H] \leq 0$), the fractional abundance of the element depleted into dust is

$$(X_{dust}/H) = (X/H)_{ISM} \cdot \left(1 - 10^{[X_{gas}/H]}\right). \quad (89)$$

Usually, establishing the degree of depletion of an element is a cumbersome affair, because the choice of the reference abundance is a difficult task and errors and inconsistencies affect the measurements (Whittet 2003, 2010). Recently, Jenkins (2009) presented a thorough study of the depletion for 17 elements along 243 lines of sight, trying to

focus on the rates of depletion and leaving aside the problem of the reference abundance. He was able to characterize the degree of depletion according to three parameters: one describes the overall level of depletion along a particular line of sight; the other two are related to the depletion of each element along that line. Once adopted the reference abundances proposed by Lodders (2003) for the proto-sun, Jenkins (2009) presents the depletion parameters for the smallest and largest depletion efficiencies (his parameter F_*), thus bracketing the region to be matched by any theoretical model. In the context of the present study, to correctly make use of the Jenkins (2009) results, the following remark is appropriate. Jenkins (2009) analysis stems from the Lodders (2003) present reference abundances (see his Table 1) which is different from the one we have adopted (see the entries of Table 1. Therefore, a suitable shift has to be applied. Furthermore, the Lodders (2003) reference abundances for the proto-solar environment have been obtained from the present-day solar+meteoritic ones by adding ~ 0.07 , which is likely too a correction (Jenkins 2009; Lodders et al. 2009; Przybilla et al. 2008). Therefore, we derive our present-day reference abundances applying the more realistic correction suggested by (Asplund et al. 2009).

Table 2 shows the reference abundances for the SoNe used by Jenkins (2009) and those adopted in our set for the proto-solar environment, together with the upper and lower limits for the smallest ($F_* = 0$) and heaviest ($F_* = 1$) depletion efficiencies adapted from Jenkins (2009) to our case. Calcium deserves some remarks. It is not included in the Jenkins (2009) list, whereas we take it into account. Furthermore, as this element is heavily depleted in the ISM (Whittet 2003; Tielens 2005), we consider the values proposed by Crinklaw et al. (1994) for the smallest and heaviest depletion. The value proposed by Whittet (2003) for the diffuse clouds falls in the middle.

In Fig. 2 we finally show the range of depletions adopted in our work to test the simulations versus the SoNe. Since the depletion is line-of-sight dependent, we show for each element the range allowed taking into account the smallest and largest depletion with relative error bars. The values of depletion for cool and warm disk are also shown. For the sake of clarity, we expanded the depletion range for C, N, O in the lower left corner of the figure.

8. Models of the ISM with dust: results

The chemical model for disk galaxies we are proposing extends the the original dust-free, multi-zone model with radial flows developed by the Padova group over the years (Chiosi 1980; Chiosi & Maeder 1986; Portinari et al. 1998; Portinari & Chiosi 1999, 2000; Portinari et al. 2004b,a) to which the reader should refer for all the details not mentioned here. The model is quite complicate and obviously contains many parameters. Therefore it would be wise to suitably select the parameters to vary guided by some general considerations to be kept in mind: (i) This study is mainly devoted to highlight the role of dust in chemical models rather than perfectly reproducing the properties of gas and stars of the MW in the local pool. Again dust properties will be the target of a forthcoming paper, just as function of the galacto-centric distance along the MW Disk (Piovan et al. 2011c). For this reason various recipes for dust formation and evolution in the ISM must

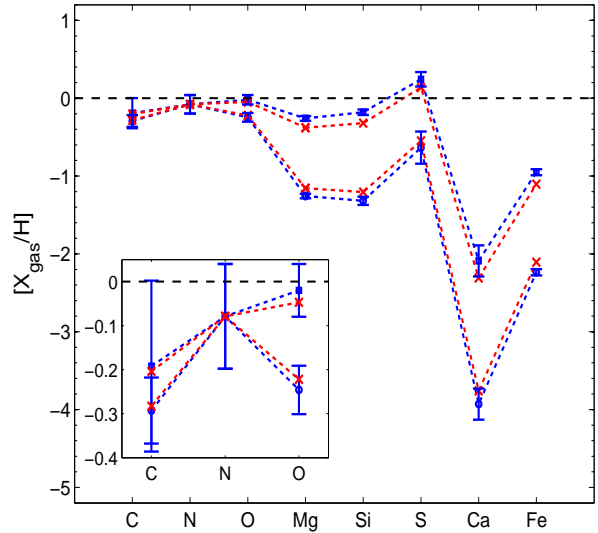


Fig. 2. The range of depletions is shown for those elements in our list that intervene in the dust formation or are present in the ejecta by AGB stars and SN α (C, N, O, Ms, Si, S, Ca and Fe). The insert shows in detail the depletions for C, N and O. Four values are plotted for each element. Filled squares and circles represent the smallest and largest depletion, respectively. The crosses determine the range for the depletion in the Warm and Cool components of the Galactic Disk, according to Jenkins (2009) and Savage & Sembach (1996). See Table 2 for more details.

be tested. (ii) A reasonable agreement between model results and observational data for gas, dust and stars (both in the solar vicinity and across the galactic disk) must be reached for the sake of physical consistency of the whole model. (iii) Finally, we will take advantage of the results already obtained by Chiosi (1980); Chiosi & Maeder (1986); Portinari et al. (1998); Portinari & Chiosi (1999, 2000); Portinari et al. (2004b,a) as far as the fine tuning of several important parameters is concerned.

In the following each model is identified by a string of nine letters (the number of parameters) in italic face whose position in the string and the alphabet corresponds to a particular parameter and choice for it. The position in the string is the same as in the list below. Let's now shortly comment on the parameters we have considered and the choices we have made for each of them together with the identification code.

- (1) **The IMF with its lower and upper limits and the fraction ζ of stars with mass $M > 1M_{\odot}$.** Eight IMF are considered as described in Sect. 3: Salpeter (*A*), Larson (*B*), Kennicutt (*C*), Kroupa original (*D*), Chabrier (*E*), Arimoto (*F*), Kroupa 2002-2007 (*G*), Scalo (*H*) and, finally, Larson adapted to the SoNe (*I*). Since some of them are similar, we will examine in particular only the results obtained for some interesting cases useful to understand the influence of the IMF. The Upper and lower mass limits (and ζ) are selected according to the default values already given in Sect. 3.
- (2) **The Star Formation law.** Five SFR are considered (Sect. 3: constant SFR (*A*), Schmidt law (*B*), Talbot & Arnett (T&A - *C*), Dopita & Ryder (D&R - *D*) and, finally, Wyse & Silk (W&S - *E*).

Table 2. In column (1) we list the elements we have considered. In columns (2) and (3) we show the chemical abundances for the proto-solar environment, according to the Lodders (2003) compilation adopted by Jenkins (2009) and the values we have adopted. In columns (4) and (5) we give $[X_{\text{gas}}/H]_0$ and $[X_{\text{gas}}/H]_1$, the smallest and largest depletion values for the various elements are obtained from Jenkins (2009), with a correction to account for the difference between the reference set of elemental abundances. In column (6) we list the abundances in the ISM and in columns (7) and (8) we show the abundances of elements in dust in units of $10^6 (X_{\text{dust}}/H)$, for the smallest and largest depletions, respectively. Finally columns (9) and (10) show the abundances for the Warm Disk and the Cool Disk, according to the fit made by Jenkins (2009) of the Savage & Sembach (1996) data

Element	$A(X)^1$	$A(X)^2$	$[X_{\text{gas}}/H]_0$	$[X_{\text{gas}}/H]_1$	$(\frac{X_{\text{ISM}}}{H})_{\odot}$	$(\frac{X_{\text{dust}}}{H})_0$	$(\frac{X_{\text{dust}}}{H})_1$	$[X_{\text{gas}}/H]_{WD}$	$[X_{\text{gas}}/H]_{CD}$
(1)	(2)	(3)	(4)	(5)	(6)	(7)	(8)	(9)	(10)
H	12.00	12.00	-	-	10^6	-	-	-	-
He	10.984 ± 0.02	10.98 ± 0.02	-	-	$9.5 \cdot 10^4$	-	-	-	-
C	8.46 ± 0.04	8.54 ± 0.06	-0.192 ± 0.194	-0.293 ± 0.075	347	124^{+80}_{-124}	170^{+28}_{-33}	-0.204	-0.283
N	7.90 ± 0.11	7.87 ± 0.05	-0.079 ± 0.119	-0.079 ± 0.119	74	12^{+15}_{-19}	12^{+15}_{-19}	-0.079	-0.079
O	8.76 ± 0.05	8.77 ± 0.05	-0.020 ± 0.060	-0.246 ± 0.055	588	27^{+73}_{-82}	255^{+40}_{-45}	-0.047	-0.222
Ne	8.08 ± 0.06	7.97 ± 0.10	-	-	93	-	-	-	-
Mg	7.62 ± 0.02	7.61 ± 0.05	-0.260 ± 0.030	-1.257 ± 0.029	41	18^{+2}_{-2}	38^{+1}_{-1}	-0.380	-1.157
Si	7.61 ± 0.02	7.57 ± 0.01	-0.180 ± 0.035	-1.319 ± 0.052	37	13^{+2}_{-2}	35^{+1}_{-1}	-0.320	-1.205
S	7.26 ± 0.04	7.18 ± 0.03	0.243 ± 0.092	-0.635 ± 0.206	15	$-11^{+6.3}_{-6}$	12^{+2}_{-2}	0.137	-0.548
Ca	6.41 ± 0.03	6.38 ± 0.04	-2.090 ± 0.200	-3.930 ± 0.200	2.4	2.38	2.398	-2.311	-3.746
Fe	7.54 ± 0.03	7.54 ± 0.04	-0.951 ± 0.038	-2.236 ± 0.041	35	31^{+1}_{-1}	34^{+0}_{-0}	-1.105	-2.107

Abundances $A(X)$ of the element X are in units of $\log_{10} (N(X)/N(H)) + 12$. ¹Proto-solar abundances adopted in (Jenkins 2009). ²Proto-solar abundances adopted in this work. ³The positive depletion of sulfur means that instead of observing a depletion of the element the gas seems to be enriched of sulfur atoms respect to the reference set.

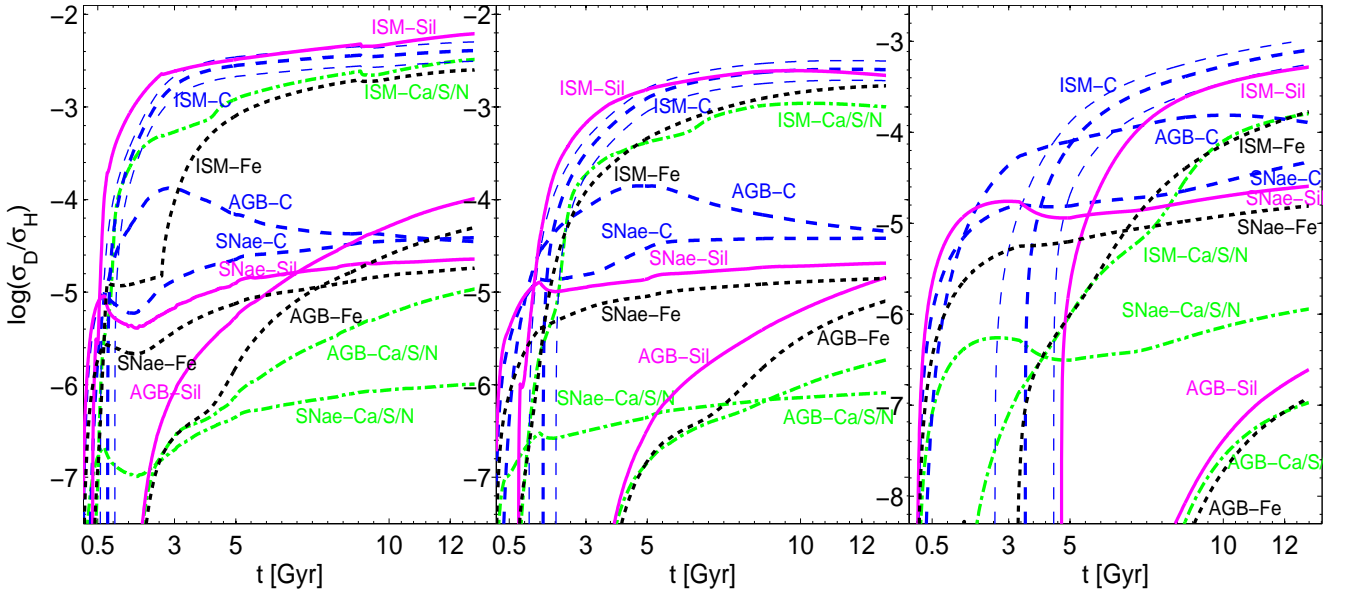


Fig. 3. Temporal evolution of the contribution to the abundance of dust by the four types of grain (on which we distributed the single elements) and the three sources. All the contributions have been properly corrected for the destruction of dust. **Left panel:** results for an inner ring of the MW centered at 2.3 kpc. We show: silicates (continuous lines), carbonaceous grains (dashed lines), iron dust (dotted lines) and, finally, other grains bearing S, Ca and N (dot-dashed lines). For each group we distinguish the net contributions from the ISM accretion, AGB and SNae, that is: ISM-C, AGB-C and SNae-C for carbon grains, ISM-Sil, AGB-Sil and SNae-Sil for silicates, ISM-Fe, AGB-Fe and SNae-Fe for the iron dust and finally, ISM-Ca/S/N, AGB-Ca/S/N and SNae-Ca/S/N for the other grains. The two thin dashed lines represent the same *GDABBCBBB* model but with 15% (upper dashed line) and 45% (lower dashed line) of CO. In all cases $\xi_{\text{CO}} = 0.30$ as default value. **Central panel:** the same as in the left panel but for the SoNe at 8.5 kpc. **Right panel:** the same as in the left panel but for an outer ring at 15.1 kpc. Since the ratio σ_D/σ_H is lower, the scale of the y-axis is shifted respect to the scales for the inner region and the SoNe in the left and central panels.

- (3) The fraction of MCs in which dust accretion takes place. This quantity must be specified because the chemical model in use does not contain a real multi-phase description of the ISM. Two cases are included: a constant fraction (\mathcal{A}) based on the SoNe data ($\chi_{MC} = 0.2$) and a varying χ_{MC} (\mathcal{B}) related to the local SFR and total gas density (see Sect. 4.2).
- (4) The model for the accretion of grains in cold molecular regions. Two choices are available: the simple model by Dwek (1998) based on typical accretion timescales for dust grains as modified by Calura et al. (2008) (see Sect. 4.1) (\mathcal{A}) and the recent and more refined model by Zhukovska et al. (2008) (see Sect. 4.2) (\mathcal{B}).
- (5) The condensation efficiencies for dust in Type Ia SN α . Two cases are possible: Dwek (1998) (\mathcal{A}) and Zhukovska et al. (2008) (\mathcal{B}). In the former they contribute to the dust budget in a way comparable to that of Type II SN α , whereas in the latter their role is negligible except for a small amount of iron in agreement with the observations. The different choices for this parameter have been discussed in Piovan et al. (2011a).
- (6) The condensation efficiencies for dust in Type II SN α . Three choices are possible. The first one by Dwek (1998) who suggests a high condensation efficiency (\mathcal{A}), the efficiencies by Nozawa et al. (2003, 2006, 2007) based on dust nucleation models and taking into account the effects of the reverse and forward shocks (\mathcal{B}), and finally those by Zhukovska et al. (2008) who favor a low condensation efficiency in SN α based upon pre-solar grain observations. The impact of these different choices on the results has been discussed in Piovan et al. (2011a).
- (7) The condensation efficiencies for dust from AGB stars. Two choices are available: the simple recipes by Dwek (1998) (\mathcal{A}) and the condensation efficiencies obtained by full calculations of dust formation in synthetic AGB models by Ferrarotti & Gail (2006) (\mathcal{B}). Again, for more details on these different possibilities for AGB stardust production, see Piovan et al. (2011a).
- (8) The age at which a bar is introduced to reproduce the radial distribution of the gas in the Galactic disk, in particular in the region of the molecular ring around 4 kpc. For the purposes of this work we do not play with the bar effect: the pattern of velocity to simulate the bar effect in the radial flows mechanism is simply taken from Portinari & Chiosi (2000), (to which the reader should refer for all the details) and is suitably chosen for every SFR law. There is no bar-effect on the SoNe, for this reason between the three cases included (no bar effect (\mathcal{A}), an onset of the bar 4 Gyr ago (\mathcal{B}) and 1 Gyr ago (\mathcal{C}), we will simply just fix the bar effect at the case (\mathcal{B}). For more details and discussion on this point, see Piovan et al. (2011c), where the dust formation and evolution on the whole disk is examined.
- (9) The parameters of the SFR laws: these are chosen according to the discussion by (Portinari & Chiosi 1999). While the exponents k or m and n are fixed (see Sect. 3) we let the efficiency of the star formation ν vary and assume three values more or less in the ranges suggested by (Portinari & Chiosi 1999) for every SF law. The minimum value for ν_{min} is case \mathcal{A} and the maximum value for ν_{max} is case \mathcal{C}). The average case is \mathcal{B} .

Table 3 summarizes the parameters we have just described together with their associated identification code: the se-

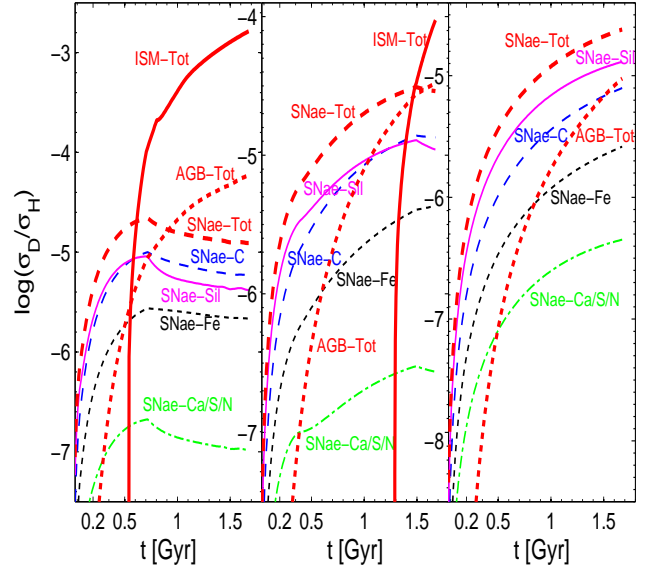


Fig. 4. Temporal evolution of the contribution to the abundance of dust during the *first 1.5 Gyr-2 Gyr*. All the contributions have been properly corrected for the destruction of dust. **Left panel:** results for the inner ring of the MW at 2.3 kpc. We show for the SN α injection: silicates (thin continuous line SN α -Sil), carbonaceous grains (thin dashed line, SN α -C), iron dust (thin dotted line, SN α -Fe) and, finally, other grains bearing S, Ca and N (thin dot-dashed line, SN α -Ca/S/N). The *thick* lines represent the total contribution from one source to the dust budget sub-divided in: SN α (thick dashed line, SN α -tot), ISM (thick continuous line) and AGB (thick dotted line). **Central panel:** the same as in the left panel but for the SoNe at 8.5 kpc. **Right panel:** the same as in the left panel but for the outer ring at 15.1 kpc.

quence must be read from top to bottom. For example, the string *DBAABABAB* corresponds to Kroupa 1998 IMF, Schmidt SFR, ANN model for χ_{MC} , Dwek (1998) accretion model, Zhukovska et al. (2008) type Ia SN α recipe for dusty yields, Dwek (1998) condensation efficiencies for type II SN α , Ferrarotti & Gail (2006) yields for AGB stars, no bar and high efficiency ν of the SFR. If not otherwise specified radial flows and bar effect will always be included by default.

Obviously, these are not the only parameters of chemical models: even the classical ones are themselves very rich of parameters and when including also radial flows, bars and dust formation/evolution the parameter space acquires many more dimensions so that a full exploration of it is a cumbersome affair. However, it may happen that: (1) some variables play a secondary role, thus not influencing that much the results (in particular we focus on the effects related to dust, the target of the work) and just adding second order corrections; (2) some variables, even if playing an important role and influencing significantly the results, have a well defined and/or restricted sphere of influence therefore are not of much interest here because their effect is clear. The parameters belonging to these two classes are not varied in the models, but kept fixed to a suitable value. In the following we examine the effect of some primary and secondary parameters and the general behaviour of the dust model. To this purpose we adopt the

Table 3. Parameters of the models. Column (1) is the parameter number, column (2) the associated physical quantity, and column (3) the source and the italic symbols are the identification code we have adopted. See the text for some more details and Piovan et al. (2011b) for a detailed description.

n ^o	Parameter	Source and identification label
1	IMF	Salpeter ¹ (<i>A</i>), Larson ² (<i>B</i>), Kennicutt ³ (<i>C</i>) Kroupa orig. ⁴ (<i>D</i>), Chabrier ⁵ (<i>E</i>), Arimoto ⁶ (<i>F</i>), Kroupa 2007 ⁷ (<i>G</i>), Scalo ⁸ (<i>H</i>), Larson SN ⁹ (<i>I</i>)
2	SFR law	Constant SFR (<i>A</i>), Schmidt ¹⁰ (<i>B</i>), Talbot & Arnett ¹¹ (<i>C</i>), Dopita & Ryder ¹² (<i>D</i>), Wyse & Silk ¹³ (<i>E</i>)
3	χ_{MC} model	Artificial Neural Networks model ¹⁴ (<i>A</i>), Constant χ_{MC} as in the Solar Neigh. ¹⁵ (<i>B</i>)
4	Accr. model	Modified Dwek (1998) and Calura et al. (2008) (<i>A</i>); adapted Zhukovska et al. (2008) model (<i>B</i>)
5	SNæ Ia model	Dust injection adapted from: Dwek (1998), Calura et al. (2008) (<i>A</i>), Zhukovska et al. (2008) (<i>B</i>)
6	SNæ II model	Dust injection adapted from: Dwek (1998) (<i>A</i>), Zhukovska et al. (2008) (<i>B</i>), Nozawa et al. (2003, 2006, 2007) (<i>C</i>)
7	AGB model	Dust injection adapted from: Dwek (1998) (<i>A</i>), Ferrarotti & Gail (2006) (<i>B</i>)
8	Galactic Bar ¹⁶	No onset (<i>A</i>), onset at $t_G - 4$ Gyr (<i>B</i>), onset at $t_G - 1$ Gyr (<i>C</i>)
9	Efficiency SFR ¹⁷	Low efficiency (<i>A</i>), medium efficiency (<i>B</i>), high efficiency (<i>C</i>)

¹Salpeter (1955). ²Larson (1986, 1998). ³Kennicutt (1983); Kennicutt et al. (1994). ⁴Kroupa (1998). ⁵Chabrier (2001). ⁶Arimoto & Yoshii (1987). ⁷Kroupa (2002b, 2007). ⁸Scalo (1986). ⁹Larson (1986); Scalo (1986); Portinari et al. (2004b). ¹⁰Schmidt (1959). ¹⁰Talbot & Arnett (1975). ¹¹Talbot & Arnett (1975). ¹²Dopita & Ryder (1994). ¹³Wyse & Silk (1989). ¹⁴Piovan et al. (2011c). ¹⁵Zhukovska et al. (2008). ¹⁶Portinari & Chiosi (2000). ¹⁷Piovan et al. (2011b).

GDABBCBBB model as the ‘default’ one, with radial flows and bar included (Portinari & Chiosi 2000) as the reference case. This model uses the most detailed theoretical recipes for the yields of dust and the amounts of MCs, while the SFR and the IMF are simply selected between the available ones.

8.1. Fraction of CO in the ISM

As already discussed in Sects. 5.1 and 5.3, a percentage from 20% to 40% of the Carbon and up to 20% of the Oxygen is locked in the CO molecules (see van Dishoeck et al. 1993; van Dishoeck & Blake 1998). This affects the amount of Carbon available as key-element for the growth process owing to the lowered abundance of this element in the gaseous phase. Furthermore, in the dense and cold regions of the ISM, CO tends to condense onto dust grains (Goldsmith 2001; Bacmann et al. 2002; Whittet 2010), leaving the gas phase and sticking efficiently to dust (Whittet 2010). The depletion of the CO can reach in pre-stellar cores even a factor of 10 (Tafalla et al. 2002; Walmsley et al. 2004). All this is parameterized by the fraction ζ_{CO} of CO. The effect of ζ_{CO} on the key-elements ¹²C and ¹³C (and of ζ'_{CO} on ¹⁷O and ¹⁸O) is straightforward: the higher is the amount in CO, the lower is the amount of free atoms in the gas-phase available for the growth, thus implying longer timescales and slower dust formation. Therefore, we expect a lower contribution by the accretion to the dust budget of the ISM when high values of ζ_{CO} are adopted.

In Fig. 3, we present the time evolution of the contributions to the dust budget for three regions of the MW: a central region ($r_k = 2.3\text{kpc}$), the SoNe ($r_k = 8.5\text{kpc}$) and an outer region ($r_k = 15.1\text{kpc}$). First of all, we do not show the temporal evolution of the single elements, but of important groups of elements representative of the main typical ISM dust types. These are the silicates (olivines+pyroxenes+quartz+silicon in SiC), carbonaceous grains (carbon grains+carbon in SiC), iron grains and, finally, other grains containing S, N and Ca. All the dust abundances have been normalized to the local hydrogen

density and corrected for dust destruction so as to represent the effective net contribution to the dust budget. The contributions are split in three main sources: AGBs, SNæ and ISM accretion. In order to explore the effect of CO, in the *GDABBCBBB* model we vary the CO abundance from 15% up to 45%: the two thin dashed lines in Fig. 3 bracket the region of variation of the ISM contribution. Carbon accretion in the ISM is the only process varying with the CO abundance: the lower ζ_{CO} the higher is the ISM contribution. This effect can be significant and we cannot easily get rid of it when evaluating carbon depletion: however, it is clear and straightforward and limited to the only carbon. Even if ¹⁶O is a component of the CO molecule, due to its high abundance and never being a key-element, it is scarcely affected by variations of ζ_{CO} . The same holds true for ¹⁷O and ¹⁸O but in this case due to their low abundance: their budget depends on ζ_{CO} , but their contribution to the global budget is negligible. Therefore, the variations of ζ_{CO} do not affect the silicates budget.

From the analysis of Fig. 3 we can notice several general features of the dust evolution common to all the models that are worth to be underlined: (i) the main contribution to the dust enrichment during most of the Galaxy lifetime is due to the accretion process in the ISM. Furthermore, dust production is much higher in the inner regions of the Galactic Disk compared to the outer ones where the weight of the ISM gets smaller so that during many Gyr the star-dust injected from AGB stars and SNæ drives the total yields. This is ultimately due to the low number densities of metals that do not favour the accretion process; (ii) the inner regions reach higher metallicities than the outer ones: therefore, all physical processes depending on the metallicities are much enhanced in the central regions of the Galaxy, e. g. the yields of dust from oxygen rich M-stars; (iii) even if some sources (like AGB-C stars in the inner regions) may vary their contributions with time, in general the *total* amount of dust keeps growing monotonically. In some way, this mirrors the metallicity enrichment of the ISM and the fact that dust formation is very sensitive to metals.

In Fig. 4 we show in detail the evolution of the contri-

butions of AGB stars, SN α and ISM to the total budget of dust during the first 1.5-2 Gyr for the three selected regions of the Galactic disk. For AGB, SN α and ISM we show the total budget. However, limited to SN α , we also distinguish the various types of grains. During the early stages, stardust dominates the scene: going from the innermost to the outermost regions it takes more and more time for the ISM accretion to overcome the stellar contribution. This is ultimately due to the higher densities and metal content of the inner regions that favors the onset of accretion. For the outer regions, with low density and low SFR, the ISM starts to be important only at $t > 4$ Gyr (see Fig. 3). It is interesting to note how the dust-to-gas ratio for net yield by SN α is nearly constant going from the innermost regions (left panels of Fig. 4 and 3) to the external ones (right panels of the same figures), even if the associated timescales are much different. Toward the center of the Galaxy, we have more hydrogen, higher SFR, higher SN α rate and higher yields of dust. Both gas (via infall) and SN α dust (via infall, SFR and SN α explosions) grow in absolute value moving from outside to inside, whereas their ratio does not change in the same proportions (considered that in any case the yields of dust by SN α do not depend on the metallicity, at least according to the kind of theoretical results to our disposal).

8.2. The effect of the IMF

Different IMFs influence in a crucial way the injection of dust into the ISM. For every generation of stars, the relative amount of newly born massive objects able to produce dust via the SNa channel and the amount of low and intermediate mass stars refueling the ISM with the dust produced through the TP-AGB phase, both depend on the IMF. This last one also determines the timescales of stardust injection and the relative contribution by SN α and AGB stars.

In Fig. 5 we compare the degree of dust enrichment obtained using nine different IMFs chosen among those widely used in literature. The reference case is always given by the model $\mathcal{GDABBCBBB}$. All the others are obtained from this by varying the first parameter of the list from case \mathcal{A} to case \mathcal{I} . First of all, let us examine the effects of the IMF during the first evolutionary stages, when the dust enrichment is mainly due to SN α , which also supply the seeds and metals for the accretion process in the ISM. We begin with the the solar vicinity displayed in the left panel of Fig. 5. We note that, at varying the IMF and keeping fixed all the other parameters of the model, the age at which the dust enrichment by the accretion in the ISM becomes comparable to that by SN α can vary by about ~ 0.5 Gyr. The time difference can be easily explained as due to the different percentage of massive stars exploding as SN α (and thus refueling the ISM) with the different IMF (see the entries of Table 4).

Some IMFs (like those by Kroupa, Larson SoNe and Scalo) predict a small number of SN α compared to others (like those by Larson, Kennicutt or Chabrier) that are more generous in the number of massive stars and hence Type II SN α . Therefore, in the former case a small injection of dust by SNa explosions and a slow accretion (fewer seeds to disposal) are expected. The opposite holds true with the latter case favouring the formation of massive stars. Furthermore, with the former case the time at which the ISM gets dust-rich by accretion is delayed with respect to the other case. This is also shown in the panels of Fig. 5

Table 4. Mass fractions in different mass intervals predicted by different IMFs. All IMFs are normalized to unity over the mass range of validity. The following nine IMFs are considered: Salpeter, Larson, Kennicutt, original/old Kroupa, Chabrier, Arimoto, new Kroupa multi-slope power law 2002-2007, Scalo and, finally, Larson adapted to the Solar Neighbourhood (See Sect. 3 for more details). The upper mass limit is always $100 M_{\odot}$, whereas the lower limit is chosen according to the discussion made in Sect. 3. Three mass intervals are considered according to the different stardust factories. All masses are in solar units.

IMF	$M < 1$ ¹	$1 \leq M < 6$ ²	$M \geq 6$ ³
Salpeter	0.6075	0.2285	0.1640
Larson	0.3470	0.3568	0.2962
Kennicutt	0.4094	0.3883	0.2023
Kroupa (old)	0.5948	0.3016	0.1036
Chabrier	0.4550	0.3517	0.1933
Arimoto	0.5000	0.1945	0.3055
Kroupa 2002-2007	0.6198	0.2830	0.0972
Scalo	0.6802	0.2339	0.0859
Larson SoNe	0.5614	0.3130	0.1256

¹Fractional mass of stars that do not contribute to the dust budget of stellar origin. ²Fractional mass of stars that contribute to the stardust budget via the AGB channel. ³Fractional mass of stars that contribute to the stardust budget via the type II SN α channel.

where the time when the ISM accretion equalizes the dust enrichment by SN α at decreasing the relative percentage of massive stars in the IMF is marked. It is also evident that IMFs skewed toward massive stars produce much more dust of stellar origin. Consequently, before accretion in the ISM starts driving the evolution of the dust, large differences brought by the IMF are possible.

So far we have examined the solar vicinity with a relatively mild star formation efficiency. What about the innermost region of the MW characterized by a much higher SFR? The situation is shown in the left panel of Fig. 6 which displays the dust enrichment due to SN α as in Fig. 5. Compared to the solar vicinity, we note that SN α produce many more seeds and metals, accretion in the ISM develops faster and becomes important very earlier on. However, in the ISM the dust production by accretion becomes more or less comparable to that by SN α at the same time *independently* of the IMF (see the large dots marked in the left panel of Fig. 6). In the case of the solar vicinity, the crossover stage hardly occurred below 1 Gyr extending up to 1.5 Gyr, whereas now they all fall in the age range 0.6-0.7 Gyr. In a medium rich of seeds, dust accretion grows faster and the effect of the IMF somehow loses importance.

The differences both in the amounts of dust of stellar origin injected and the timescale of earlier enrichment in dust by SN α are very large. In general, the effects induced by variations in the IMF can be very large during the earliest stages of evolution. Along this line of thought, we can expect that in high-redshift obscured galaxies with high SFR (easily even higher than the early SFR of the inner regions of the MW) some IMFs may not be able to produce the amounts of observed dust of stellar origin before the dust accretion process has become significant. The immediate implication of this for primeval galaxies can be easily foreseen. According Draine (2009), some accretion in the ISM

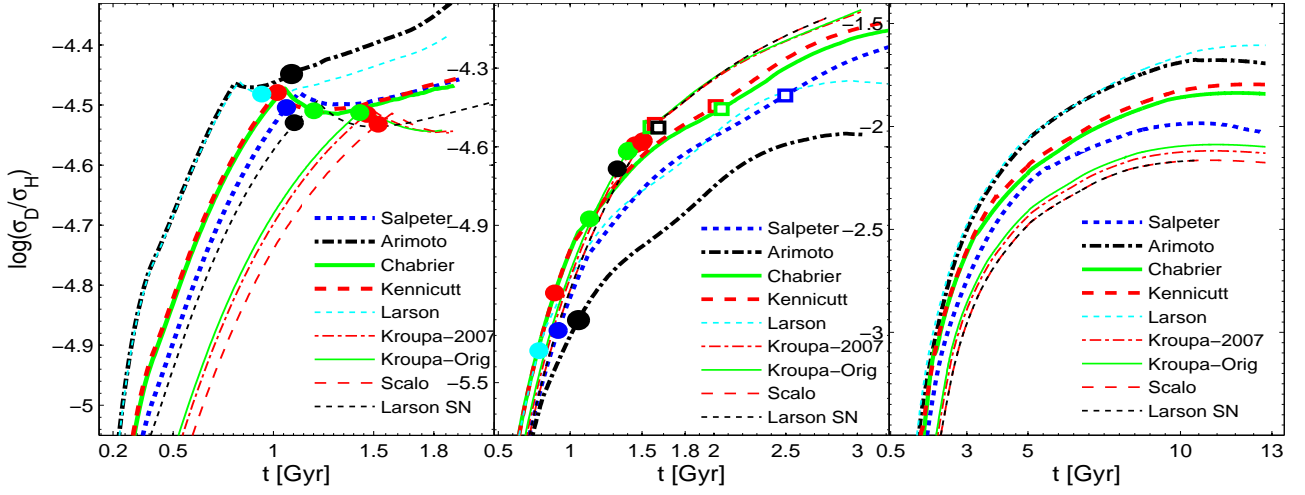


Fig. 5. Temporal evolution of the contribution to the abundance of dust during the *first 2 Gyr-3 Gyr* in the SoNe at 8.5 kpc and for *different IMFs*. All the contributions have been corrected for the destruction of dust. Nine IMFs have been considered: Salpeter (thick dotted line), Arimoto (thick dot dashed line), Chabrier (thick continuous line), Kennicutt (thick dashed line), Larson (thin dotted line), Kroupa-2007 (thin dot-dashed line), Kroupa original (thin continuous line), the Scalo IMF (thin dashed line) and, finally, the Larson IMF adapted to the SoNe (thin dashed line). See Sect. 3 for more details. **Left panel:** temporal evolution of the total contribution to the dust budget by SNæ in the MW SoNe. The filled symbols represent the instant when the contribution by ISM accreted dust *equalizes* the SNæ injected dust amount. **Middle panel:** time evolution of the total contribution to the dust budget by AGB stars for the MW SoNe. The filled symbols represent the instant when the contribution by AGB injected dust *equalizes* the ISM dust production by accretion, while the empty symbols represent the instant (if eventually it happens) when AGB dust equalizes the SNæ injected dust. **Right panel:** time evolution of the total dust budget for different IMFs.

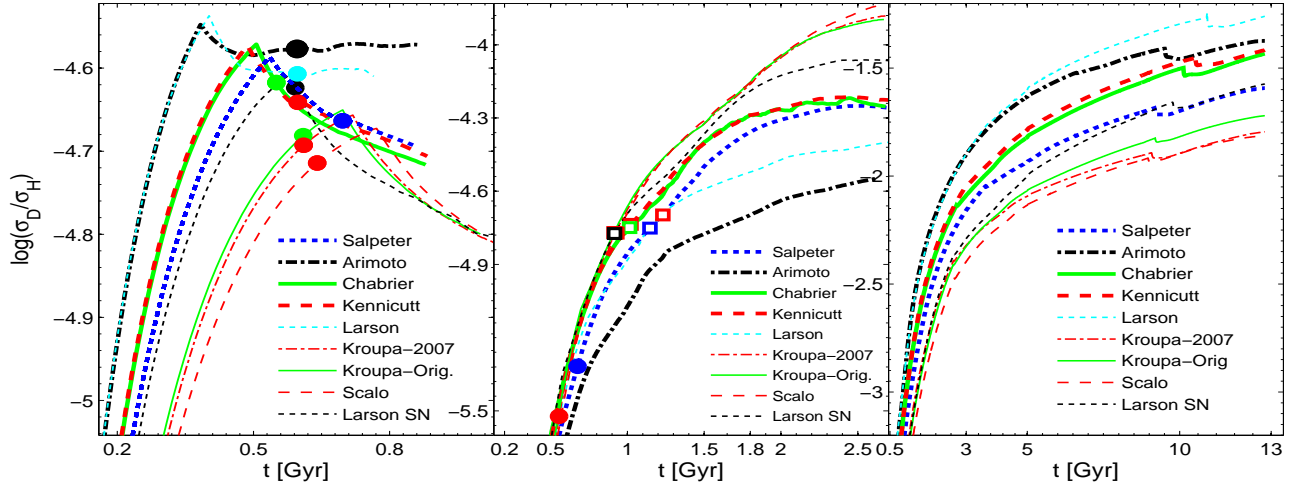


Fig. 6. Temporal evolution of the contribution to the abundance of dust during the *first 1-2 Gyr* in the *inner part* of the MW disk at 2.3 kpc from the centre and for *different IMFs*. All the contributions have been corrected for the destruction of dust. Nine IMFs have been considered as in Fig. 5. See Sect. 3 for more details. The meaning of all the symbols is the same as in Fig. 5.

to explain the amount of dust in observed primeval galaxies is required. The picture should be as follows: (i) before dust by accretion in the ISM and dust injected by stars become comparable, the effect of the IMF prevails and determines the amounts of dust present in the Galaxy; (ii) if the SFR is high, the IMF does not play an important role in determining the onset of the dust accretion process in the ISM, whereas if (iii) the SFR is low, different IMFs cause an important spread in the ages at which dust by accretion becomes important.

We pass now to examine the role played by AGB stars.

In the middle panels of Figs. 5 and 6 we see for the same regions of the left panels the contribution of the AGB stars to the total dust budget. The AGB stars contribute significantly over a longer time-scale: the filled symbols show the age at which dust produced by AGB stars and dust accreted in the ISM become comparable, whereas the empty ones show the same but for AGB stars versus SNæ. In both cases the age is marked when and if the equality among the three contributions can be established. There are indeed some extreme IMFs, where massive stars are favored with respect to the intermediate mass ones progenitors of

AGB stars (like the Arimoto IMF), in which during the first Gyrs AGB stars never reach SN α in the inner MW regions (Fig. 6 - middle panel). Furthermore, IMFs richer in intermediate mass stars produce bigger amounts of dust by AGB stars. This may somehow be correlated with the delayed appearance in a galaxy spectral energy distribution of the PAHs features: the delay may depend on efficiency of dust injection by AGB stars.

Finally, in the right panels of Figs. (5) and (6) we show the evolution of the total dust content in the ISM: it is interesting to note how the differences between the various IMFs in the early stages are the same as those expected (observed) at the present age, keeping constant all other parameters. The IMFs producing more dust by SN α (and of course seeds for accretion) in the early stages are the same for which we get higher amounts of dust at the current age. The differences among the various IMFs can be significant. Indeed, a fast enrichment of dust during the early stages caused by SN α , (keeping fixed all other parameters, the condensation coefficients in particular) goes together with a strong enrichment in metals. More metals means more atoms available for dust to grow in the ISM. For this reason IMFs skewed toward massive stars favor the accretion of dust in the ISM and lead to higher final contents of dust.

8.3. The effect of the SF law

As presented in Sect. 3, four SF laws have been considered. The results are shown in the four panels of Fig. 7 limited to the early stages of the evolution. The reference model is *GDABBCBBB*, in which the SFR is changed as indicated.

The parameters k and ν of the SFR are chosen in agreement with the analysis made by Portinari & Chiosi (1999), in such a way that the sole effect of the SFR law is isolated. All other parameters of the model are kept fixed. At given k and ν , the different SF laws widely adopted for the MW disk produce a similar dust budget. Some differences can be noted (i) in the amount of dust before the onset of the ISM accretion, with the Schmidt and/or Wyse & Silk laws favouring a higher amount of dust by SN α and (ii) in the age at which the production of dust by accretion in the ISM becomes more important than that by SN α . Depending on the SF law, the time interval in which SN α dominate the total dust budget gets short or long.

Given that the specific expression for the SF law is not of primary importance here (at least choosing among the ones we included in this study), we turn the attention to the efficiency of SF represented by the parameter ν . In Fig. 8 we show the contribution to the dust budget in the usual three significant rings of the MW at varying ν from $\nu = 0.30$ to $\nu = 0.70$. As expected lower values of ν imply a smaller rate of SN α and number of AGB stars, therefore a delay in the ISM dust accretion process because there are less seeds/metals injected by stars into the ISM from the stars, and finally a lower total production of dust. As expected, varying the SF parameters affects the system in the early phases of the evolution when the SF is strong. This can be noticed once comparing thin and thick lines in Fig. 8.

Does the efficiency ν affect also the dust budget at the present epoch? In Fig. 9 we show the evolution of the same three regions of Fig. 8 up to the present age of the MW. As we can see, in the inner regions and the solar vicinity, even if there is a significant difference in the past, at the

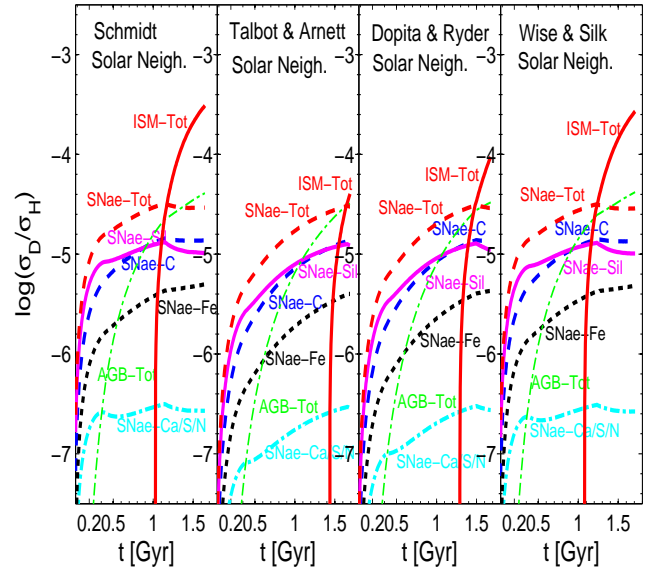


Fig. 7. Temporal evolution of the dust budget in the SoNe during the early stages until 1.5-2.5 Gyr. Four SF laws are shown in the four panels: Schmidt, Talbot & Arnett, Dopita & Ryder and Wyse & Silk. We display: the amount of dust grains accreted in the ISM (continuous lines), the amount of dust injected by AGB stars (thin dot-dashed line), the total amount of SN α stardust (dashed line) also subdivided into the various grain families, respectively, i.e. dotted line (iron-dust), silicates (continuous line), carbonaceous grains (dashed line), and S/Ca/N based grains (dot-dashed line). **Left panel:** Temporal evolution of the dust budget injected in the SoNe by the various sources and the Schmidt law. **Central-left panel:** the same as in the left panel but for the Talbot & Arnett law. **Central-Right panel:** the same as in the left panel but for the Dopita & Ryder SF law. **Right panel:** the same as in the left panel but for the Wyse & Silk SF law.

present time the difference gets negligible, whereas in the outer regions the difference in the dust budgets (both total and partial ones) remains remarkable. This is an effect of the adopted SF laws that are all scaled to the current star formation at the solar neighbourhood and for this reason tend to ultimately produce the same result as the evolution proceeds. However, we expect that if the SF law is not tied up to normalization or scaling factor, the adoption of different SF laws would have a strong impact on the whole evolution. The difference in the outer regions is explained by the long delay in onset of the ISM dust accretion process in the case of low efficiencies ν (very low star forming environment): when eventually the ISM accretion process becomes important, there is not enough time to reach the dust budget produced in the high ν case. This behaviour is also strengthened by the inward radial flows that remove gas from the outermost regions.

8.4. The effects of different models for dust accretion in the ISM

In this study we consider two models of dust accretion in the ISM (see Sects. 4.1, 4.2 and 5 for details): model \mathcal{A} based on Dwek (1998) where accretion is simply included with a general timescale depending on the destruc-

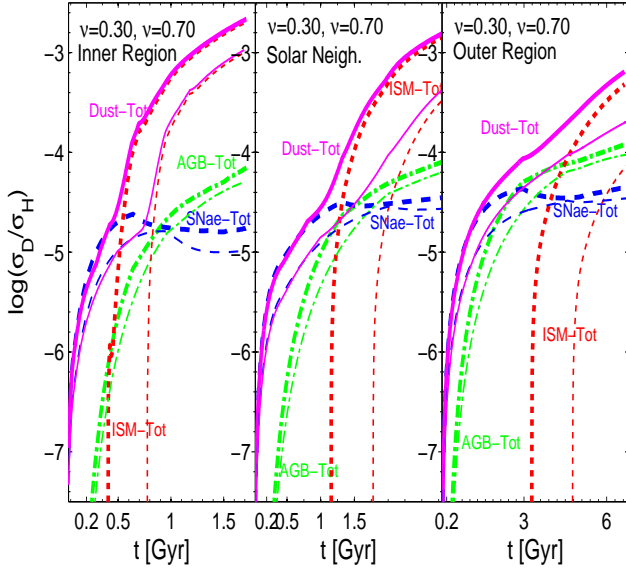


Fig. 8. Temporal evolution of the contribution to the dust budget during the first Gyrs at varying the coefficient ν of the star formation law, namely the Dopita & Ryder SF law, for *three regions* of the MW. The thin line is $\nu = 0.30$ (low efficiency), while the thick line is for $\nu = 0.70$ (high efficiency). We show: the total amount of dust (from accretion in the ISM plus dust ejected by SNæ and AGB stars - continuous line); the contribution by accretion of dust grain in the ISM (dotted line); the total contribution by SNæ (dashed line); the contribution by AGB stars (dot-dashed line). **Left panel:** the results for an inner ring of the MW. **Central panel:** the same as in the left panel but for the SoNe. **Right panel:** the same as in the left panel but for an outer ring of the MW.

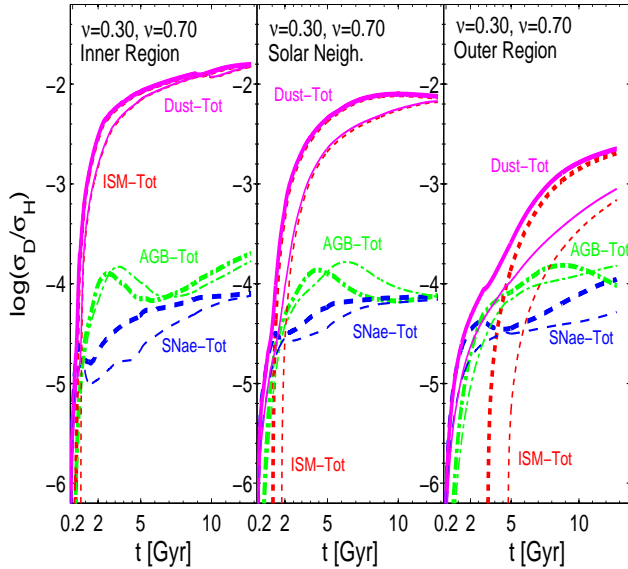


Fig. 9. Temporal evolution of the contribution to the dust budget up to the present age at varying the coefficient ν of the star formation law from 0.30 to 0.70. The meaning of the symbols is the same as in Fig. 8. **Left panel:** the results for an inner ring of the MW. **Central panel:** the same as in the left panel but for the SoNe. **Right panel:** the same as in the left panel but for an outer MW ring.

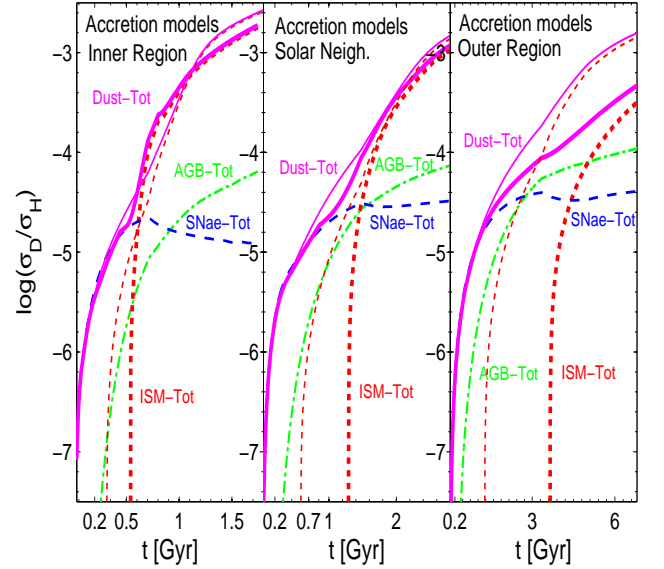


Fig. 10. Temporal evolution of the dust production during the early phases of the MW evolution at varying the accretion model used to describe dust formation in the ISM. Three regions have been considered as usual: an inner one (left panel), the SoNe (middle panel), and an outer region (right panel). Thick lines represent model \mathcal{A} based upon Dwek (1998) and Calura et al. (2008), whereas thin lines represent model \mathcal{B} based upon Zhukovska et al. (2008). For AGB (dot-dashed line) and SNæ (dashed line) we only show one line as the contribution is fixed. We show: the total amount of dust grains in the ISM (continuous lines) and the total amount of accreted dust in the ISM (dotted lines). **Left panel:** The results for an inner region. **Central panel:** The results for the SoNe. **Right panel:** The results for an outer region.

tion timescale. Indeed, the accretion timescale is half of the destruction timescale, and the same value is used for all the elements (Dwek 1998; Calura et al. 2008). Model \mathcal{B} based on Zhukovska et al. (2008) in which a different timescale for each element is adopted and the evolution of the dust abundances for a number of elements, supposedly contained in a several species of dust grains, is followed. Furthermore, there is no *a priori* connection between the destruction and accretion timescales.

In Fig. 10, we show the evolution of the dust budget for the two accretion models. The amounts of dust produced by SNæ and AGB stars and all the other parameters are kept fixed. In particular, the description of the dust destruction process is the same in both cases: therefore we can examine the sole effect of accretion. In the very early stages there is no difference: the budget is dominated by SNæ. The accretion process however starts to be significant very fast in model \mathcal{A} , because it simply depends on the adopted timescale, while in model \mathcal{B} it is more sensitive to the physical conditions of the environment: in general it tends to slow down at decreasing SFR and densities (i.e. passing from the innermost to the outermost regions). Even if there is some difference between model \mathcal{A} and \mathcal{B} , the behaviour of the *total* dust budget is similar. This finding means that if we are interested in the total amount of dust produced, we can do it simply choosing a suitable timescale for dust formation. This holds everywhere but the

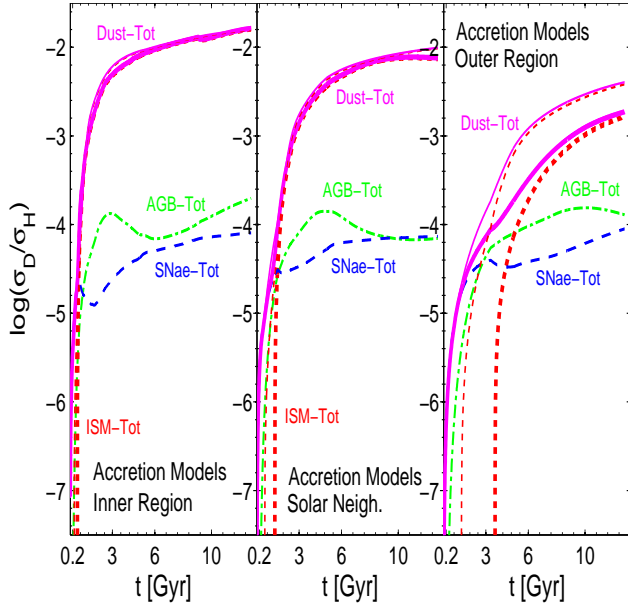


Fig. 11. Temporal evolution of the dust production in the MW up to the present age at varying the accretion model used to describe dust formation in the ISM. **Left panel:** The results for the inner ring. **Central panel:** The same but for the Solar Neighborhood. **Right panel:** The same but for the outer ring.

outer regions where for model \mathcal{A} we probably need a longer timescale of dust formation to closely agree with model \mathcal{B} . This sounds reasonable because it is likely that the accretion timescale varies with the environment. In any case even the simple model of dust accretion with constant timescale is fully adequate to follow the evolution of the *total* dust budget in the early stages of evolution.

In Fig. 11 we extend the evolution up to the present time: in the inner regions and solar vicinity of the MW the differences between the two models are quite small, whereas as expected they are large in the external regions of the disk. In brief, in model \mathcal{A} the accretion in the ISM starts very early independently from the environment and consequently it gives rise to a higher dust content compared to model \mathcal{B} .

A deeper insight of the differences brought by the models of dust accretion is possible looking at the evolution of the single elements composing the dust. In Fig. 12 we show the evolution of some depleted elements up to the present time, namely C, O, Mg, Si and Fe. As expected there is a strong disagreement between the two accretion models in all the regions. In the case of oxygen the difference is striking: model \mathcal{A} with a fixed timescale produces a lot of oxygen in dust. Since there is no description of how the various elements enter the different dust grains, with a fixed timescale the most abundant element is also the most abundant in dust. With a simple model we can not follow, for instance, the different ways in which oxygen is bound in silicates, or iron is bound both in iron-dust and silicates. Of course, only the comparison with the observational depletion factors can highlight the issue. Most likely, model \mathcal{B} taking into account the physical conditions of the medium and following in detail the evolution of typical dust grains should better reproduce the observational depletion factors.

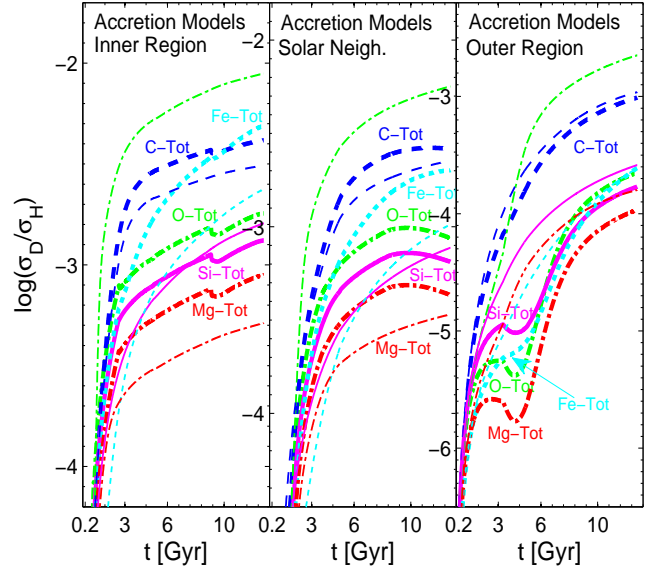


Fig. 12. Temporal evolution of the dust production in the MW up to the present age at varying the accretion model used to describe dust formation in the ISM. In this plot we put into elements the contribution of individual element to the total dust budget. **Left panel:** The results for an inner ring of the MW. **Central panel:** The same but for the SoNe. **Right panel:** The same but for an outer ring of the MW.

8.5. A final note on the model parameters

We have just discussed the main parameters entering the problem of the calculation of the dust enrichment of the ISM. However we must underline the following point: classical chemical models are widely used in literature to follow the metal enrichment in galaxies of different morphology. They are already complicated because of the many physical ingredients entering the problem, like the law of SF, the IMF, the stellar yields and the geometrical description of the galaxy. When the dust is added to the problem, the parameter space literally blows up, because in addition to the classical parameters we have to consider also those governing the dust content. The amount of dust of stellar origin injected in the ISM, the way in which the dust content increases/decreases by accretion/destruction and other physical processes, all these concur to extend the list of parameters. In addition to those we have already discussed, a couple of them deserves some discussion.

- (1) The chemical model we are working with has a single-phase description of the gas content and in particular of the MC component in which the dust accretion takes place. For this reason we have included two possibilities for the MC fraction χ_{MC} . Either χ_{MC} is assumed to be constant and equal to the present day value in the solar vicinity, or it stands on the data for the MW and it correlates the fraction of MCs to the SFR and the gas density through ANNs. In this latter option, that is described in detail in Piovan et al. (2011c), we are therefore assuming a variable amount of MCs. Both the recipes tend to the same value for the current time and produce similar results for the SoNe, that is for our target, since the differences in χ_{MC} , most striking in the early stages of the evolution, are not enough to pro-

duce significant differences. The reason for this can be traced in the SFRs and densities of the SoNe that are never characterized by extreme values. Instead, quite different results between the two recipes are expected for the outer or inner regions of the MW, because of the more significant excursion of the physical variables (Piovan et al. 2011c).

- (2) All our models includes radial flows of matter and the effects of a galactic bar. All the details and typical parameters are taken from Portinari & Chiosi (1999) and Portinari & Chiosi (2000). Radial flows and bar have been taken into account to better reproduce a wide number of properties of the MW disk, in particular to simultaneously reproduce the radial gradients and the peak of gas observed around 4 kpc. The main motivation for including the radial flows and the bar is therefore the consistency between theory and observation as far as the depletion factors, radial/local abundances and gas masses are concerned. However, the bar influences the innermost properties of the MW and it is of no interest in this work. Again, the influence of the radial flows of matter mainly applies to the radial properties of the disk (Piovan et al. 2011c). If limited to the SoNe, their effect could be mimicked with a slightly different choice of the parameters. Concerning the radial flows, it must be finally observed that in principle the pattern of velocities of gas and dust could be different. For the sake of simplicity, we assume here that gas and dust are moving with the same velocities. Thanks to this gas and dust should have similar radial behaviour (see Piovan et al. 2011c, for all details).

9. Models and observations

The final step of our study is to compare the theoretical results with the data in the Solar Vicinity, thus ultimately validating the model we have built up to describe the dust enrichment of the ISM. As we already discussed, the model has many parameters, which together with the many observational data to match would make the search of best-fit solution a huge task to be accomplished. However, pursuing this strategy would not lead us to get a deeper physical insight of the dust formation in the MW Disk and Solar Vicinity in particular. Therefore, instead of looking for the absolute best-fit model, we are more interested in the model response to thoughtful choices of the parameters and in the comparison of model results with data on element depletion, local abundances. The following observational data for the MW are taken in consideration:

- (1) The depletion of the elements in the local ISM (see Sect. 7) is the main check for a dust accretion model. This one to be physically consistent must reproduce the observational depletion of many elements. Obviously the depletion is line-of-sight dependent and we can only estimate the range of plausible values (See Fig. 2).
- (2) The local evolution of the elemental abundances in the Solar Vicinity. This is observationally indicated by many diagnostic planes such as $[El/H]$ vs. $[Fe/H]$ and $[El/Fe]$ vs. $[Fe/H]$ for some elements that are also involved in the dust formation process, derived from large samples of F and G stars. The models need to match those diagnostic planes. This allows us to check that not only the process of dust formation/injection is properly

simulated but also that the total enrichment process, as observed in the different generations of stars, is realistically reproduced.

- (3) The large scale properties of the MW in the Solar Vicinity like the surface densities of stars and gas, rate of SN α , dust-to-gas ratio, and present day SFR must be reproduced.
- (4) The age-metallicity relation in the $[Fe/H]$ vs. Age plane as observed in stars of the Solar Vicinity.
- (5) The metallicity of the Sun at the current age and of the proto-Sun about 4.56 Gyr ago.

The reference model is always $\mathcal{GDABBCBBB}$ according to the parameter list contained in Table 3 and it includes the radial flows and the bar. The main parameters we are going to play with are the star formation efficiency ν , the infall timescale τ and the IMF. For this latter we consider those by Kroupa, Larson (however adapted to the Solar Vicinity in the high mass tail as discussed in Sect. 3) and by Salpeter (usually taken as the reference case for comparison). As already listed in Table 4, we limit ourselves to the IMFs that do not predict a high number of SN α . IMFs of this type are perhaps more suited to other dust-rich environments, like starburst galaxies or ellipticals (Valiante et al. 2009; Gall et al. 2011a,b; Pipino et al. 2011). The MW disk and the Solar Vicinity in particular seem to require IMFs somewhat poor in massive stars (Dwek 1998; Calura et al. 2008; Zhukovska et al. 2008). Four infall timescales are considered, that is $\tau = 1$, $\tau = 3$, $\tau = 6$ and $\tau = 9$, from the shortest to the longest, and four values of the star formation efficiency, $\nu = 0.3$, $\nu = 0.7$, $\nu = 1.1$ and $\nu = 1.5$, from the lowest to the highest efficiencies.

The results of these models are presented in the various panels of Fig. 13. In general, moving from the upper right to the bottom left corner of the figure, the depletion of the elements gets easier to obtain. We find that: (i) in the case with the Kroupa IMF the observational range of abundances is easily reproduced over ample ranges for the remaining two parameters (ν and τ); (ii) models with the other two IMFs lead good results only if the infall timescale τ and the efficiency ν are properly chosen. About the depletion of the individual elements we note what follows:

Carbon: carbon depletion is simulated assuming that the fraction of carbon hidden in the CO molecules amounts to 0.3. This parameter plays a key role as shown in Fig. 3. At varying ξ_{CO} it is possible to allow for less or more dust embedded in C grains, whose accretion depends on the C atoms free to accrete. Carbon depletion is, in any case, well reproduced for the most common sets of the parameters.

Nitrogen: to reproduce the small depletion of nitrogen we find that the simple choice of the longest timescale between the oxygen and carbon, and the use of a mean nitrogen dust grain were not enough to keep low the amount of nitrogen condensed into dust. To this aim, we introduce a multiplicative factor N_X for the accretion time scale $\tau_{N,N}^{gr}$ that enters Eqn. (71) and tune it so that the low observational depletion is reproduced. The results shown in Figs. 13 and 14 include the scaling factor N_X . We get that $N_X \gtrsim 10$ is required to fetch the small accretion of nitrogen.

Magnesium and Silicon: magnesium is embedded into dust thank to the presence of olivines/pyroxenes and in our best simulations it is found to be easily very depleted. The preference goes toward the maximum allowed depletion

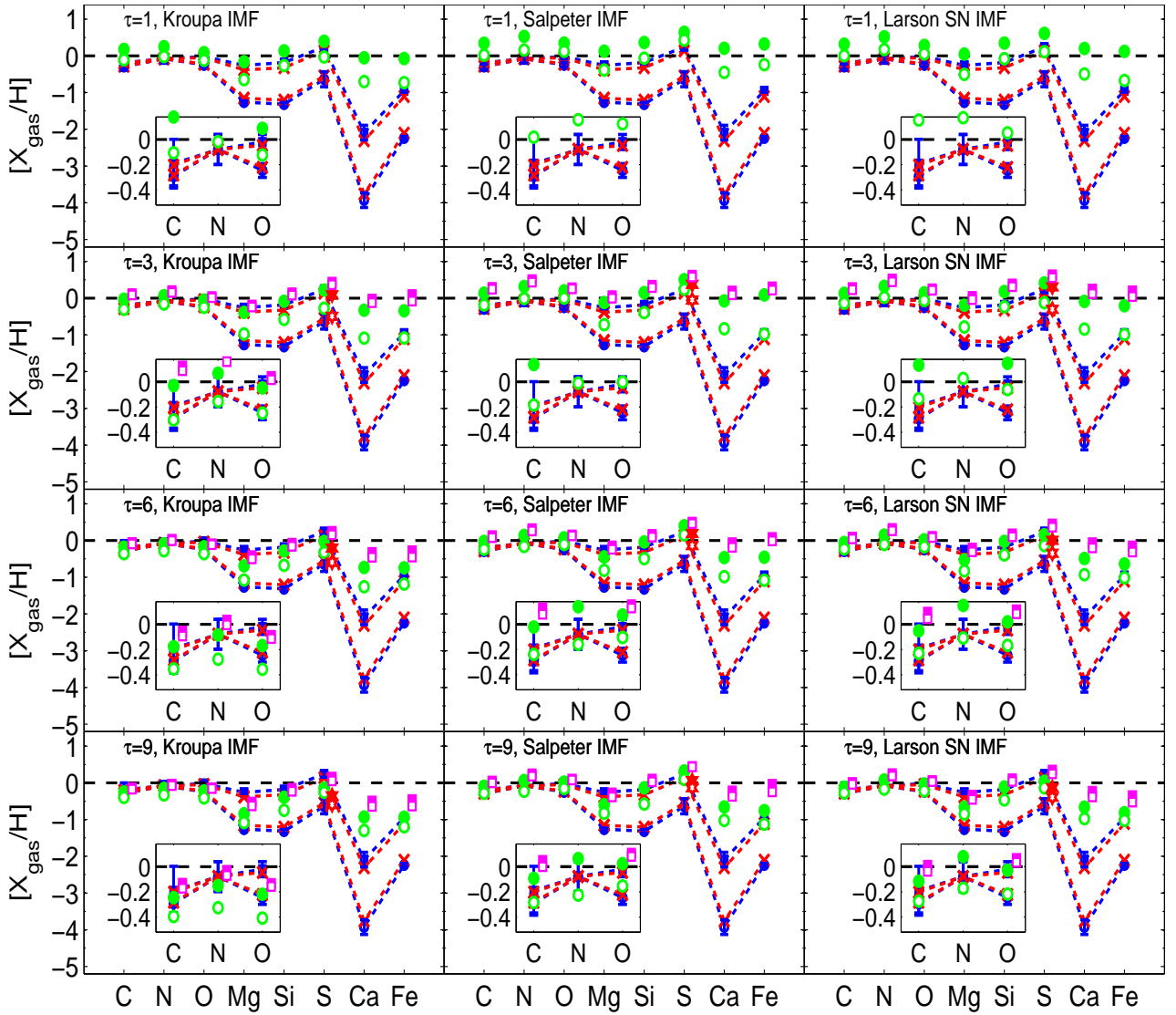


Fig. 13. Depletion of C, N, O, Mg, Si, S, Ca and Fe in the ISM as observed in the SoNe. The observations are compared with the models at varying three important parameters, namely the IMF, the SF efficiency ν , and the mass accretion time scale τ . For the IMF we consider : the recent Kroupa IMF (left panels), the classical Salpeter one (central panels) and the Larson IMF adapted to the SoNe (right panels). These IMFs are all described in Sect. 3). Four cases are considered for ν , that is $\nu = 0.30$ (empty circles), $\nu = 0.70$ (filled circles), $\nu = 1.10$ (empty squares) and $\nu = 1.50$ (filled squares). Finally, four values are used for the accretion time scale, namely $\tau = 1$, $\tau = 3$, $\tau = 6$ and $\tau = 9$ Gyr , from the top line to the bottom line of each panel.

rather than the minimum one. The opposite happens for silicon which is more often found close to the minimum depletion limit (see Fig. 13). This common behavior for Mg and Si can be explained with the under-production of Mg characterizing the SN α e yields by Portinari et al. (1998) that are ultimately based on Woosley & Weaver (1995): This is a long known problem (Timmes et al. 1995; François et al. 2004) that becomes crucial in our case, because Mg is one of the possible key elements driving the accretion process of the silicates. If the amount of Mg atoms available to form dust is under-abundant, this will set up an upper limit to the amount of olivines/pyroxenes that can be formed. In this study, first we calculate models with the original

yields by Portinari et al. (1998)¹ (filled and empty circles and squares in Fig. 13). This choice leads to a dust mixture where Mg (already under-abundant) is usually more depleted than Si. The case is well illustrated in Fig. 13. According to Zhukovska et al. (2008), the yields of Mg based on Woosley & Weaver (1995) could be suited to reproduce the Milky Way once scaled by a factor of 2-3 in order to obtain Mg/Si/Fe ratios in agreement with the observational ones for the MW, thus leading to a dust mixture closer to reality. Keeping in mind this suggestion, we calculate the same models of Fig. 13 slightly modifying the yields of Mg for Type II SN α e, in practice changing the tabulations of Portinari et al. (1998) according to the sug-

¹ The latest version of the yields is used in which the under-abundance of Mg is partially corrected (Portinari, 2011 private communication).

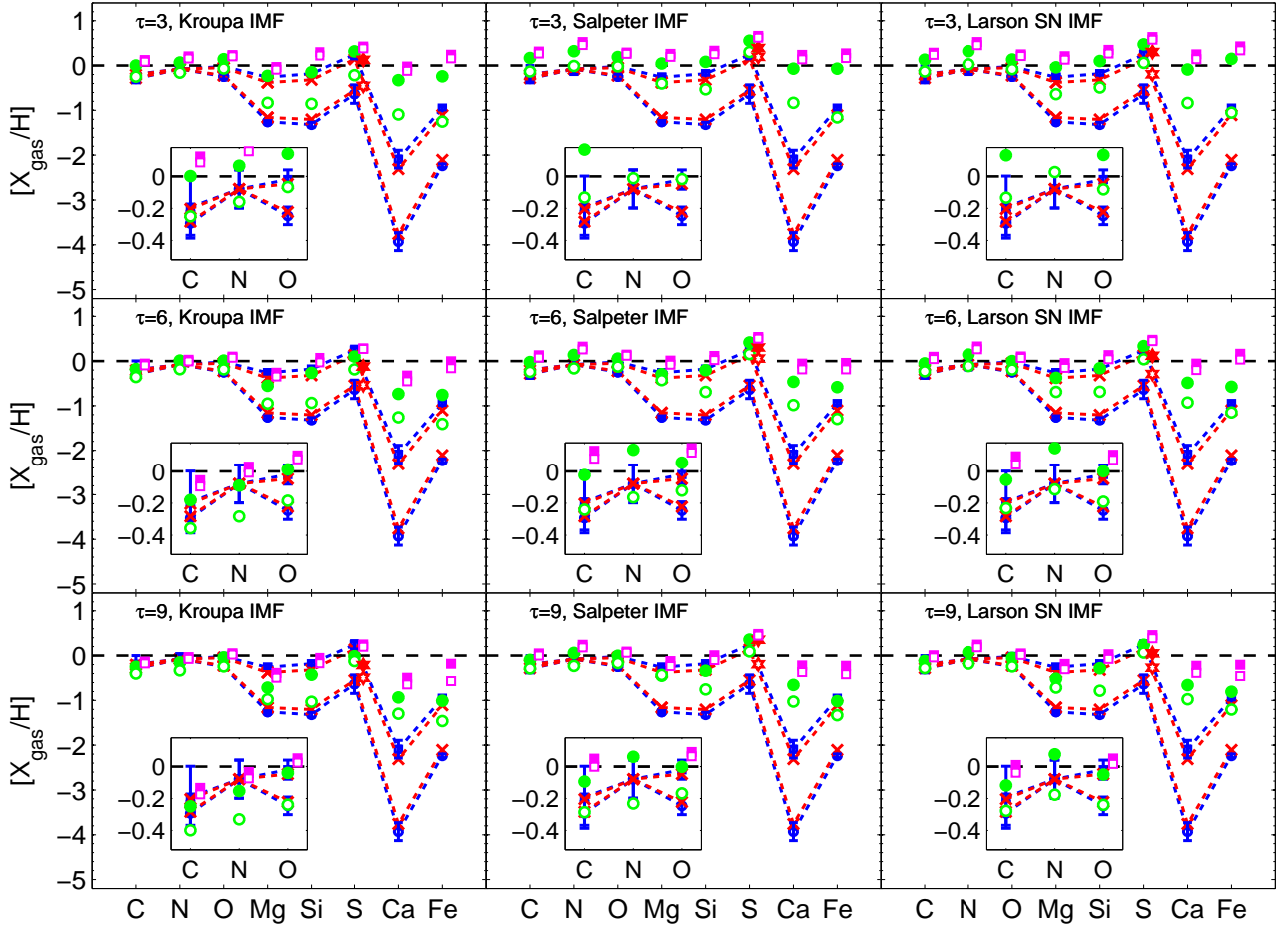


Fig. 14. Depletion of C, N, O, Mg, Si, S, Ca and Fe in the ISM as observed in the Solar Neighbourhood compared with models calculated with enhanced yields of Mg. The observational data is compared with the models at varying of the IMF (three choices), the efficiency of the star formation ν (four choices) and the infall timescale τ (three choices). The meaning of the symbols is the same as in Fig. 2.

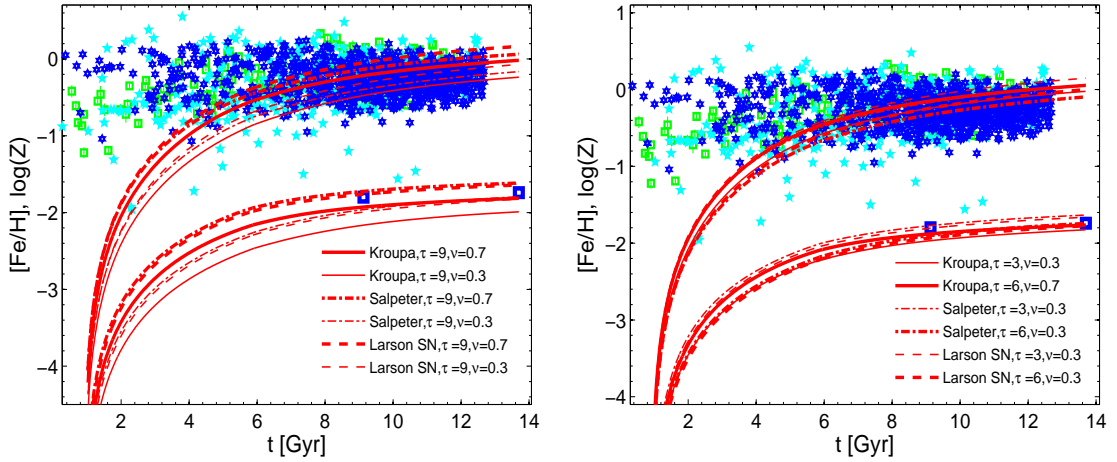


Fig. 15. Temporal evolution of the metallicity Z and the iron abundance $[Fe/H]$ in the Solar Neighborhood for a wide sample of models. Data are taken from Ibukiyama & Arimoto (2002) (dark stars: photometric $[Fe/H]$; light stars: spectroscopic $[Fe/H]$), Ramírez et al. (2007) (squares: sample of thin and thick disk stars). Open squares represent the metallicity of the solar system and of present-day ISM (Gail et al. 2009). **Left panel:** six models are represented, at varying the IMF, the efficiency of the star formation ν and the infall timescale between the values $\tau = 3$ and $\tau = 6$ Gyr. **Right panel:** six models are shown at varying the IMF and the efficiency ν between 0.3 and 0.7 with a fixed infall timescale $\tau = 9$ Gyr.

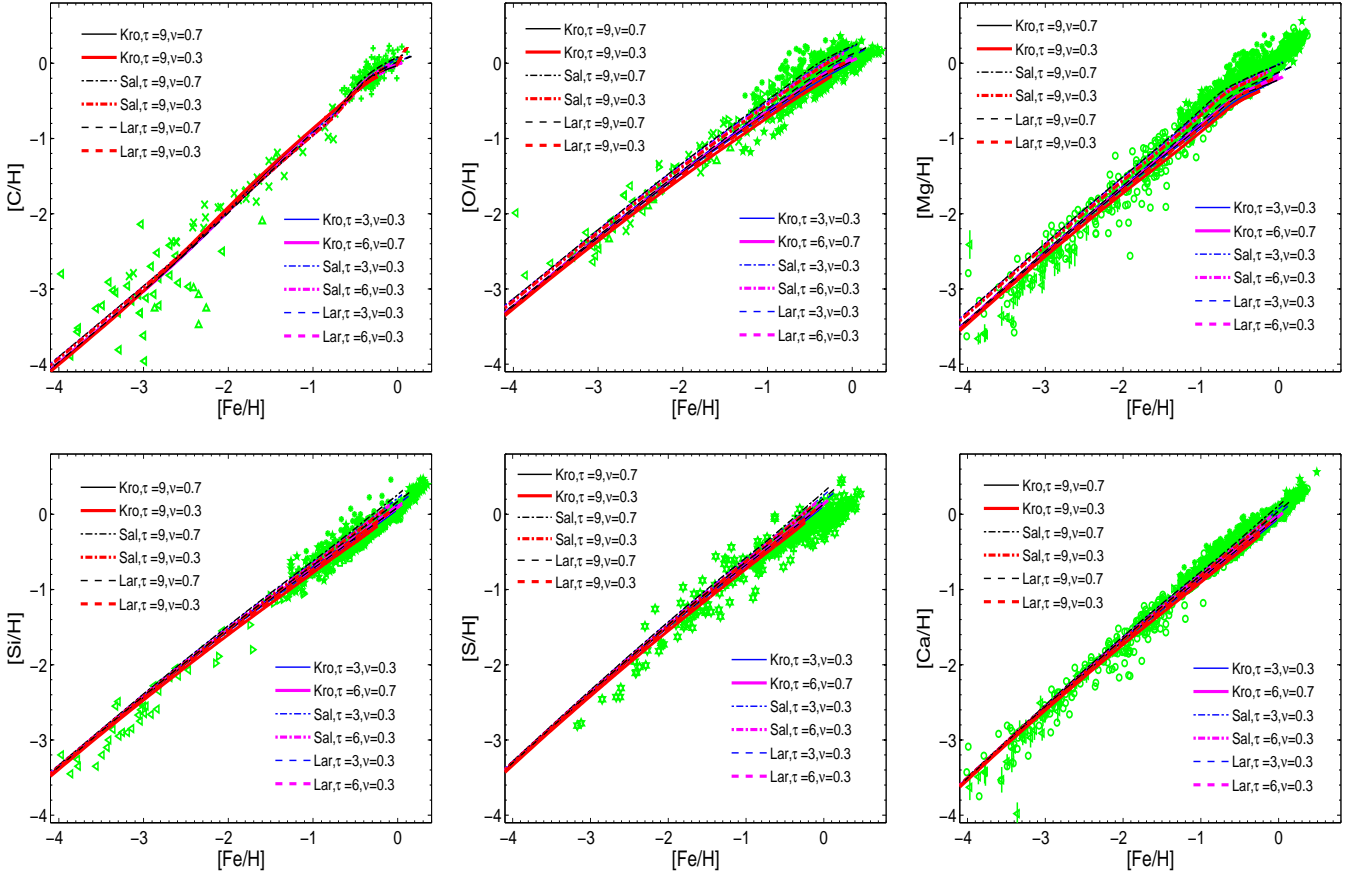


Fig. 16. Evolution of the elemental abundances in the Solar Neighborhood as measured by a sample of F and G stars and compared with the simulations. The evolution of $[A/H]$ vs. $[Fe/H]$ is represented for six elements of interest, namely C, O, Mg, Si, S and Ca. The data are taken from the following databases: Oxygen from Chen et al. (2000); Meléndez & Barbuy (2002); Reddy et al. (2003); Gratton et al. (2003); Akerman et al. (2004); Cayrel et al. (2004); Jonsell et al. (2005); Soubiran & Girard (2005); Carbon from Meléndez & Barbuy (2002); Reddy et al. (2003); Akerman et al. (2004); Cayrel et al. (2004); Magnesium from Chen et al. (2000); Gratton et al. (2003); Reddy et al. (2003); Soubiran & Girard (2005) and Venn et al. (2004) (circle); Silicon from Chen et al. (2000); Gratton et al. (2003); Reddy et al. (2003); Cayrel et al. (2004); Jonsell et al. (2005); Soubiran & Girard (2005); Sulphur from Reddy et al. (2003) and Caffau et al. (2005) (six-point star) and, finally, Calcium from Chen et al. (2000); Gratton et al. (2003); Reddy et al. (2003); Venn et al. (2004); Cayrel et al. (2004); Soubiran & Girard (2005); Jonsell et al. (2005). Twelve models are superposed to the data, at varying the IMF (three cases are considered: Kroupa, Salpeter and Larson adapted to the Solar Neighborhood), the efficiency of the star formation ν (two values: $\nu = 0.3$ and $\nu = 0.7$) and the infall timescale τ (three values: $\tau = 3$, $\tau = 6$ and $\tau = 9$ Gyr). Not all the combinations are shown but only the most interesting ones according to Figs. 13 and 14.

gestion by Zhukovska et al. (2008). These new calculations allow us to test the model response to variations of the Mg yields. The results are shown in Fig. 14 where we note that the agreement with the observational data is better for all the IMFs, in particular with the Kroupa IMF the results are very good. Furthermore, the whole range of observational depletions is now better covered by varying the star formation efficiency than with the original yields of Mg: changing ν from 0.3 to 0.7 all the range of observational values is obtained. However, as in the previous case of Fig. 13, the highest star formation rates enrich too much the ISM in metals and the process of dust formation is hardly able to deplete the ISM. The models clarify that the process of dust formation *crucially* depends on the the amounts of metals injected by the stars via mass loss and/or SNæ. They also make clear that the set of abundances at the base of the

theoretical models for metal enrichment and dust production of the ISM must be strictly identical, otherwise there would be no consistency between the two descriptions (consistency is of course always secured in reality).

Iron: in normal circumstances iron is highly depleted. In most of the models in Fig. 13 the best we can obtain at varying the parameters is to reach the upper limit of the observational depletion range, i.e. $-2 \leq [Fe_{\text{gas}}/H] \leq -1$. Even if two possible processes for the formation of dust (iron dust and silicates) are included, the mechanism of iron formation in cold regions of our models is not able to reach such lower values. Probably a more complex model, for instance with a spectrum of MCs with different lifetimes and/or some processes of accretion in other parts of the ISM different from MCs, is needed to reach the severe -2 depletion limit. With the modified Mg abundances, the

Table 5. Comparison of the properties of the MW in the SoNe with model results¹ and with the Zhukovska et al. (2008) model from which the observational data is taken:

Observable	Observed	ZGT08 ²	This work	Reference
Total surface density $\sigma(r_\odot, t_G)$ [$M_\odot \text{pc}^{-2}$]	50 - 62	56	52	Holmberg & Flynn (2004)
ISM surface density $\sigma_{\mathcal{M}}(r_\odot, t_G)$ [$M_\odot \text{pc}^{-2}$]	7 - 13	9.7	10 - 19.5	Dickey (1993)
	~ 8	9.7	10 - 19.5	Dame (1993)
	13 - 14	9.7	10 - 19.5	Olling & Merrifield (2001)
Gas fraction $\sigma_{\mathcal{M}}(r_\odot, t_G) / \sigma(r_\odot, t_G)$	0.05 - 0.2	0.17	0.2 - 0.39	
Surface density of visible stars $\sigma_*(r_\odot, t_G)$ [$M_\odot \text{pc}^{-2}$]	30 - 40	38.6	23 - 35	Gilmore et al. (1989)
Surface density of stellar remnants [$M_\odot \text{pc}^{-2}$]	2 - 4	7.7	6 - 10	Mera et al. (1998)
Star Formation Rate [$M_\odot \text{pc}^{-2} \text{Gyr}^{-1}$]	3.5 - 5	3.1	1.6 - 4	Rana (1991)
SN $\bar{\alpha}$ II rate [$\text{pc}^{-2} \text{Gyr}^{-1}$]	0.009-0.0326	0.016	0.01 - 0.04	Tammann et al. (1994)
SN $\bar{\alpha}$ Ia rate [$\text{pc}^{-2} \text{Gyr}^{-1}$]	0.0015-0.0109	0.0024	0.0035 - 0.0078	Tammann et al. (1994)
Infall Rate [$M_\odot \text{pc}^{-2} \text{Gyr}^{-1}$]	0.5 - 5	1.45	0.25 - 1.80	Braun & Thilker (2004)

¹The range of values for the entries of column (4) refers to the models discussed in this section, for the case with no correction to Mg abundance. Of all the models shown in Fig. 13, we select only the twelve models presented in Fig. 15. ²Zhukovska et al. (2008).

results improve a bit due to the higher amount of silicates and hidden iron, but still we are not able to fully span the interval from -1 to -2 .

Calcium: some of the considerations we made for the iron apply to calcium, for which the observed depletion is even more severe than that of iron. For calcium, there is no overlap at all with the observational interval. As described in Sect. 5.6, we introduce a multiplicative factor Ca_X in the accretion time scale $\tau_{Ca, Ca}^{gr}$ and try to calibrate it against the observational values. Even using $Ca_X \lesssim 0.05$ it is not possible to describe the strong depletion of Ca. The results presented in Figs. 13 and 14 are for a small scaling factor ~ 0.1 .

Sulfur: sulfur can be very depleted along some lines of sight, much less along other. Since a typical sulfur dust grain is not available to simulate the accretion process, we used a simple prescription for the average accretion with sulfur atoms accreting on themselves (see Sect. 5.7 for more details). A multiplicative factor S_X has been introduced to calibrate the timescale τ_S^{gr} , the longest between the timescales of the refractory elements and the accretion of sulfur atoms on themselves. The results displayed in Figs. 13 and 14 show the sulfur depletion with (filled and empty hexagons) and without (filled and empty circles) the effect of S_X on the accretion time scale τ_S^{gr} . With S_X going from 1 (no correction - circles) to 0.6-0.4 (small correction - hexagons) the theory fairly agrees with observational data.

Oxygen: this element does not participate as a key-element in any accretion process of dust formation. However it takes part to the formation of the silicates and it is an ingredient of the dust yields from stars of different masses. Because of its high abundance, the depletion is small, even if lots of oxygen atoms are contained in olivines/pyroxenes. In Figs. 13 and 14 we can see that the theoretical predictions well reproduce the observational data, in particular when Mg is corrected for under-abundance in the yields. The agreement simply follows from using the correct Mg/Si ratio.

Abundances and Depletions in the Solar Vicinity. To check the internal consistency of the depletion models, we must secure that the theoretical evolution of the abundances

of the various elements in the Solar Neighborhood is able to reproduce the observational data. It would be a point of strong contradiction if the models can reproduce the elemental abundances in the dust, but fail to reproduce the pattern of abundances in the gas and stars. In Fig. 15 we show the evolution of the metallicity Z and iron abundance $[\text{Fe}/\text{H}]$ for a wide selection of models, taking into account more or less the combinations of IMF, ν and τ that best reproduce the depletion measured in the SoNe. In such a case, one should discard the models with $\tau = 1$ that hardly fit the data for depletion in the SoNe. Most of the remaining models fairly agree with the observational data with the exception of the case with the Kroupa IMF, slow infall ($\tau = 9$), and low SFR ($\nu = 0.3$) that is not able to grow fast enough in metals. In Table 5 we present the check of the minimum/maximum values obtained in our models vs. the observations in the SoNe of various physical quantities of interest. The same simulations presented in Fig. 15 are compared with both the results obtained by Zhukovska et al. (2008) and the observational data. The general agreement between our results and the observations is good and it allows to conclude that we are employing a correct modelling of the SoNe. Once that the more general quantities, like the mass of stars, gas, the SNa rates and the total surface mass are satisfactorily reproduced we can proceed to examine the evolution of the abundances of the single elements in the SoNe and how they match up with the local data.

In the panels of Fig. 16 we show the time evolution in the Solar Neighborhood of the abundances of six elements heavily involved in dust formation, namely C, O, Mg, Si, S and Ca, in the diagnostic planes $[A/\text{Fe}]$ vs. $[\text{Fe}/\text{H}]$. The observational data refers to F and G stars (see Fig. 16 for more details on the data and associated legend). Twelve models are displayed at varying the IMF (Larson SoNe, Salpeter and Kroupa), efficiency of star formation ($\nu = 0.3$ and 0.7), and the infall timescale τ (3, 6 and 9 Gyr). Not all the cases are shown for $\tau = 3$ and $\tau = 6$ but only the most interesting ones as far as the degree of depletion is concerned (see Figs. 13 and 14). In general, the agreement is good for $\tau = 3$ and

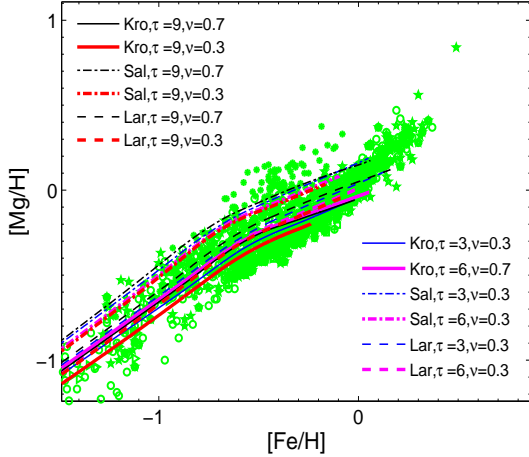


Fig. 17. Evolution of the Mg abundance in the Solar Neighborhood as measured in a sample of F and G stars. The yields have been slightly corrected for the Mg under-abundance. This corrected abundance is the same as in Fig. 14.

$\tau = 6$, while for $\tau = 9$, during the first 2 Gyr (in practice until $[\text{Fe}/\text{H}] \sim -1.5$) the enrichment in metals is too slow with respect to the observations. The only exception is carbon which always agrees with the observations. It must be pointed out that we are using infall models with a single timescale. This simplified picture leads to models that in the $[\text{A}/\text{Fe}]$ vs. $[\text{Fe}/\text{H}]$ planes cannot reach regions of very low or very high $[\text{Fe}/\text{H}]$. In reality, during the lifetime of the MW different time scales could be involved in the evolution of the describe the Solar Neighborhood, e.g. a fast early enrichment followed by a much slower one. Double infall models (Chiosi 1980; Chiappini et al. 1997) or more complicated scenarios are however beyond the aims of this study. Finally, it is worth noticing: (i) the under-abundance of Mg in the top right panel; (ii) the marginal agreement of the models with sulfur evolution.

In Fig. 17 we show the evolution of the Mg abundance in the SoNe once corrected for the under-abundance problem. The same models already presented in Fig. 16 are shown, but for the correction of the Magnesium abundance. With this correction not only we have a better pattern of depletions (See Fig. 14), but also a better reproduction of the local data.

To enforce the argument we examine the evolution of the most important elements involved in the dust formation process looking at the $[\text{A}/\text{Fe}]$ vs. $[\text{Fe}/\text{H}]$ diagrams relative to the SoNe. The most striking points of disagreement with the observational data are the under-abundance of Mg and the evolution of Sulphur. For the sake of comparison, we also show the models by Zhukovska et al. (2008), calculated after revising the yields by Woosley & Weaver (1995) and Nomoto et al. (2006). In both cases the yields of Sulphur do not lead to a good fit of the observations. The yields by Nomoto et al. (2006) give indeed the worst model. Our yields produce similar results in the sense that they tend to keep the abundance of Sulphur too high. Fortunately, this has no effect on the overall production of dust as Sulphur drives its own accretion efficiency (See Sect. 5.7) and does not affect other channels of dust production. Apart from these minor uncertainties, the observational data and the-

oretical abundances fairly agree and consequently dust formation stands on a realistic description of the evolution of the elemental abundances in the Solar Neighborhood.

10. Discussion and conclusions

In the first paper of this series of three (Piovan et al. 2011a), we presented and discussed the prescriptions currently in use to describe the type and amounts of dust injected into the ISM by AGB stars and SNa explosions. The condensation coefficients of the dust have tested and analyzed referring to a suitable chemical model for the MW Disk and the Solar Neighbourhood in particular. This reference model and its physical ingredients are described in great detail in this paper. In particular, we focused on the mechanism of dust accretion in the ISM, dust destruction by various processes, the main parameters of the chemical model, namely IMF, star formation efficiency and infall timescale. The main conclusions can be summarized as follows:

- The CO molecules influence the formation of C-based dust, thus introducing into the estimates an unavoidable uncertainty. The higher the amount of carbon embedded into CO, the slower is the accretion process and the smaller the amount of carbonaceous grains that are formed.
- During most of the MW evolutionary history, the main process enriching the ISM in dust is the accretion in the cold regions. Only in the very early stages, SN α dominate, and the duration of this phase tends to shorten in regions of high star formation and fast enrichment in metals (innermost regions of the MW). The opposite for the regions of low star formation (the outskirts of the MW), where the accretion in the ISM becomes significant much later so that for many Gyr SN α govern the total dust budget. In this case, AGB stars play an important role, because there is enough time for them to significantly contribute to the dust budget, without being overwhelmed by the SN α (earlier phases) or the ISM accretion (later phases). The time interval during which SN α are the main dust producer can slightly change at varying the upper mass limit of stars undergoing the AGB phase.
- Our conclusions for the MW Disk could be extended to galaxies characterized by continuous star formation on the notion that the outer regions of the MW Disk might correspond to low star forming galaxies and the inner ones to high star forming objects. Very high values of SFR (See for example Gall et al. 2011a,b, for detailed simulations of starburst galaxies and QSOs), which are not reached in the MW, not even in the early phases of the evolution in the inner regions, somehow elude this simple scheme. In any case, star-dust dominates the mild SF environments for a long period of time. This time scale tends to decrease in environments with IMFs skewed toward the mass interval in which the star-dust/metals factories (AGB stars and SN α) are important, thus helping the onset of the accretion phase in the ISM.
- In the high SFR/high metallicity regions AGB stars mainly produce silicates, whereas in the low SFR/low metallicity ones, carbon stars can contribute significantly to the C-based dust.

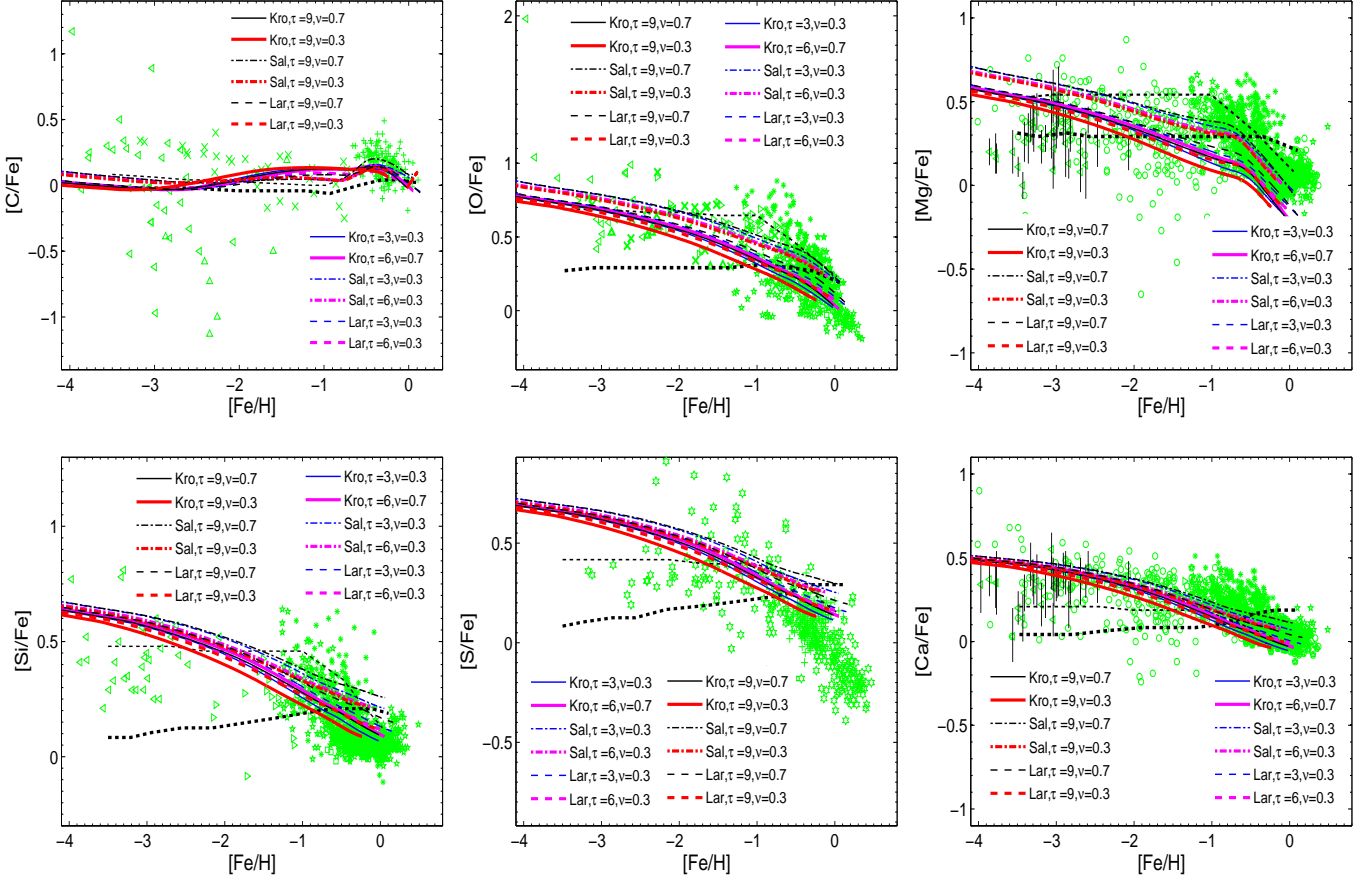


Fig. 18. Evolution of the elemental abundances in the Solar Neighborhood as measured in a sample of F and G stars. The evolution of $[A/Fe]$ vs. $[Fe/H]$ is shown for six elements of interest, that is C, O, Mg, Si, S and Ca. For the sake of comparison we plot the results by Zhukovska et al. (2008) for the SNa yields by Woosley & Weaver (1995) where Mg and Fe have been corrected to get a better agreement with the observations (the thick dotted line), and the yields by Nomoto et al. (2006), the thin dotted line. The meaning of the symbols for the observational data is the same as in Fig. 16.

– The IMF plays a fundamental role because it controls the relative amounts of low, intermediate and massive stars (see the entries of Table 4). We found that IMF's skewed toward massive stars are not suitable to reproduce the properties of dust in the MW, the SoNe in particular, (see also Dwek 1998; Zhukovska et al. 2008; Calura et al. 2008), whereas it seems that for star-burst galaxies (Gall et al. 2011a), ellipticals (Pipino et al. 2011) and QSOs (Gall et al. 2011b; Valiante et al. 2011) IMF's more biased toward higher mass stars are required, because otherwise it would be more difficult to reproduce the amount of dust observed already on site in very high- z objects. The alternative is to introduce very high condensation efficiencies in SN α . This possibility is somehow supported by the recent FIR/sub-mm observations on the SN 1987A by Matsuura et al. (2011). In such a case normal IMF's in high- z galaxies and QSOs cannot be excluded. The use of different IMF's for different galaxies in order to reproduce dust properties is a subject of vivid debate, and tightly related to the wider question about the universality of the IMF. The debate seems to favour an IMF sensitive to the initial conditions of star formation (see for instance the recent Elmegreen 2009; Bastian et al. 2010; Myers et al.

2011; Gunawardhana et al. 2011; Kroupa 2011, to mention a few). This possibility was suggested long ago by Chiosi et al. (1998) to solve the apparent contradiction between the spectral and chemical properties of early type galaxies. Similar conclusions are reached by Valiante et al. (2011), trying to match the observed properties of the QSOs SDSS J1148+5251, where a top-heavy IMF allow a more coherent match between different observations. Finally, when the SFR is high (inner regions), the effect of the IMF on the dust budget tends to disappear at the current time, because the accretion in the ISM becomes dominant early on in the evolution, while if the SFR is low we can see the effect of different IMF's spreading until the current time.

- Lower efficiencies ν of the SF, in the range adopted for the SoNe, correspond to a slower onset of the accretion in the ISM and a lower final dust budget.
- We tested different descriptions of the process of dust accretion in the ISM. A simple approach adopts an average time-scale of accretion to estimate the *total* dust budget at least in the early stages and for normal star forming environments. More complicated descriptions are require to follow the evolution of the abundance of single elements in dust or low star forming regions.

- The range of depletions observed for most of the elements, that is C, N, O, Mg, Si and S, is nicely reproduced by reasonable combinations of the parameters. IMFs with the classical slope in the high mass range, more easily fit the data for depletion. The only exceptions are: (i) iron, for which probably a more complex mechanism of accretion in the ISM than the simple one on cold regions is required (Zhukovska et al. 2008); (ii) calcium whose extreme depletion can not be reproduced by our model.
- The ratio between the abundances of Mg and Si is crucial in the formation of silicates and it is important to tune it according to the ratio expected from models. We had to correct the slightly under-abundance of the Mg in our gaseous yields, to obtain a better agreement with the observed depletion for the refractory elements involved into the silicates formation.

To conclude, the classical chemical models nicely reproduce the observed depletion and properties of the SoNe. The theoretical ingredients, like condensation coefficients and accretion models, behave in a satisfactory way. What can be improved? Clearly the major weak point is the one-phase description of the ISM. At least a two-phases ISM is required. Finally, work is in progress to introduce a multi-phase description of the ISM with dust in N-Body-TSPH simulations of galaxies.

Acknowledgements. L. Piovan acknowledges A. Weiss and the Max Planck Institut Für AstroPhysik (Garching - Germany) for the very warm and friendly hospitality and for providing unlimited computational support during the visits as EARA fellow when a significant part of this study has been carried out. The authors are also deeply grateful to S. Zhukovska and H. P. Gail for many explanations and clarifications about their model of dust accretion, T. Nozawa and H. Umeda for many fruitful discussions about SNa dust yields. This work has been financed by the University of Padua with the dedicated fellowship "Numerical Simulations of galaxies (dynamical, chemical and spectrophotometric models), strategies of parallelization in dynamical lagrangian approach, communication cell-to-cell into hierarchical tree codes, algorithms and optimization techniques" as part of the AACSE Strategic Research Project.

References

- Akerman, C. J., Carigi, L., Nissen, P. E., Pettini, M., & Asplund, M. 2004, *A&A*, 414, 931
- Allende Prieto, C., Lambert, D. L., & Asplund, M. 2001, *ApJL*, 556, L63
- . 2002, *ApJL*, 573, L137
- Anders, E. & Grevesse, N. 1989, *Geochim. Cosmochim. Acta*, 53, 197
- Antia, H. M. & Basu, S. 2005, *ApJL*, 620, L129
- . 2006, *ApJ*, 644, 1292
- Arimoto, N. & Yoshii, Y. 1987, *A&A*, 173, 23
- Asplund, M., Grevesse, N., & Sauval, A. J. 2005a, in *Astronomical Society of the Pacific Conference Series*, Vol. 336, *Cosmic Abundances as Records of Stellar Evolution and Nucleosynthesis*, ed. T. G. Barnes III & F. N. Bash, 25–+
- Asplund, M., Grevesse, N., Sauval, A. J., Allende Prieto, C., & Blomme, R. 2005b, *A&A*, 431, 693
- Asplund, M., Grevesse, N., Sauval, A. J., Allende Prieto, C., & Kiselman, D. 2004, *A&A*, 417, 751
- Asplund, M., Grevesse, N., Sauval, A. J., & Scott, P. 2009, *ARA&A*, 47, 481
- Bacmann, A., Lefloch, B., Ceccarelli, C., Castets, A., Steinacker, J., & Loinard, L. 2002, *A&A*, 389, L6
- Bahcall, J. N., Basu, S., Pinsonneault, M., & Serenelli, A. M. 2005a, *ApJ*, 618, 1049
- Bahcall, J. N., Serenelli, A. M., & Basu, S. 2005b, *ApJL*, 621, L85
- Bastian, N., Covey, K. R., & Meyer, M. R. 2010, *ARA&A*, 48, 339
- Basu, S. & Antia, H. M. 2008, 457, 217
- Bertoldi, F., Carilli, C. L., Cox, P., Fan, X., Strauss, M. A., Beelen, A., Omont, A., & Zylka, R. 2003, *A&A*, 406, L55
- Bianchi, S. & Schneider, R. 2007, *MNRAS*, 378, 973
- Blitz, L., Fukui, Y., Kawamura, A., Leroy, A., Mizuno, N., & Rosolowsky, E. 2007, in *Protostars and Planets V*, ed. B. Reipurth, D. Jewitt, & K. Keil, 81–96
- Boissier, S. & Prantzos, N. 1999, *MNRAS*, 307, 857
- . 2000, *MNRAS*, 312, 398
- Braun, R. & Thilker, D. A. 2004, *A&A*, 417, 421
- Bressan, A., Chiosi, C., & Fagotto, F. 1994, *ApJS*, 94, 63
- Caffau, E., Bonifacio, P., Faraggiana, R., François, P., Gratton, R. G., & Barbieri, M. 2005, *A&A*, 441, 533
- Caffau, E. & Ludwig, H. 2008, in *IAU Symposium*, Vol. 252, *IAU Symposium*, ed. L. Deng & K. L. Chan, 35–39
- Caffau, E., Ludwig, H., Bonifacio, P., Faraggiana, R., Steffen, M., Freytag, B., Kamp, I., & Ayres, T. R. 2010, *ArXiv e-prints*
- Caffau, E., Ludwig, H., Steffen, M., Ayres, T. R., Bonifacio, P., Cayrel, R., Freytag, B., & Plez, B. 2008, *A&A*, 488, 1031
- Caffau, E., Maiorca, E., Bonifacio, P., Faraggiana, R., Steffen, M., Ludwig, H., Kamp, I., & Busso, M. 2009, *A&A*, 498, 877
- Calura, F., Dessauges-Zavadski, M., Prochaska, J. X., & Matteucci, F. 2009, *ApJ*, 693, 1236
- Calura, F., Pipino, A., & Matteucci, F. 2008, *A&A*, 479, 669
- Cayrel, R., Depagne, E., Spite, M., Hill, V., Spite, F., François, P., Plez, B., Beers, T., Primas, F., Andersen, J., Barbuy, B., Bonifacio, P., Molaro, P., & Nordström, B. 2004, *A&A*, 416, 1117
- Chabrier, G. 2001, *ApJ*, 554, 1274
- . 2002, *ApJ*, 567, 304
- Chen, Y. Q., Nissen, P. E., Zhao, G., Zhang, H. W., & Benoni, T. 2000, *A&AS*, 141, 491
- Chiappini, C., Matteucci, F., & Gratton, R. 1997, *ApJ*, 477, 765
- Chiosi, C. 1980, *A&A*, 83, 206
- Chiosi, C., Bressan, A., Portinari, L., & Tantalo, R. 1998, *A&A*, 339, 355
- Chiosi, C. & Maeder, A. 1986, *ARA&A*, 24, 329
- Cioffi, D. F., McKee, C. F., & Bertschinger, E. 1988, *ApJ*, 334, 252
- Clayton, D. D. 1988, *ApJ*, 334, 191
- Clayton, R. N. 2003, *Treatise on Geochemistry*, 1, 129
- Crinklaw, G., Federman, S. R., & Joseph, C. L. 1994, *ApJ*, 424, 748
- Dame, T. M. 1993, in *American Institute of Physics Conference Series*, Vol. 278, *Back to the Galaxy*, ed. S. S. Holt & F. Verter, 267–278
- Deneault, E., Clayton, D. D., & Heger, A. 2003, *ApJ*, 594, 312
- Dickey, J. M. 1993, in *Astronomical Society of the Pacific Conference Series*, Vol. 39, *The Minnesota Lectures on the Structure and Dynamics of the Milky Way*, ed. R. M. Humphreys, 93–+
- Dopita, M. 1985, *ApJ*, 295, L5
- Dopita, M. & Ryder, S. D. 1994, *ApJ*, 430, 163
- Draine, B. T. 2009, *ArXiv:astro-ph/0903.1658*
- Dwek, E. 1998, *ApJ*, 501, 643
- Dwek, E. 2005, in *American Institute of Physics Conference Series*, Vol. 761, *The Spectral Energy Distributions of Gas-Rich Galaxies: Confronting Models with Data*, ed. C. C. Popescu & R. J. Tuffs, 103
- Dwek, E., Arendt, R. G., Fixsen, D. J., Sodroski, T. J., Odegard, N., Weiland, J. L., Reach, W. T., Hauser, M. G., Kelsall, T., Moseley, S. H., Silverberg, R. F., Shafer, R. A., Ballester, J., Bazell, D., & Isaacman, R. 1997, *ApJ*, 475, 565
- Dwek, E. & Cherchneff, I. 2011, *ApJ*, 727, 63
- Dwek, E., Galliano, F., & Jones, A. 2009, *ArXiv:astro-ph/0903.0006*
- Elmegreen, B. G. 2009, in *The Evolving ISM in the Milky Way and Nearby Galaxies*
- Ferrarotti, A. S. & Gail, H. 2006, *A&A*, 447, 553
- François, P., Matteucci, F., Cayrel, R., Spite, M., Spite, F., & Chiappini, C. 2004, *A&A*, 421, 613
- Gail, H., Zhukovska, S. V., Hoppe, P., & Trieloff, M. 2009, *ApJ*, 698, 1136
- Gall, C., Andersen, A. C., & Hjorth, J. 2011a, *A&A*, 528, A13+
- . 2011b, *A&A*, 528, A14+
- Gallerani, S., Maiolino, R., Juarez, Y., Nagao, T., Marconi, A., Bianchi, S., Schneider, R., Mannucci, F., Oliva, T., Willott, C. J., Jiang, L., & Fan, X. 2010, *A&A*, 523, A85+

- Gibson, B. K. 1994, *J. R. Astron. Soc. Can.*, 88, 383
- Gilmore, G., Wyse, R. F. G., & Kuijken, K. 1989, in *Evolutionary Phenomena in Galaxies*, ed. J. E. Beckman & B. E. J. Pagel, 172–200
- Goldsmith, P. F. 2001, *ApJ*, 557, 736
- Grassi, T., Krstić, P., Merlin, E., Buonomo, U., Pivon, L., & Chiosi, C. 2010, *ArXiv e-prints*
- Gratton, R. G., Carretta, E., Claudi, R., Lucatello, S., & Barbieri, M. 2003, *A&A*, 404, 187
- Greggio, L. & Renzini, A. 1983, *A&A*, 118, 217
- Grevesse, N., Asplund, M., & Sauval, A. J. 2007, *Space Science Reviews*, 130, 105
- Grevesse, N. & Noels, A. 1993, *Phys. Scr.*, 47, 133
- Grevesse, N. & Sauval, A. J. 1998, *Space Science Reviews*, 85, 161
- Gunawardhana, M. L. P., Hopkins, A. M., Sharp, R. G., Brough, S., Taylor, E., Bland-Hawthorn, J., Maraston, C., Tuffs, R. J., Popescu, C. C., Wijesinghe, D., Jones, D. H., Croom, S., Sadler, E., Wilkins, S., Driver, S. P., Liske, J., Norberg, P., Baldry, I. K., Bamford, S. P., Loveday, J., Peacock, J. A., Robotham, A. S. G., Zucker, D. B., Parker, Q. A., Conselice, C. J., Cameron, E., Frenk, C. S., Hill, D. T., Kelvin, L. S., Kuijken, K., Madore, B. F., Nichol, B., Parkinson, H. R., Pimbblet, K. A., Prescott, M., Sutherland, W. J., Thomas, D., & van Kampen, E. 2011, *ArXiv e-prints*
- Holmberg, J. & Flynn, C. 2004, *MNRAS*, 352, 440
- Hoppe, P., Strebler, R., Eberhardt, P., Amari, S., & Lewis, R. S. 2000, *Meteoritics and Planetary Science*, 35, 1157
- Hou, J. L., Yin, J., Boissier, S., Prantzos, N., Chang, R. X., & Chen, L. 2008, *ArXiv:astro-ph/0807.2492*
- Ibukiyama, A. & Arimoto, N. 2002, *A&A*, 394, 927
- Jenkins, E. B. 2009, *ApJ*, 700, 1299
- Jones, A. P. 2004, in *Astronomical Society of the Pacific Conference Series*, Vol. 309, *Astrophysics of Dust*, ed. A. N. Witt, G. C. Clayton, & B. T. Draine, 347–+
- Jones, A. P. & Nuth, J. A. 2011, *A&A*, 530, A44+
- Jonsell, K., Edvardsson, B., Gustafsson, B., Magain, P., Nissen, P. E., & Asplund, M. 2005, *A&A*, 440, 321
- Jonsson, P., Groves, B. A., & Cox, T. J. 2010, *MNRAS*, 403, 17
- Kemper, F., Markwick, A. J., & Woods, P. M. 2011, *MNRAS*, 413, 1192
- Kennicutt, Jr., R. C. 1983, *ApJ*, 272, 54
- . 1998, *ApJ*, 498, 541
- Kennicutt, Jr., R. C., Tamblyn, P., & Congdon, C. E. 1994, *ApJ*, 435, 22
- Kroupa, P. 1998, in *Astronomical Society of the Pacific Conference Series*, Vol. 134, *Brown Dwarfs and Extrasolar Planets*, ed. R. Rebolo, E. L. Martin, & M. R. Zapatero Osorio, 483
- Kroupa, P. 2001, in *Astronomical Society of the Pacific Conference Series*, Vol. 228, *Dynamics of Star Clusters and the Milky Way*, ed. S. Deiters, B. Fuchs, A. Just, R. Spurzem, & R. Wielen, 187–+
- Kroupa, P. 2002a, in *Astronomical Society of the Pacific Conference Series*, Vol. 285, *Modes of Star Formation and the Origin of Field Populations*, ed. E. K. Grebel & W. Brandner, 86
- Kroupa, P. 2002b, *Science*, 295, 82
- . 2007, *ArXiv:astro-ph/0703124*
- Kroupa, P. 2011, in *IAU Symposium*, Vol. 270, *IAU Symposium*, ed. J. Alves, B. G. Elmegreen, J. M. Girart, & V. Trimble, 141–149
- Kroupa, P., Tout, C. A., & Gilmore, G. 1993, *MNRAS*, 262, 545
- Krumholz, M. R., Matzner, C. D., & McKee, C. F. 2006, *ApJ*, 653, 361
- Landi, E., Feldman, U., & Doschek, G. A. 2007, *ApJ*, 659, 743
- Larson, R. B. 1986, *MNRAS*, 218, 409
- Larson, R. B. 1998, *MNRAS*, 301, 569
- Lee, J., Bergin, E. A., & Lyons, J. R. 2008, *Meteoritics and Planetary Science*, 43, 1351
- Leshin, L. A., Rubin, A. E., & McKeegan, K. D. 1997, *Geochim. Cosmochim. Acta*, 61, 835
- Li, A. & Draine, B. T. 2001, *ApJ*, 554, 778
- Liszt, H. S. 2007, *A&A*, 476, 291
- Lodders, K. 2003, *ApJ*, 591, 1220
- Lodders, K., Palme, H., & Gail, H. 2009, *ArXiv e-prints*
- Ludwig, H., Caffau, E., Steffen, M., Bonifacio, P., Freytag, B., & Cayrel, R. 2009, *ArXiv e-prints*
- Ludwig, H. & Steffen, M. 2008, in *Precision Spectroscopy in Astrophysics*, ed. N. C. Santos, L. Pasquini, A. C. M. Correia, & M. Romaniello, 133–138
- Maiorca, E., Caffau, E., Bonifacio, P., Busso, M., Faraggiana, R., Steffen, M., Ludwig, H., & Kamp, I. 2009, *Publications of the Astronomical Society of Australia*, 26, 345
- Mashonkina, L., Korn, A. J., & Przybilla, N. 2007, *A&A*, 461, 261
- Matsuura, M., Dwek, E., Meixner, M., Otsuka, M., & Babler, B., e. a. 2011, *ArXiv e-prints*
- Matteucci, F. & François, P. 1989, *MNRAS*, 239, 885
- Matteucci, F. & Greggio, L. 1986, *A&A*, 154, 279
- Mattsson, L. 2011, *MNRAS*, 451
- Matzner, C. D. 2002, *ApJ*, 566, 302
- Meléndez, J. & Asplund, M. 2008, *A&A*, 490, 817
- Meléndez, J. & Barbuy, B. 2002, *ApJ*, 575, 474
- Mera, D., Chabrier, G., & Schaeffer, R. 1998, *A&A*, 330, 937
- Meyer, B. S. 2009, *Meteoritics and Planetary Science Supplement*, 72, 5340
- Michalowski, M. J., Murphy, E. J., Hjorth, J., Watson, D., Gall, C., & Dunlop, J. S. 2010a, *A&A*, 522, A15+
- Michalowski, M. J., Watson, D., & Hjorth, J. 2010b, *ApJ*, 712, 942
- Morel, T. & Butler, K. 2008, *A&A*, 487, 307
- Myers, A. T., Krumholz, M. R., Klein, R. I., & McKee, C. F. 2011, *ArXiv e-prints*
- Narayanan, D., Dey, A., Hayward, C. C., Cox, T. J., Bussmann, R. S., Brodwin, M., Jonsson, P., Hopkins, P. F., Groves, B., Younger, J. D., & Hernquist, L. 2010, *MNRAS*, 407, 1701
- Nieva, M. F. & Przybilla, N. 2008a, in *Revista Mexicana de Astronomía y Astrofísica Conference Series*, Vol. 33, *Revista Mexicana de Astronomía y Astrofísica Conference Series*, 35–37
- Nieva, M. F. & Przybilla, N. 2008b, *A&A*, 481, 199
- Nomoto, K., Tominaga, N., Umeda, H., Kobayashi, C., & Maeda, K. 2006, *Nuclear Physics A*, 777, 424
- Nozawa, T., Kozasa, T., & Habe, A. 2006, *ApJ*, 648, 435
- Nozawa, T., Kozasa, T., Habe, A., Dwek, E., Umeda, H., Tominaga, N., Maeda, K., & Nomoto, K. 2007, *ApJ*, 666, 955
- Nozawa, T., Kozasa, T., Umeda, H., Maeda, K., & Nomoto, K. 2003, *ApJ*, 598, 785
- Olling, R. P. & Merrifield, M. R. 2001, *MNRAS*, 326, 164
- Omont, A., Cox, P., Bertoldi, F., McMahon, R. G., Carilli, C., & Isaak, K. G. 2001, *A&A*, 374, 371
- Ostriker, J. P. & McKee, C. F. 1988, *Rev. Mod. Phys.*, 60, 1
- Pagel, B. E. J. 1997, *Nucleosynthesis and Chemical Evolution of Galaxies (Nucleosynthesis and Chemical Evolution of Galaxies, by Bernard E. J. Pagel, pp. 392. ISBN 0521550610. Cambridge, UK: Cambridge University Press, October 1997.)*
- Piersanti, L., Straniero, O., & Cristallo, S. 2007, *A&A*, 462, 1051
- Pivon, L., Chiosi, C., Merlin, E., Grassi, T., Tantaló, R., & Cassarà, L. P. 2011a, *A&A*
- . 2011b, *A&A*
- . 2011c, *A&A*
- Pivon, L., Tantaló, R., & Chiosi, C. 2006, *MNRAS*, 370, 1454
- Pipino, A., Fan, X. L., Matteucci, F., Calura, F., Silva, L., Granato, G., & Maiolino, R. 2011, *A&A*, 525, A61+
- Popescu, C. C., Tuffs, R. J., Dopita, M. A., Fischera, J., Kylafis, N. D., & Madore, B. F. 2011, *A&A*, 527, A109+
- Portinari, L. & Chiosi, C. 1999, *A&A*, 350, 827
- . 2000, *A&A*, 355, 929
- Portinari, L., Chiosi, C., & Bressan, A. 1998, *A&A*, 334, 505
- Portinari, L., Moretti, A., Chiosi, C., & Sommer-Larsen, J. 2004a, *ApJ*, 604, 579
- Portinari, L., Sommer-Larsen, J., & Tantaló, R. 2004b, *MNRAS*, 347, 691
- Prantzos, N. & Boissier, S. 2000, *MNRAS*, 313, 338
- Prantzos, N. & Silk, J. 1998, *ApJ*, 507, 229
- Przybilla, N., Nieva, M., & Butler, K. 2008, *ApJL*, 688, L103
- Ramírez, I., Allende Prieto, C., & Lambert, D. L. 2007, *A&A*, 465, 271
- Rana, N. C. 1991, *ARA&A*, 29, 129
- Reddy, B. E., Tomkin, J., Lambert, D. L., & Allende Prieto, C. 2003, *MNRAS*, 340, 304
- Roberts, W. W. 1969, *ApJ*, 158, 123
- Robson, I., Priddey, R. S., Isaak, K. G., & McMahon, R. G. 2004, *MNRAS*, 351, L29
- Romano, D., Matteucci, F., Salucci, P., & Chiappini, C. 2000, *ApJ*, 539, 235
- Salpeter, E. E. 1955, *ApJ*, 121, 161
- Savage, B. D. & Sembach, K. R. 1996, *ARA&A*, 34, 279
- Scalo, J. M. 1986, *Fundam. Cosmic Phys.*, 11, 1
- Schmelz, J. T., Nasraoui, K., Roames, J. K., Lippner, L. A., & Garst, J. W. 2005, *ApJL*, 634, L197
- Schmidt, M. 1959, *ApJ*, 129, 243
- Schurer, A., Calura, F., Silva, L., Pipino, A., Granato, G. L., Matteucci, F., & Maiolino, R. 2009, *MNRAS*, 394, 2001

- Scott, P. C., Asplund, M., Grevesse, N., & Sauval, A. J. 2006, *A&A*, 456, 675
- Shapley, A., Fabbiano, G., & Eskridge, P. B. 2001, *ApJS*, 137, 139
- Shu, F. H., Milione, V., Gebel, W., Yuan, C., Goldsmith, D. W., & Roberts, W. W. 1972, *ApJ*, 173, 557
- Silva, L., Granato, G. L., Bressan, A., & Danese, L. 1998, *ApJ*, 509, 103
- Sommer-Larsen, J. 1996, *ApJ*, 457, 118
- Soubiran, C. & Girard, P. 2005, *A&A*, 438, 139
- Tafalla, M., Myers, P. C., Caselli, P., Walmsley, C. M., & Comito, C. 2002, *ApJ*, 569, 815
- Talbot, R. J. & Arnett, D. W. 1975, *ApJ*, 197, 551
- Tammann, G. A., Loeffler, W., & Schroeder, A. 1994, *ApJS*, 92, 487
- Tielens, A. G. G. M. 2005, *The Physics and Chemistry of the Interstellar Medium*, ed. Tielens, A. G. G. M.
- Timmes, F. X., Woosley, S. E., & Weaver, T. A. 1995, *apjs*, 98, 617
- Tinsley, B. M. 1980, *Fundam. Cosmic Phys.*, 5, 287
- Turck-Chièze, S., Couvidat, S., Piau, L., Ferguson, J., Lambert, P., Ballot, J., García, R. A., & Nghiem, P. 2004, *Physical Review Letters*, 93, 211102
- Turck-Chièze, S., Phi Nghiem, P. A., & Mathis, S. 2008, *Journal of Physics Conference Series*, 118, 012030
- Turcotte, S. & Wimmer-Schweingruber, R. F. 2002, *Journal of Geophysical Research (Space Physics)*, 107, 1442
- Valiante, R., Schneider, R., Bianchi, S., & Andersen, A. C. 2009, *MNRAS*, 397, 1661
- Valiante, R., Schneider, R., Salvadori, S., & Bianchi, S. 2011, *ArXiv e-prints*
- van Dishoeck, E. F. & Black, J. H. 1988, *ApJ*, 334, 771
- van Dishoeck, E. F. & Blake, G. A. 1998, *ARA&A*, 36, 317
- van Dishoeck, E. F., Blake, G. A., Draine, B. T., & Lunine, J. I. 1993, in *Protostars and Planets III*, ed. E. H. Levy & J. I. Lunine, 163–241
- Venn, K. A., Irwin, M., Shetrone, M. D., Tout, C. A., Hill, V., & Tolstoy, E. 2004, *AJ*, 128, 1177
- Visser, R., van Dishoeck, E. F., & Black, J. H. 2009, *A&A*, 503, 323
- Walmsley, C. M., Flower, D. R., & Pineau des Forêts, G. 2004, *A&A*, 418, 1035
- Wang, B. & Silk, J. 1994, *ApJ*, 427, 759
- Wang, R., Carilli, C. L., Wagg, J., Bertoldi, F., Walter, F., Menten, K. M., Omont, A., Cox, P., Strauss, M. A., Fan, X., Jiang, L., & Schneider, D. P. 2008a, *ApJ*, 687, 848
- Wang, R., Wagg, J., Carilli, C. L., Benford, D. J., Dowell, C. D., Bertoldi, F., Walter, F., Menten, K. M., Omont, A., Cox, P., Strauss, M. A., Fan, X., & Jiang, L. 2008b, *AJ*, 135, 1201
- Weingartner, J. C. & Draine, B. T. 2001, *ApJ*, 563, 842
- Whittet, D. C. B., ed. 2003, *Dust in the galactic environment*
- Whittet, D. C. B. 2010, *ApJ*, 710, 1009
- Woosley, S. E. & Weaver, T. A. 1995, *ApJS*, 101, 181
- Wyse, R. F. G. & Silk, J. 1989, *ApJ*, 339, 700
- Yamasawa, D., Habe, A., Kozasa, T., Nozawa, T., Hirashita, H., Umeda, H., & Nomoto, K. 2011, *ArXiv e-prints*
- Young, P. R. 2005, *A&A*, 444, L45
- Zhukovska, S., Gail, H.-P., & Tieloff, M. 2008, *A&A*, 479, 453